Catalytic Conversion of Biomass-derived Oxygenates to α,ω-Diols

By

Kevin J. Barnett

A dissertation submitted in partial fulfillment of

the requirements for the degree of

Doctor of Philosophy

(Chemical Engineering)

at the

UNIVERSITY OF WISCONSIN-MADISON

2018

Date of final oral examination: 5/21/2018

This dissertation is approved by the following members of the Final Oral Committee:

George W. Huber, Professor, Chemical and Biological Engineering

James A. Dumesic, Professor, Chemical and Biological Engineering

Manos Mavrikakis, Professor, Chemical and Biological Engineering

Thatcher W. Root, Professor, Chemical and Biological Engineering

Ive Hermans, Professor, Chemistry

Abstract

Commodity chemical production from lignocellulosic biomass resources has the potential to sustainably replace petroleum-derived chemicals and to improve the economic feasibility of biofuels production. One class of chemicals of interest are α,ω-diols, particularly those with four, five, and six carbon atoms (C4-C6): 1,4-butanediol (1,4-BD), 1,5-pentanediol (1,5-PD) and 1,6-hexanediol (1,6-HD), respectively. These α,ω-diols are primarily used as monomers in the synthesis of polycarbonate polyols, polyester polyols, and polyurethanes and represent a combined $7 billion annual market that is growing at 7% per year.

C5 and C6 α,ω-diols were synthesized from biomass-derived oxygenates tetrahydrofurfuryl alcohol (THFA) and tetrahydropyran-2-methanol (THP2M), respectively. A three-step Dehydration-Hydration-Hydrogenation (DHH) pathway form THFA was shown to decrease catalyst costs by >50x and non-feedstock production costs by 6.6x versus the direct hydrogenolysis of THFA over oxophilically-promoted noble metal catalysts (e.g. RhRe). Here, 1,5-PD is produced via vapor-phase **D**ehydration of THFA to dihydropyran (DHP), **H**ydration of DHP to 2-hydroxytetrahydropyran (2-HTHP) in water, and **H**ydrogenation of the ring-opened tautomer of 2-HTHP, 5-hydroxyvaleraldehyde (5HVal), to 1,5-PD. The DHH pathway afforded 87% overall yields of 1,5-PD from THFA. The DHH chemistry applied to the analogous C6 route yielded 34% 1,6-HD from THP2M. Increased side product formation in the THP2M dehydration step to 2,3,4,5-tetrahydrooxepine (THO) led to the lower overall yield, but 86% 1,6-HD yields were achieved from the hydration-hydrogenation of THO.

The keys to the high yields and low costs achieved in the DHH pathway were the high thermodynamic favorability to desired products and increased reactivities of the reaction intermediates. Gas-phase THFA dehydration yielded 90% yield to DHP over a γ-Al_2O_3 catalyst due to the high thermodynamic favorability to the DHP product, as shown by gas-phase thermochemistry calculations and ^{13}C labelling studies. DHP, a vinyl cyclic ether, hydrated at over six orders of magnitude faster than cyclohexene. Gas-phase thermochemistry calculations showed the increased hydration rate of vinyl cyclic ethers over other unsaturated species is due to the formation of a very stable oxocarbenium intermediate. DHP is autocatalyzed by liquid- and solid-phase acids formed in situ during hydration, leading to over 28x increased in hydration rates in continuous flow reactors. Addition of pre-synthesized solid acid catalysts greatly increased

DHP hydration rates over autocatalytic hydration and improved 1,5-PD yields from 20% to 86% in the combined hydration-hydrogenation of DHP to 1,5-PD. The cyclic hemiacetal 2-HTHP hydration product spontaneously tautomerizes to its ring-opened aldehyde form, 5HVal, in solution, leading to a ~50:50 mixture of 2-HTHP:5Hval at 120˚C. Hydrogenation of the aldehyde group (at 120˚C) enables the use of monometallic catalysts and 80x increased reaction rates versus the direct hydrogenolysis of THFA.

Hydration-hydrogenation chemistry was applied to C4 feedstocks to produce 1,4-BD from biomass-derived chemicals. 2,5-dihydrofuran - which can be synthesized from biomass-derived erythritol - was isomerized, hydrated, and hydrogenated in a single batch reaction step over solid-acid hydration and metal hydrogenation catalysts, giving a 82% yield to 1,4-BD. γ-Butyrolactone (GBL) – which can be synthesized from biomass-derived furfural – was hydrogenated to 1,4-BD at >95% yields over bimetallic $CuCo/TiO_2$ catalyst. GBL hydrogenation rates were improved by 2.5x over monometallic Co and 20x over monometallic Cu catalysts, respectively, when employing a bimetallic $CoCu/TiO_2$ catalyst with a 90:10 Co:Cu ratio.

Acknowledgements

I would like to thank all the people that have helped me get to this exciting point in my life. First, I would like to thank my advisor Professor George Huber. George has always been supportive of my research and I appreciate his mentorship. I also appreciate his willingness to support my professional development outside of the laboratory, including my internship in China and my efforts in starting Pyran. I would also like to thank Professors James Dumesic, Christos Maravelias, and Ive Hermans for their collaborations and their efforts in aiding in my research. The Department of Energy Bioenergy Technologies Office (DOE BETO) was a great project to work on and I thank DOE for the financial support. I would also like to acknowledge my undergraduate advisor, Dr. Benjamin Wilhite, and undergraduate mentor, Dr. Daejin Kim, at Texas A&M for inspiring me to pursue a PhD degree and a career in research. The same goes to the people at the National Renewable Energy Laboratory who opened my eyes to the world of catalysis and biomass and were great mentors as well.

Dr. Zach Brentzel, Dr. Sam Burt, and Dr. Kefeng Huang were extremely hard-working and talented co-workers and I would not have gotten half as much done here if not for them. Fellow 5th year Huber group members Joe Chada and Dan McClelland not only helped me immensely with my research and provided great advice throughout my PhD, but were also good friends over the years and I wish them the best in the future. 4th year Huber group members Nat Eagan and Siddarth Krishna were ok, too. Visiting scholars Zhiwei Huang and Ling Li contributed a lot to the work in this thesis. Other people that I'd like to thank include former and current graduate students Dr. Jechan Lee, Dr. Pranav Karanjkar, Dr. Insoo Ro, Dr. Zhuoran Xu, Dr. Dongting Zhao, Peter Galebach, Kei$$hla Rivera-Dones, Ted Walker, Mark Lindsay and Anthony Anderson;

postoc Dr. Jiayue He; and undergraduate researchers Emily Gasteyer, Ian Henderson, and Andrew Einspanier.

I would not have gotten through my PhD without such great friends in the department, including Frank Nguyen, Parth Mangrolia, Michael Risbeck, Loukas Goulatis, and Travis and Hannah Nelson. It was also fun to get to see my friends from back at Texas A&M a couple times a year and having such good friends during my undergrad helped me get to this point. I also fondly remember the friends I made in Dalian, China during my internship and I thank them for the memories.

Most importantly I would like to thank my family, who have been there for me my whole life up to this point. It is hard to go wrong with a family so supportive. Firstly, my girlfriend Merve: meeting her in my 3rd year here was easily the best thing that could've happened to me. She was incredibly supportive and loving and always cheered me up when I got home from a long day. She is a very strong, talented, and caring woman and I am more than excited about our bright future together. My parents, Jean and Gary Barnett were always by my side through my childhood – at soccer games, band practice, Boy Scouts and on and on. They gave me everything I needed and more and I couldn't have asked for more involved and loving parents and I appreciate them for that. My sister Lauren Barnett had to put up with me and my craziness all during our childhood (and still now) and I am proud of the person she has grown up to be. I also thank all my extended family, including my grandma Martha Barnett, for also being there from the start. Last, but not least, I would like to thank my cat Slippers for causing mischief in general, but also for being a really cool cat.

Table of Contents

List of Figures

List of Tables

Chapter 1. Introduction

1.1 Fuels and Chemicals from Lignocellulosic Biomass

The need for a clean and sustainable source of fuels and chemicals is becoming more pressing with the depletion of petroleum resources, increase in greenhouse gas emissions, and desire for a diversified national energy profile. Biomass represents the only renewable resource that can foreseeably replace the carbon-based fuels and chemicals that are currently made from oil. Lignocellulosic biomass holds particular promise due to its relative abundance, low cost, and the fact that it is inedible and does not compete with the food supply.[1] The U.S. Department of Energy has estimated that over 1.3 billion dry tons/year of biomass can be produced domestically by 2030 with the utilization of energy crops.[2] This represents 3.8 billion barrels of oil equivalent, or roughly the amount consumed by the U.S. transportation sector per year.[3] For biofuels to be produced at large enough scales to reasonably replace petroleum, however, biofuels technologies must continue to be improved to increase efficiencies and lower production costs.[4]

Commodity chemical production from biomass is desirable because it both improves the economics of producing biofuels and provides a renewable alternative to petroleum-based chemicals. Figure 1.1 shows the market prices and volumes in 2013 for several widely used commodity chemicals. Integration of high-value chemical production with fuels would increase the overall profitability of biorefineries, creating a drive for further investment and increased biofuels production.[5] To this end, we have shown that the co-production of high-value chemical 1,5-pentanediol with cellulosic ethanol can lower the price of the bio-ethanol by over $2.00 per gallon.[6] Biochemical production is also important from an environmental point-of-view: while chemicals comprise a much lower percentage of oil end-use than fuels, they represent a large and

growing portion of oil that will also need to be replaced by a renewable carbon resource such as biomass.[7]

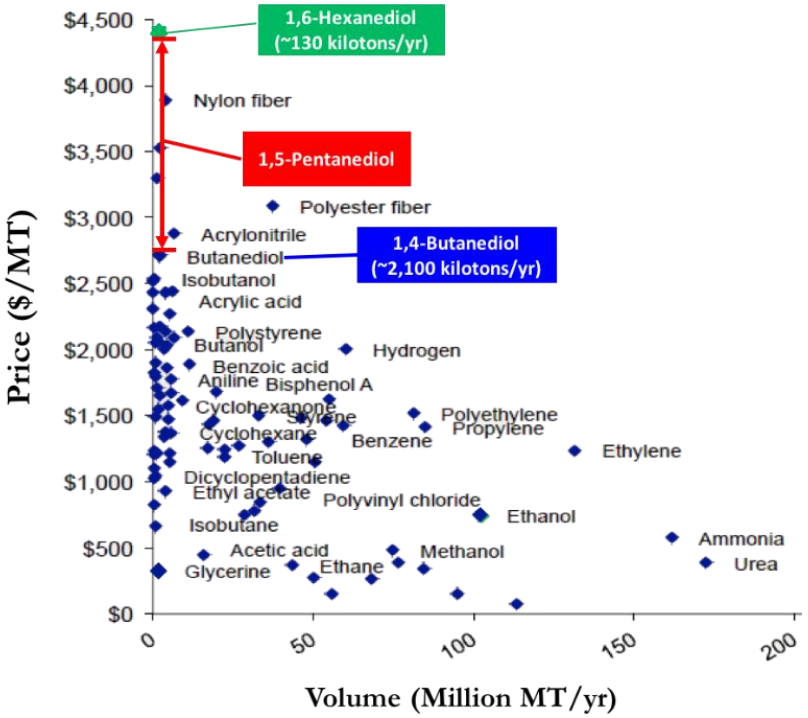

Adapted from ref. 17 with permission from Royal Society of Chemistry

Figure 1.1 Market price of commodity chemicals in 2013.[8]

1.2 α,ω-Diols from Petroleum

A class of high-value commodity chemicals that shows promise for production from biomass are α,ω-diols. Of particular interest are those with four, five, and six carbons (C4-C6): 1,4-butanediol (1,4-BD), 1,5-pentanediol (1,5-PD), and 1,6-hexanediol (1,6-HD), respectively. Figure 1.2 shows the current production volumes of C4-C6 α,ω-diols from oil and how these molecules could by replaced via the upgrading of biomass-derived xylose (C5) and glucose (C6). These α,ω-diols are largely utilized for the production of polycarbonate polyols, polyester polyols, and polyurethanes – industries that are growing rapidly worldwide.[9]

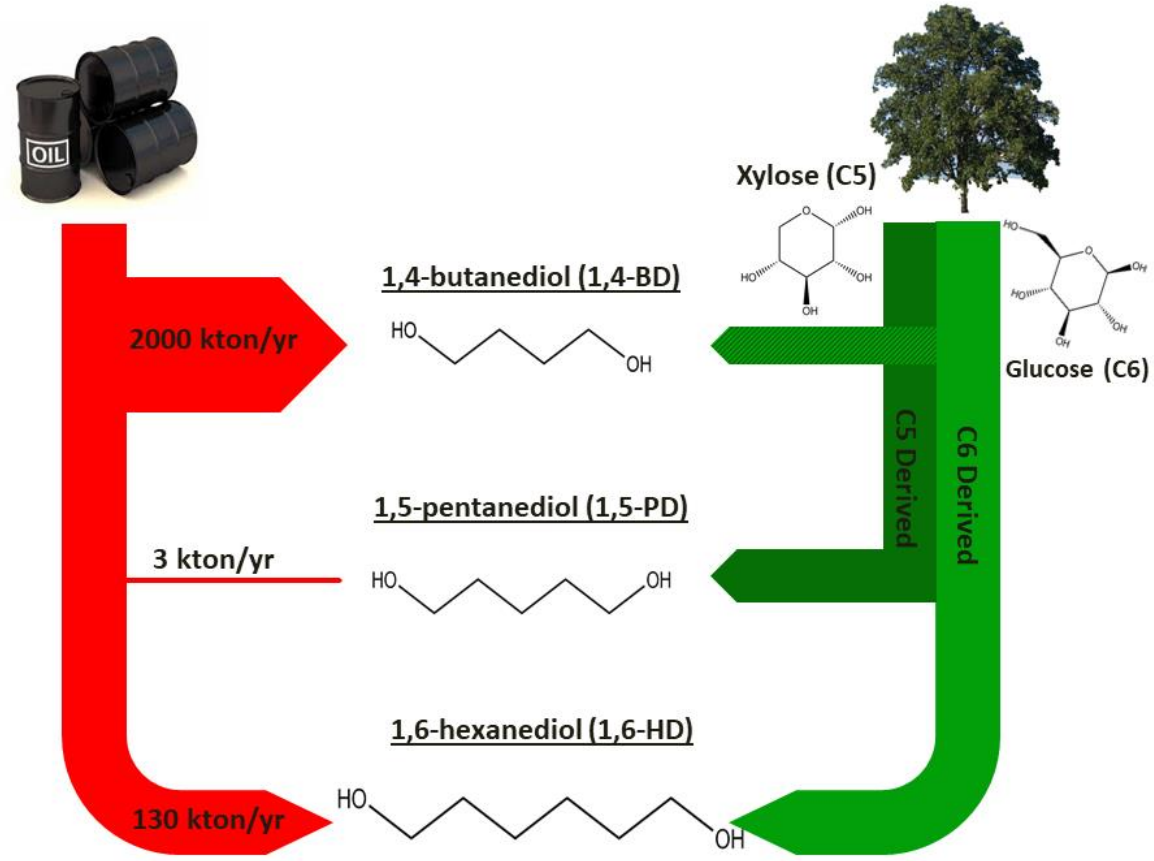

Figure 1.2 Replacement of oil-derived C4-C6 α,ω-diols using lignocellulosic biomass

C4-C6 α,ω-diols together comprise a $7 billion annual market that is growing at 7% per year.[10,11] 1,6-HD is the most expensive diol (selling price of $3000-4700/ton with a $900M annual market) followed by 1,4-BD (selling price of $1600-3300/ton with a $6.2 billion annual market).[10–12] 1,5-PD currently has a very high selling price ($6000/ton), but it's market is very small due to the high cost of making it from oil. Despite having some variance in applications, C4-C6 diols are highly interchangeable with each other as far in regards to the properties of the polymer end-products. For instance, polyester polyols made with 1,5-PD have similar properties as those made with 1,4-BD and 1,6-HD, while they are different enough to give unique and versatile plastics systems (e.g. low thermal transition temperature).[13]

Industrial synthesis of 1,6-HD is carried out via the oxidation of oil-derived cyclohexane to adipic acid in multiple steps followed by the hydrogenation of adipic acid (Figure 1.3).[14] There is currently no on-purpose synthesis of 1,5-PD from petroleum because of the lack of readily available C5 feedstocks from petroleum and resulting high production costs; 1,5-PD is only made as a byproduct in 1,6-HD production from adipic acid. 1,4-BD is commercially produced by three major routes: 1) hydrogenation of butynediol produced via carbonylation of acetylene with formaldehyde (Reppe process), 2) hydrogenation of maleic anhydride (MA), and 3) acetoxylation of butadiene.[15,16] Many of the α,ω-diol synthesis routes above suffer from low conversion reactions, many reaction steps (lower yields), homogeneous chemistry involving toxic chemicals (HNO_3 or KCN), and nonrenewable, petroleum feedstocks which contribute to climate change (see Figure 1.3 for 1,6-HD route).[17] It would thus be preferable to develop production routes for α,ω-diols from renewable biomass feedstocks

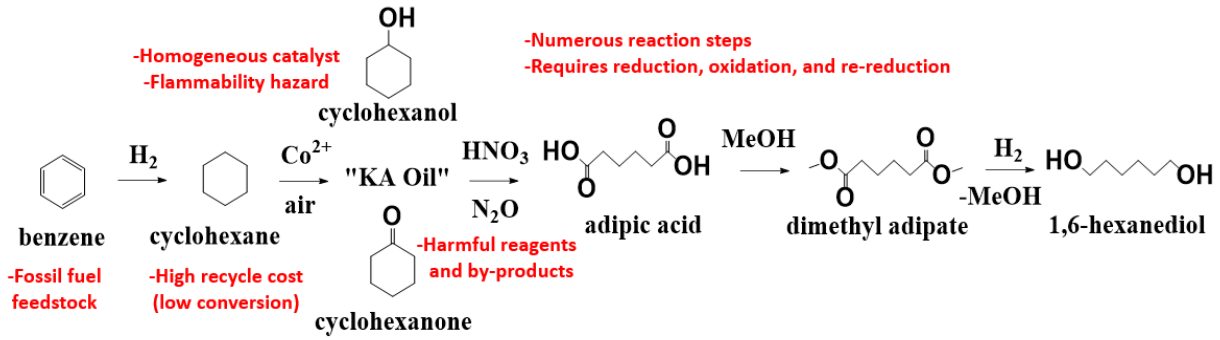

Adapted from ref. 17 with permission from Royal Society of Chemistry

Figure 1.3 Production of 1,6-hexanediol from petroleum-derived benzene.[17]

1.3 α,ω-Diols from Biomass

The inherently highly oxygenated nature of lignocellulosic biomass along with its high density of C5 and C6 units make it an ideal feedstock for the production of long-chain α,ω-diols. The three main components of lignocellulosic biomass – hemicellulose, cellulose, and lignin - can

be solubilized and purified using a novel thermal separation technique utilizing gamma-valerolactone and water solvent and an H_2SO_4 acid catalyst.[18,19] The hemicellulose stream can undergo downstream upgrading to the C5 platform molecule, furfural, while the cellulose stream can be upgraded to the C6 platform molecule, hydroxymethyl furfural (HMF).[20,21] Both furfural and HMF can then undergo complete hydrogenation to tetrahydrofurfuryl alcohol (THFA) and tetrahydrofuran dimethanol (THFDM), respectively, over Ni- and Ru-based catalysts.[22–24] In the C6 route, THFDM can then be converted to tetrahydropyran-2-methanol (THP2M) through a 1,2,6-hexanetriol intermediate.[25]

Most academic literature on THFA conversion to 1,5-PD and THP2M conversion to 1,6-HD has focused on direct hydrogenolysis (Figure 1.4A).[26–28] Noble metal catalysts (e.g. Rh or Pt) doped with an oxophilic promoter (e.g. Re or Mo) have been shown to give >90% yields to α,ω-diol products[27] due to the formation of very stable ring-opened oxocarbenium ion intermediates.[28] However, the relatively low reaction rates and high cost the noble metal catalysts make the direct hydrogenolysis route economically unfeasible.[29] Some work has been attempted in directly converting THFA to 1,5-PD over base metal catalysts at high temperatures, but this has resulted in the formation of low 1,5-PD selectivity with a large degree of byproduct formation in form of tetrahydropyran and 1-pentanol.[30] In fact, preliminary work to this thesis tested the high temperature (250˚C) direct hydrogenolysis of THFA over Ni/TiO_2 catalysts, resulting in only ~50% selectivity to 1,5-PD at ~10% conversion of THFA. Another 1,5-PD upgrading strategy involves incomplete hydrogenation of furfural to furfuryl alcohol (FA)[31] and hydrogenolysis of FA to 1,5-PD.[32] While having the benefit of using a strong metal-support interaction (SMSI)-stabilized Co/TiO_2 catalyst, overall 1,5-PD yields from FA were still fairly low at 30%.[32]

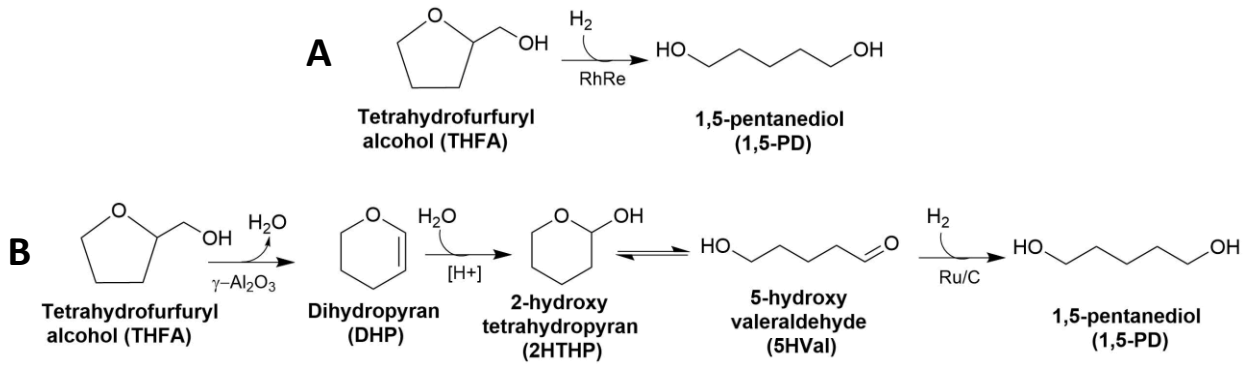

Figure 1.4 A) Direct hydrogenolysis and B) Dehydration-hydration-hydrogenation (DHH) routes to produce 1,5-pentanediol from biomass-derived THFA

Alternative methods to the costly (RhRe) or non-selective (Cu, Ni, Co) conversion of THFA and THP2M to α,ω-diols have been proposed. One route for THFA conversion to 1,5-PD is the "DHH" pathway. Here, 1,5-PD is produced via vapor-phase **D**ehydration of THFA to dihydropyran (DHP), **H**ydration of DHP to 2-hydroxytetrahydropyran (2-HTHP) in water, and **H**ydrogenation of the ring-opened tautomer of 2-HTHP, 5-hydroxyvaleraldehyde (5HVal), to 1,5-PD (Figure 1.4B). This pathway was first proposed in the 1940s by Geller et. al,[33] but has largely been unstudied since. The "DHH" chemistry was also applied to the analogous C6 route from THP2M to 1,6-HD in the 1960s and 1970s.[34,35]

1.4 Overview of the Dissertation

The present dissertation focuses on the development of alternative routes to the direct hydrogenolysis pathway for making C4-C6 α,ω-diols. The main contribution was the detailed study of the three step "DHH" pathway for 1,5-pentanediol (1,5-PD) production from THFA.[29,36] We were able to make several improvements to the early work by Geller et. al.,[33] including higher overall yields (87% vs. 70%), no use of homogeneous acids, and no purification of the 5HVal intermediate prior to hydrogenation.[29] The "DHH" pathway was also be applied to analogous C6

chemistry from THP2M to 1,6-HD.[37] Moreover, we show that this chemistry can also be applied to biomass-derived C4 streams to produce 1,4-BD.[38,39] A roadmap for the production of C4-C6 α,ω-diols using the hydration-hydrogenation chemistry is shown in Figure 1.5.

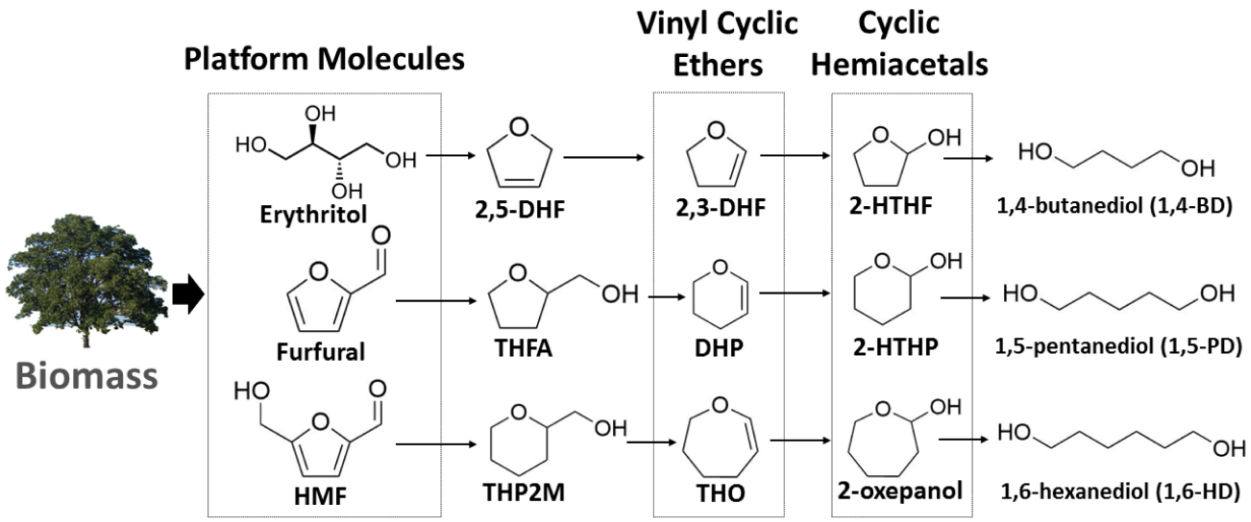

Figure 1.5 Roadmap for producing C4-C6 α,ω-diols from biomass-derived chemicals utilizing (dehydration)-hydration-hydrogenation chemistry

Chapter 2 focuses on the DHH pathway for the C5 Route from THFA to 1,5-PD. Here we show that a trio of unique reactions in series lead to much improved reaction rates and lower catalyst costs (by 50x), versus the direct hydrogenolysis of THFA.[29] First, THFA is dehydrated in the gas phase at 375˚C over a γ-Al_2O_3 catalyst to DHP in 90% yield. A carbon-13 (^{13}C) labeling study showed that the THFA undergoes ring-opening and Wagner-Meerwein rearrangement to the 6-membered ring DHP product. DHP is then hydrated without the use of an externally added catalyst to the cyclic hemiacetal, 2-HTHP. A key finding in Chapter 2 is the 2-HTHP undergoes spontaneous tautomerization to its ring-opened aldehyde form in solution. The aldehyde is then hydrogenated nearly quantitatively to the 1,5-PD product over monometallic catalysts at much faster rates than direct hydrogenolysis, thus enabling the much improved economics of the DHH

approach. Over 87% overall yields of 1,5-PD were obtained from THFA using the DHH pathway.[29]

Chapter 3 explores the same DHH chemistry for the production of 1,6-HD from the C6 biomass-derived chemical, THP2M. Here, many types of zeolite cage structures with different exchanged cations were studied for the THP2M dehydration step to 2,3,4,5-tetrahydrooxepine (THO), the C6 analog of the 5-carbon DHP.[37] However, yields for the dehydration step were lower than for the C5 route, with a maximum THO yield of 40% achieved. We were able to show that this is due to the increased thermodynamic favorability of side product formation from THO than for the C5 analog, DHP. Product selectivities were studied as a function of space velocity in a flow reactor in order to propose a detailed reaction pathway for the C6 dehydration step. We also showed that the C6 cyclic hemiacetal, 2-oxepanol, is very favorable to ring opening, with 50% of it converted to the ring-opened aldehyde, 6-hydroxyhexanal, at room temperature. The hydration and hydrogenation steps of the C6 route performed similarly well to the C5 route, with 86% total yields to 1,6-HD achieved.[37]

Chapters 4 and 5 focus in on the hydration reaction (step 2) of the DHH pathway. In Chapter 4, the autocatalytic nature of DHP hydration to 2-HTHP is explored. While in Chapter 2 we simply state that the DHP hydrates in water with no catalyst, in Chapter 4 we explain that this reaction actually forms an acidic species *in situ*, which further catalyzes DHP hydration and increases the reaction rate. We show that a liquid-phase acids form in batch reactors and that solid-phase acidic species form in continuous flow reactors, with both respectively increasing the DHP hydration rate.[40]

In Chapter 5, we investigate the thermodynamics of the hydration of cyclic vinyl ethers (e.g. DHP) in an attempt to explain why these molecules are so reactive for hydration. We were

able to show that the vinyl cyclic ethers hydrate over 7 orders of magnitude faster than similar molecules that do not have the cyclic oxygen atom present (e.g. cyclohexene) and concluded that the higher rates occur due to the formation of a very stable oxocarbenium intermediate upon hydration. We also demonstrate that solid acid catalysts can be added to the reactor to increase hydration rates, which can improve the selectivity to α,ω-diol products when combining the hydration and hydrogenation reactions in one reactor.[38]

Chapter 6 investigates the hydrogenation of the C4 lactone, gamma-butryolactone (GBL), to produce 1,4-BD over bimetallic CuCo catalysts.[39] Furfural can be oxidized to form SA,[41] MA[42] and 2(5H)-furanone,[16,41] all of which can be hydrogenated to GBL.[41] Hydrogenation of GBL in 1,4-dioxane solvent was shown to likely proceed through the same type of cyclic hemiacetal intermediate that enabled rapid hydrogenation to α,ω-diol products in the C5 and C6 routes. Moreover, a bimetallic CoCu/TiO_2 catalyst with a 90:10 Co:Cu ratio was shown to increase the rate of GBL conversion by 2.5 and 20 times than that over monometallic Co and monometallic Cu catalysts, respectively. Another important outcome of this study is the demonstration of a potential route to produce the C4 α,ω-diol, 1,4-BD, from the C5 biomass stream.[39]

1.5 References

1. Huber, G. W.; Iborra, S.; Corma, A. Synthesis of Transportation Fuels from Biomass: Chemistry, Catalysts, and Engineering. *Chem. Rev.* **2006**, *106* (9), 4044–4098.
2. 2016 Billion-Ton Report. United States Department of Energy: Washington, DC, 2016.
3. Annual Energy Outlook 2014. Www.Eia.Gov. Accessed 2014-12-19.
4. Routray, K.; Barnett, K. J.; Huber, G. W. Hydrodeoxygenation of Pyrolysis Oils. *Green Chem.* **2017**, 80–93.
5. Werpy, T.; Petersen, G. *Top Value Added Chemicals from Biomass*; 2004.
6. Huang, K.; Won, W.; Barnett, K. J.; Brentzel, Z. J.; Alonso, D. M.; Huber, G. W.; Dumesic, J. A.; Maravelias, C. T. Improving Economics of Lignocellulosic Biofuels: An Integrated Strategy for Coproducing 1,5-Pentanediol and Ethanol. *Appl. Energy* **2018**, *213* (July 2017),

585–594.

7. U.S. Department of Energy. The How's and Why's if Replacing the Whole Barrel https://energy.gov/articles/hows-and-whys-replacing-whole-barrel (accessed Feb 2, 2018).

8. Lux Research. *Bio-Based Materials and Chemicals Intelligence Service*; 2013.

9. Schlaf, M. Selective Deoxygenation of Sugar Polyols to Alpha,Omega-Diols and Other Oxygen Content Reduced Materials--a New Challenge to Homogeneous Ionic Hydrogenation and Hydrogenolysis Catalysis. *Dalton Trans.* **2006**, 4645–4653.

10. MarketandMarkets. *1,6-Hexanediol Market by Application (Polyurethanes, Coatings, Acrylates, Adhesives, Polyester Resins, Plasticizers), and Region (Europe, North America, Asia-Pacific, South America, and Middle East & Africa) - Global Forecasts to 2021*; 2016.

11. Grand View Research. *1,4 Butanediol (1,4-BD) Market Analysis by Application (Tetrahydrofuran (THF), Polybutylene Terephthalate (PBT), Gamma-Butyrolactone (GBL), Polyurethane (PU)), By Region (North America, Europe, Asia Pacific, CSA, MEA), And Segment Forecasts, 2014-2025*; 2017.

12. ICIS News. BASF seeks to raise North American 1,4-BD in July https://www.icis.com/resources/news/2016/06/01/10004049/basf-seeks-to-raise-north-american-1,4-BD-in-july/.

13. Desalvo, J.; Miller, R.; Van Gorp, J. Susterra Propanediol - Renewability, Sustainability, and Differentiating Performance in Urethane Applications http://www.duponttateandlyle.com/sites/default/files/2010 CPI Susterra White Paper.pdf.

14. Vyver, S. Van De; Román-Leshkov, Y. Emerging Catalytic Processes for the Production of Adipic Acid. *Catal. Sci. Technol.* **2013**, *3*, 1465.

15. Haas, T.; Jaeger, B.; Weber, R.; Mitchell, S. F.; King, C. F. New Diol Processes: 1,3-Propanediol and 1,4-Butanediol. *Appl. Catal. A Gen.* **2005**, *280* (1), 83–88.

16. Li, F.; Lu, T.; Chen, B.; Huang, Z.; Yuan, G. Pt Nanoparticles over TiO2-ZrO2mixed Oxide as Multifunctional Catalysts for an Integrated Conversion of Furfural to 1,4-Butanediol. *Appl. Catal. A Gen.* **2014**, *478*, 252–258.

17. He, J.; Huang, K.; Barnett, K. J.; Krishna, S.; Martin Alonso, D.; Brentzal, Z.; Burt, S. P.; Walker, T. W.; Banholzer, W.; Maravelias, C. T.; et al. New Catalytic Strategies for Alpha-Omega Diol Production from Lignocellulosic Biomass. *Faraday Discuss.* **2017**, *202*, 247-267.

18. Luterbacher, J. S.; Rand, J. M.; Alonso, D. M.; Han, J.; Youngquist, J. T.; Maravelias, C. T.; Pfleger, B. F.; Dumesic, J. a. Nonenzymatic Sugar Production from Biomass Using Biomass-Derived γ-Valerolactone. *Science* **2014**, *343* (6168), 277–280.

19. Alonso, D. M.; Hakim, S. H.; Zhou, S.; Won, W.; Hosseinaei, O.; Tao, J.; Garcia-negron, V.; Motagamwala, A. H.; Mellmer, M. A.; Huang, K.; et al. Increasing the Revenue from Lignocellulosic Biomass : Maximizing Feedstock Utilization. *Sci. Adv.* **2017**, *3* (5), 1-7.

20. Xing, R.; Qi, W.; Huber, G. W. Production of Furfural and Carboxylic Acids from Waste Aqueous Hemicellulose Solutions from the Pulp and Paper and Cellulosic Ethanol Industries. *Energy Environ. Sci.* **2011**, *4* (6), 2193.

21. Weingarten, R.; Rodriguez-Beuerman, A.; Cao, F.; Luterbacher, J. S.; Alonso, D. M.; Dumesic, J. a.; Huber, G. W. Selective Conversion of Cellulose to Hydroxymethylfurfural in Polar Aprotic Solvents. *ChemCatChem* **2014**, *6*, 2229–2234.

22. Nakagawa, Y.; Tomishige, K. Total Hydrogenation of Furan Derivatives over Silica-Supported Ni-Pd Alloy Catalyst. *Catal. Commun.* **2010**, *12* (3), 154–156.

23. Nakagawa, Y.; Tamura, M.; Tomishige, K. Catalytic Reduction of Biomass-Derived Furanic Compounds with Hydrogen. *ACS Catal.* **2013**, *3*, 2655–2668.

24. Alamillo, R.; Tucker, M.; Chia, M.; Pagán-Torres, Y.; Dumesic, J. The Selective Hydrogenation of Biomass-Derived 5-Hydroxymethylfurfural Using Heterogeneous Catalysts. *Green Chem.* **2012**, *14* (5), 1413.

25. Buntara, T.; Noel, S.; Phua, P. H.; Melián-Cabrera, I.; De Vries, J. G.; Heeres, H. J. Caprolactam from Renewable Resources: Catalytic Conversion of 5-Hydroxymethylfurfural into Caprolactone. *Angew. Chemie - Int. Ed.* **2011**, *50*, 7083–7087.

26. Koso, S.; Ueda, N.; Shinmi, Y.; Okumura, K.; Kizuka, T.; Tomishige, K. Promoting Effect of Mo on the Hydrogenolysis of Tetrahydrofurfuryl Alcohol to 1,5-Pentanediol over Rh/SiO2. *J. Catal.* **2009**, *267* (1), 89–92.

27. Nakagawa, Y.; Tomishige, K. Production of 1,5-Pentanediol from Biomass via Furfural and Tetrahydrofurfuryl Alcohol. *Catal. Today* **2012**, *195*, 136–143.

28. Chia, M.; Pagán-Torres, Y. J.; Hibbitts, D.; Tan, Q.; Pham, H. N.; Datye, A. K.; Neurock, M.; Davis, R. J.; Dumesic, J. a. Selective Hydrogenolysis of Polyols and Cyclic Ethers over Bifunctional Surface Sites on Rhodium-Rhenium Catalysts. *J. Am. Chem. Soc.* **2011**, *133*, 12675–12689.

29. Brentzel, Z. J.; Barnett, K. J.; Huang, K.; Maravelias, C. T.; Dumesic, J. A.; Huber, G. W. Chemicals from Biomass: Combining Ring-Opening Tautomerization and Hydrogenation Reactions to Produce 1,5-Pentanediol from Furfural. *ChemSusChem* **2017**, *10* (7), 1351–1355.

30. Yoshida, Y.; Hirotsu, K.; Fujimoto, R.; Katsura, R.; Fujitsu, S.; Doi, T.; Kashiwagi, K. Method for Producing High-Purity 1,5-Pentanediol. US 8,940,946 B2, 2015.

31. O'Neill, B. J.; Jackson, D. H. K.; Crisci, A. J.; Farberow, C. a.; Shi, F.; Alba-Rubio, A. C.; Lu, J.; Dietrich, P. J.; Gu, X.; Marshall, C. L.; et al. Stabilization of Copper Catalysts for Liquid-Phase Reactions by Atomic Layer Deposition. *Angew. Chemie - Int. Ed.* **2013**, *52*, 13808–13812.

32. Lee, J.; Burt, S. P.; Carrero, C. A.; Alba-Rubio, A. C.; Ro, I.; O'Neill, B. J.; Kim, H. J.; Jackson, D. H. K.; Kuech, T. F.; Hermans, I.; et al. Stabilizing Cobalt Catalysts for Aqueous-Phase Reactions by Strong Metal-Support Interaction. *J. Catal.* **2015**, *330*, 19–27.

33. Schneipp, L. E.; Geller, H. H. Preparation of Dihydropyran, δ-Hydroxyvaleraldehyde and 1,5-Pentanediol from Tetrahydrofurfuryl Alcohol. *J. Am. Chem. Soc.* **1946**, *68* (6), 1646–1648.

34. Misono, A.; Osa, T.; Sanami, Y. The Hydrogenation of Pyran Derivatives. IV. The Skeletal Rearrangement in the Gas-Phase Dehydration of Tetrahydropyran-2-Methanol. *Bull. Chem. Soc. Jpn.* **1968**, *41* (10), 2447–2453.

35. Tysee, D. A. Preparation of 2,3,4,5-Tetrahydrooxepin. U.S. 6,636,053, 1972.

36. Huang, K.; Brentzel, Z. J.; Barnett, K. J.; Dumesic, J. A.; Huber, G. W.; Maravelias, C. T. Conversion of Furfural to 1,5-Pentanediol: Process Synthesis and Analysis. *ACS Sustain. Chem. Eng.* **2017**, *5* (6), 4699–4706.

37. Burt, S. P.; Barnett, K. J.; McClelland, D. J.; Wolf, P.; Dumesic, J. A.; Huber, G. W.; Hermans, I. Production of 1,6-Hexanediol from Tetrahydropyran-2-Methanol by Dehydration–hydration and Hydrogenation. *Green Chem.* **2017**, *19* (5), 1390–1398.

38. Barnett, K. J.; Brentzel, Z. J.; Dumesic, J. A.; Huber, G. W. Hydration of Highly Reactive Vinyl Cyclic Ethers over Solid-Acid Catalysts for the Production of α,ω-Diols. *Prep.* **2018**.

39. Huang, Z.; Barnett, K. J.; Chada, J. P.; Brentzel, Z. J.; Xu, Z.; Dumesic, J. A.; Huber, G. W. Hydrogenation of γ-Butyrolactone to 1,4-Butanediol over CuCo/TiO $_2$ Bimetallic Catalysts. *ACS Catal.* **2017**, 8429–8440.

40. Barnett, K. J.; McClelland, D. J.; Huber, G. W. Autocatalytic Hydration of Dihydropyran to 1,5-Pentanediol Precursors via in Situ Formation of Liquid- and Solid-Phase Acids. *ACS Sustain. Chem. Eng.* **2017**, *5* (11), 10223–10230.

41. Li, X.; Lan, X.; Wang, T. Highly Selective Catalytic Conversion of Furfural to γ-Butyrolactone. *Green Chem.* **2016**, *18* (3), 638–642.

42. Alonso-Fagúndez, N.; Granados, M. L.; Mariscal, R.; Ojeda, M. Selective Conversion of Furfural to Maleic Anhydride and Furan with VO x/Al2O3 Catalysts. *ChemSusChem* **2012**, *5* (10), 1984–1990.

Chapter 2. Combining Dehydration, Hydration, and Ring-Opening Tautomerization/Hydrogenation Reactions for 1,5-Pentanediol Production from Furfural

2.1 Introduction

The low cost of petroleum and large capacity of petroleum refineries, combined with challenges in implementing technologies at scale, have made it difficult to commercialize technologies to produce liquid transportation fuels from lignocellulosic biomass. [1–4] An alternative, economically viable approach, that could help transition society to a more sustainable society, is to synthesize high volume commodity chemicals from biomass.[5,6] C3-C6 α,ω-diols are a class of high value, high volume (with a α,ω-diols global production of 2.3 million tons/year) oxygenated commodity chemicals that have found a variety of applications in the production of polyurethanes, coatings, acrylates, adhesives, polyesters, and plasticizers.[7-9] α,ω-diols are expensive to produce from petroleum-derived feedstocks, because they involve a complex number of separations, selective oxidations, and reductions. 1,5-pentanediol (1,5-PD) is more challenging to produce than the other α,ω-diols, because C5 petroleum feedstocks are not available on a large scale. In contrast, C5 feedstocks, such as xylose and furfural, are produced at the industrial scale from biomass. However, current approaches for the production of 1,5-PD from furfural are expensive due to high catalyst costs and low catalytic activity.[10–12] Here we report a new approach for the production of 1,5-PD from furfural-derived tetrahydrofurfuryl alcohol (THFA) that has 2 times lower capital cost and 7 times lower operating cost (not including feedstock cost)

The content of this chapter is largely adapted from the following reference, Copyright (2017), reproduced by permission of John Wiley and Sons:

Zachary J. Brentzel, Kevin J. Barnett, Kefeng Huang, Christos T. Maravelias, James A. Dumesic, George W. Huber. Chemicals from biomass: combining ring-opening tautomerization and hydrogenation reactions to produce 1,5-pentanediol from furfural. *ChemSusChem*. **2017**. *10*, 1351-1355.

* ZJB and KJB performed experiments. KH performed technoeconomic simulations. *

than current approaches to make 1,5-PD from THFA. Although this process has more reaction steps than the traditional direct hydrogenolysis of THFA, technoeconomic analyses demonstrate that this process is the economically preferred route for the synthesis of biorenewable 1,5-PD. 2-hydroxytetrahydropyran (2-HTHP) is the key reaction intermediate in our approach, and we show that the enhanced reactivity of this intermediate is a result of the ring-opening tautomerization to 5-hydoxyvaleraldehyde (5HVal) and subsequent hydrogenation to 1,5-PD.

Furfural is produced on the industrial scale (604 ktons/year) by dehydration of the hemicellulose portion of biomass and has a projected annual growth rate of 4.3%.[13,14] Furfural is hydrogenated into a variety of products, including THFA using Cu- or Ni-based catalysts.[15–17] Research on the synthesis of 1,5-PD from THFA has focused on the direct hydrogenolysis of THFA (Fig. 1A).[10-12,18–21] The most active and selective catalysts are comprised of Rh doped with an oxophilic promoter, such as Re or Mo. The acidity of the oxophilic promoter assists with the stabilization of the ring-opened oxocarbenium ion intermediates, producing high selectivity (97%) to 1,5-PD from THFA at 120˚C.[10,21] The drawback of this direct hydrogenolysis approach is low catalytic activity and high catalyst cost.

2.2 Experimental Methods

2.2.1 Catalyst Synthesis

The γ-Al_2O_3 (Strem, low soda) dehydration catalyst was crushed and sieved below 100 mesh. The catalyst was pretreated in flowing He (Airgas, industrial grade) at 400˚C for 1 hour prior to the reaction.

The zirconium phosphate (ZrP) catalyst used for dehydration of xylose to furfural was prepared by precipitation of $ZrCl_2O$-$8H_2O$ (Sigma Aldrich, 1 M, 70 mL) and $NH_4H_2PO_4$ (Sigma Aldrich, 1 M, 140 mL) at a molar ratio of P/Zr = 2. The solution was stirred and then filtered,

washed with deionized (DI) water and dried overnight at 100˚C. The catalyst was calcined at 450˚C for 4 h (5˚C/min ramp) in static air prior to reaction.

The Pd/Carbon and Ru/Carbon catalysts were purchased from Sigma-Aldrich. The 5 wt% Pd/C catalyst was not pre-reduced prior to aqueous-phase furfural hydrogenation. The 5 wt% Ru/C catalyst was re-reduced in hydrogen (Airgas, industrial grade) at 300˚C prior to use.

The 1 wt% Ru/TiO_2 catalyst used in hydrogenation reactions was synthesized by incipient wetness impregnation. The TiO_2 (Aldrich, > 99.5%) was calcined in air (Airgas, industrial grade) for 12 hours at 750˚C, with a 4˚C/min ramp, to change the phase to rutile. Ruthenium nitrosyl nitrate (Aldrich) was mixed with deionized water to give the proper concentration of Ru. The Ru was added to TiO_2 in three separate additions. Between each addition, the catalyst was dried in static air at 110˚C for 10 hours. The Ru salt solution was added dropwise and mixed with TiO_2 until the color was homogeneous. After the final addition, the catalyst was reduced in flowing hydrogen (Airgas, industrial grade) for 2 hours at 300˚C, with a 1˚C/min ramp. The catalyst was passivated at room temperature for 1 hour in a 5% air (Airgas, industrial grade) and 95% He (Airgas, 99.999%) mixture.

2.2.2 THFA Dehydration

The dehydration studies were performed in a fixed bed catalytic reactor in an up-flow configuration at 375˚C and 1 atm with a γ-Al_2O_3 (Strem, low soda) catalyst. The catalyst was loaded into a ¼" OD stainless steel tube and secured in place by alternating layers of quartz wool (Grace) and granular silicon dioxide (Sigma, 99.9%, 4-20 mesh). The silicon dioxide was used to decrease void volume and increase heat transfer. The quartz wool layers served as a buffer between the catalyst and silicon dioxide layers. The tube was secured in a furnace comprised of aluminum blocks, heating tape (Briskheat, 135W), and insulation. The vapor phase reactor

effluent was passed through an ice bath condenser. Liquid samples were collected from the condensed effluent every 2 to 8 hours. The vapor phase was sampled via online gas chromatography (Shimadzu GC2010 equipped with a flame ionization detector (FID) and a RT-Q-Bond column). Liquid samples were analyzed by gas chromatography (Shimadzu GC2010 equipped with a flame ionization detector (FID) and a DB-5MS capillary column).

The γ-Al_2O_3 catalyst was pretreated in flowing He (Airgas, industrial grade) at 400˚C for 1 hour prior to the reaction. The reactor was then cooled to a reaction temperature of 375˚C. The flowing He was then used as a sweep gas at the effluent of the reactor. Neat tetrahydrofurfuryl alcohol (Aldrich, 99%) was pumped into the reactor with an HPLC pump (Lab Alliance Series I).

2.2.3 ^{13}C THFA Dehydration Studies

D-xylose labelled with carbon-13 (^{13}C) at the 1-position (Omicron Biochemicals) was added to DI water up to 0.5 wt%. The aqueous xylose solution (25mL) was loaded into to a 45mL stainless steel autoclave (Parr systems) equipped with a magnetic stir bar. The xylose dehydration reaction was performed at over 140 mg ZrP catalyst at 160˚C and 1 atm Ar atmosphere (5 hr reaction time, 750 rpm). The resulting aqueous furfural product then underwent liquid-phase hydrogenation to THFA over 100 mg Pd/C catalyst at 100˚C and 55.2 bar H_2 atmosphere (5 hr reaction time, 750 rpm). The aqueous THFA product mixture was then subjected to vapor-phase dehydration over a γ-Al_2O_3 catalyst following the same experimental conditions stated above for the non-^{13}C-labelled THFA dehydration studies.

2.2.4 Dihydropyran Hydration

Dihydropyran (Aldrich, 97%) was used as purchased. A feed of 20 wt% DHP and 80 wt% deionized (DI) water was added to a stainless steel autoclave (Parr Instruments) with a magnetic stir bar. The autoclave was purged 3 times with He (Airgas, industrial grade) and pressurized to

35.5 bar He. The biphasic mixture was stirred at 800 rpm. The autoclave was heated to the desired temperatures and held for the set period of time before being cooled. The monophasic product mixture was sampled and analyzed by gas chromatography (Shimadzu GC2010 equipped with a flame ionization detector (FID) and an RTX-VMS column).

2.2.5 2-HTHP and Butanal Reaction Kinetics Studies

The 1% Ru/TiO_2 catalyst was pre-reduced for 2 hours at 300˚C, with a 1˚C/min ramp, in a Schlenk tube prior to experiments. The Schlenk tube was transferred to an inert glovebox (Vacuum Atmospheres Company , Genesis model) where the catalyst was stored. Prior to experiments, the catalyst was loaded into Hastelloy autoclaves (Parr Instrument, Multi Reactor System 5000). The autoclaves were seated in their housing and filled with 10 bar of H_2 (Airgas, industrial grade). 2-hydroxytetrahydropyran (Acros organics, 90%) and butanal (Aldrich, > 99.5%) feeds in deionized water (Millipore Milli-Q grade, 18 MΩ) or tetrahydrofuran (Sigma-Aldrich, 99.9%, anhydrous with 250 ppm BHT) were prepared and pumped into each autoclave. The feeds were pumped into their respective autoclaves and stirred with magnetic stir bars at 500 rpm. The autoclaves were then purged three times with H_2 and pressurized to 20 bar. The autoclaves were heated to 110˚C (6˚C/min). The autoclaves were held at 110˚C for 2 to 3 hours. After cooling, the samples were analyzed by both gas chromatography (Shimadzu GC2010 equipped with a flame ionization detector (FID) and a RTX-VMS column) and high-performance liquid chromatography (HPLC) (Waters Alliance 2695 system equipped with a Waters 410 differential refractometer and Aminex HPX-87H ion exchange column) using a 5 mM H_2SO_4 mobile phase.

2.2.6 Ru Continuous Flow Studies

The hydrogenation studies were performed in a fixed bed catalytic reactor in an up-flow configuration at 45 bar and 70 to 120˚C with Ru/TiO_2 or Ru/C. The catalyst was loaded into a ¼”

OD stainless steel tube and secured in place by alternating layers of quartz wool (Grace) and granular silicon dioxide (Sigma, 99.9%, 4-20 mesh). The silicon dioxide was used to decrease void volume and increase heat transfer. The quartz wool layers served as a buffer between the catalyst and silicon dioxide layers. The tube was secured in a furnace comprised of aluminum blocks, heating tape (Briskheat, 135W), and insulation. The reactor effluent was passed through an ice bath condenser. Liquid samples were collected from the condensed effluent every 2 to 24 hours. Liquid samples were analyzed by both gas chromatography (Shimadzu GC2010 equipped with a flame ionization detector (FID) and an RTX-VMS column) and high-performance liquid chromatography (HPLC) (Waters Alliance 2695 system equipped with a Waters 410 differential refractometer and Aminex HPX-87H ion exchange column) using a 5 mM H_2SO_4 mobile phase.

2.2.7 ^{13}C THFA Dehydration NMR

The ^{13}C THFA dehydration samples were characterized by ^{13}C NMR. D_2O was added to the sample (1:9 v/v). The ^{13}C NMR experiments were acquired on a Bruker Biospin (Billerica, MA) AVANCE III 500 MHz spectrometer fitted with a DCH (^{13}C-optimized) cryoprobe. Bruker standard pulse sequence 'zgig30' was used for the ^{13}C experiments with the following parameters: an inter-scan relaxation delay of 15 s, a sweep width of 240 ppm centered at 110 ppm, acquiring 59,520 data points with an acquisition time of 1 s, and 128 scans. Mestrelab Research's MestReNova software was used to process the spectra.

2.2.8 Variable Temperature NMR

2-hydroxytetrahydropyran (Acros organics, 90%) solutions (1 molar) were prepared in either D_2O (Sigma-Aldrich, 99.9 atomic % deuterium) or tetrahydrofuran (Sigma-Aldrich, 99.5 atomic % deuterium). A 0.7 M solution of butanal (Aldrich, > 99.5%) in D_2O (Sigma-Aldrich,

99.9 atomic % deuterium) was prepared. One half a gram of each solution was added to an NMR tube (Wilmad, 5 mm borosilicate glass).

Liquid ^{1}H and ^{13}C variable temperature NMR experiments were performed on a Bruker Avance-III 500 MHz spectrometer with a broadband fluorine observe (BBFO) probe. Variable temperature experiments were performed from 20 to 80˚C in D_2O and 20 to 50˚C in THF. The ^{2}H signals from the solvents were used as the field-frequency lock. The magnetic field shimming was performed on the ^{2}H solvent signals. ^{1}H and ^{13}C chemical shifts were referenced against solvent peaks. Prior to each experiment, the sample was equilibrated at the spectrometer set point temperature for a minimum of 30 minutes. ^{1}H experiments were performed with a standard 1D pulse sequence. ^{13}C experiments were performed with an inverse-gated decoupling pulse sequence.

2.2.9 ATR-FTIR

In situ attenuated total reflectance Fourier transform infrared (ATR-FTIR) spectroscopy experiments were performed with a Hastelloy autoclave (Parr Instruments, modified from Model 4590). The spectra were obtained by using a Mettler-Toledo AutoChem ReactIR iC10 spectrometer equipped with a photoconductive detector (MCT type). The 9.5 mm AgX DiComp Diamond ATR probe is inserted into the bottom of the autoclave to sample the liquid phase. The solvent background was used as a reference for each sample. Spectra were collected every minute with a 256 scan average and 4 cm^{-1} resolution.

The 1% Ru/TiO_2 catalyst was pre-reduced for 2 hours at 300˚C, with a 1˚C/min ramp, in a Schlenk tube prior to experiments. The catalyst was loaded into the autoclave in an inert glovebag filled with Ar (Airgas, 99.999%). After being sealed, the autoclave was seated in its housing, purged 3 times with 20 bar of H_2 (Airgas, industrial grade), and pressurized to 20 bar H_2. The

1950 mM feed of 2-hydroxytetrahydropyran (Acros organics, 90%) in either deionized water (Millipore Milli-Q grade, 18 MΩ) or tetrahydrofuran (Sigma-Aldrich, 99.9%, anhydrous with 250 ppm BHT) was pumped into the autoclave. The autoclave was stirred at 500 rpm by an overhead impellor. The autoclave was heated to and held at 110˚C (2˚C/min ramp). The step change from 20 to 0 bar H_2 was performed by depressurizing the reactor to 7 bar and repressurizing to 20 bar with Ar (Airgas, industrial grade) ten times.

2.3 Results and Discussion

2.3.1 Experimental Results

The new pathway we report here is outlined in Figure 2.1. Furfural is first hydrogenated to THFA which is then dehydrated in the gas phase (neat at 375˚C, 1 atm, and a WHSV of 9 hr^{-1}) to produce DHP in 87% yield. The DHP is then hydrated to 2-HTHP and 10-carbon dimers in yields up to 100% in the aqueous phase (20 wt% DHP in water) without a catalyst at temperatures from 70 to 130˚C. 2-HTHP is a cyclic hemiacetal that undergoes ring-opening tautomerization in the aqueous phase to form 5HVal.[22,23] The hydrogenation of 5HVal in the presence of the 2-HTHP monomers and dimers using a Ru catalyst results in 97% overall yield of 1,5-PD from DHP. This route will subsequently be referred to as the dehydration, hydration, and hydrogenation (DHH) pathway.

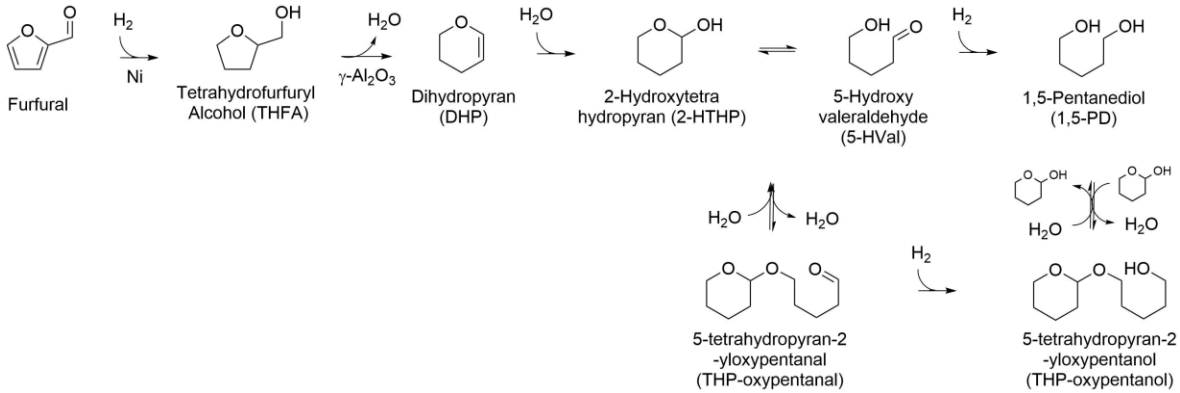

Figure 2.1 Dehydration-Hydration-Hydrogenation (DHH) pathway from furfural to 1,5-PD.

The results of this paper for the gas phase dehydration of THFA to DHP are consistent with the work of Geller et al. and Yamada et al. who used an activated alumina catalyst.[24,25] The high yields for the dehydration reaction are unique to the 5-membered ring, THFA (see Chapter 3 for full discussion on C5 vs. C6 ring dehydration thermodynamics). DHP is likely formed via acid-catalyzed dehydration of the THFA primary hydroxyl group,[26] followed by simultaneous ring-opening and Wagner-Meerwein rearrangement to the 6-membered ring DHP product.[27,28] Possible reaction mechanisms are shown in Figure 2.2.

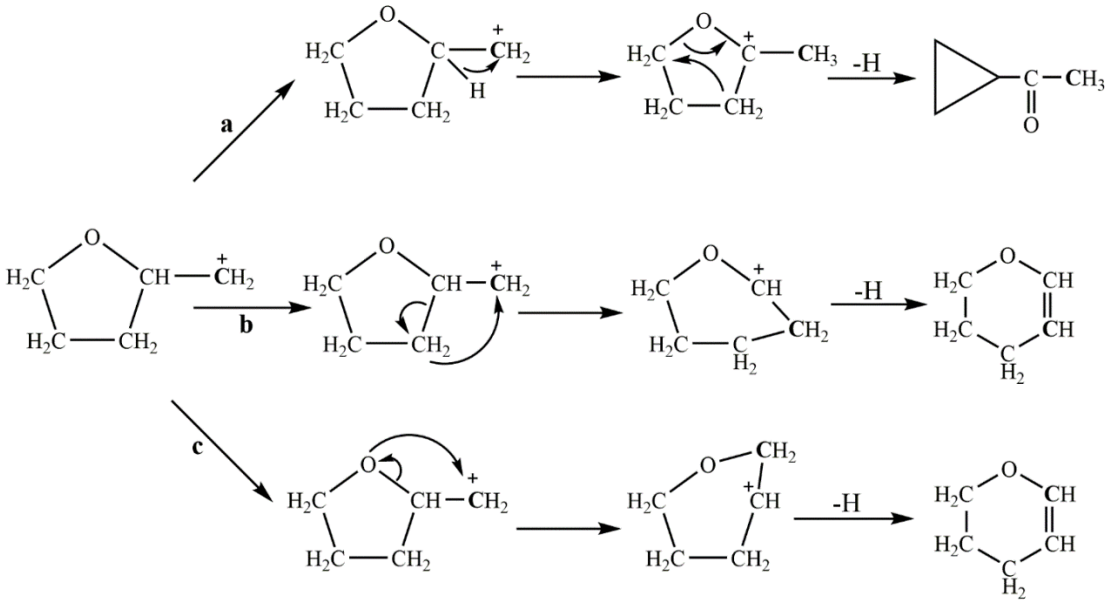

Figure 2.2 Scheme of possible reaction pathways for dehydration of THFA to DHP.

In order to probe the THFA dehydration mechanism, D-xylose labelled with carbon-13 (^{13}C) at the 1-position was first subjected to aqueous-phase dehydration to furfural over a ZrP catalyst at 160˚C and 1 atmosphere of Argon. The resulting aqueous furfural product then underwent liquid-phase hydrogenation to THFA over a Pd/C catalyst at 100˚C and 55.2 bar hydrogen atmosphere. As the anomeric carbon of the xylose is known to transform into the aldehyde carbon in furfural,[29] following hydrogenation of furfural the ^{13}C position is located alpha

to the alcohol group of THFA (see Figure 2.2). Gas phase dehydration over γ-Al_2O_3 was performed on the ^{13}C THFA, with the ^{13}C NMR spectrum of the resulting aqueous DHP mixture. By comparing the product mixture (Figure 2.3B) to a DHP standard (Figure 2.3A), we show that the ^{13}C labelled carbon is located at the 2 and 6 positions of DHP. The ^{13}C located at the α-position to the cyclic ether oxygen atom is proof that the THFA undergoes pathway c in Figure 2.3.2, in which a Wagner-Meerwein rearrangement occurs via the nucleophilic attack of the methyl carbon by the oxygen atom. This is in corroboration with the findings of Gensler et. al.,[27] but is the first study to conclusively show the reaction mechanism using quantitative ^{13}C NMR spectroscopy. The fact that we see the ^{13}C labelled position at both the 2 and 6 positions at a roughly 50:50 molar ratio suggests that there is either rapid isomerization of the double bond or hydride transfer through an intermediate species. Gensler et. al. was able to show that double bond isomerization does not occur at these conditions and that hydride transfer through the surface of γ-Al_2O_3 is responsible for the distribution of the ^{13}C at the 2 and 6 positions.[28,30]

Gas phase continuous flow studies were conducted to determine the stability of the γ-Al_2O_3 catalyst versus time on stream for the dehydration of THFA to DHP (Figure 2.4). The fresh γ-Al_2O_3 catalyst had a first order deactivation rate constant of 0.026 hr^{-1}. Coking was the primary mode of deactivation, and the catalyst was thus regenerated by a calcination treatment at 400˚C for 3 hours in air. After calcination, the catalyst regained its initial activity but deactivated more rapidly, with a first order deactivation rate constant of 0.039 hr^{-1}. The low cost of alumina allows for replacement of the catalyst every 24 hours without the need for regeneration, as we have demonstrated in more detail in our technoeconomic analyses.

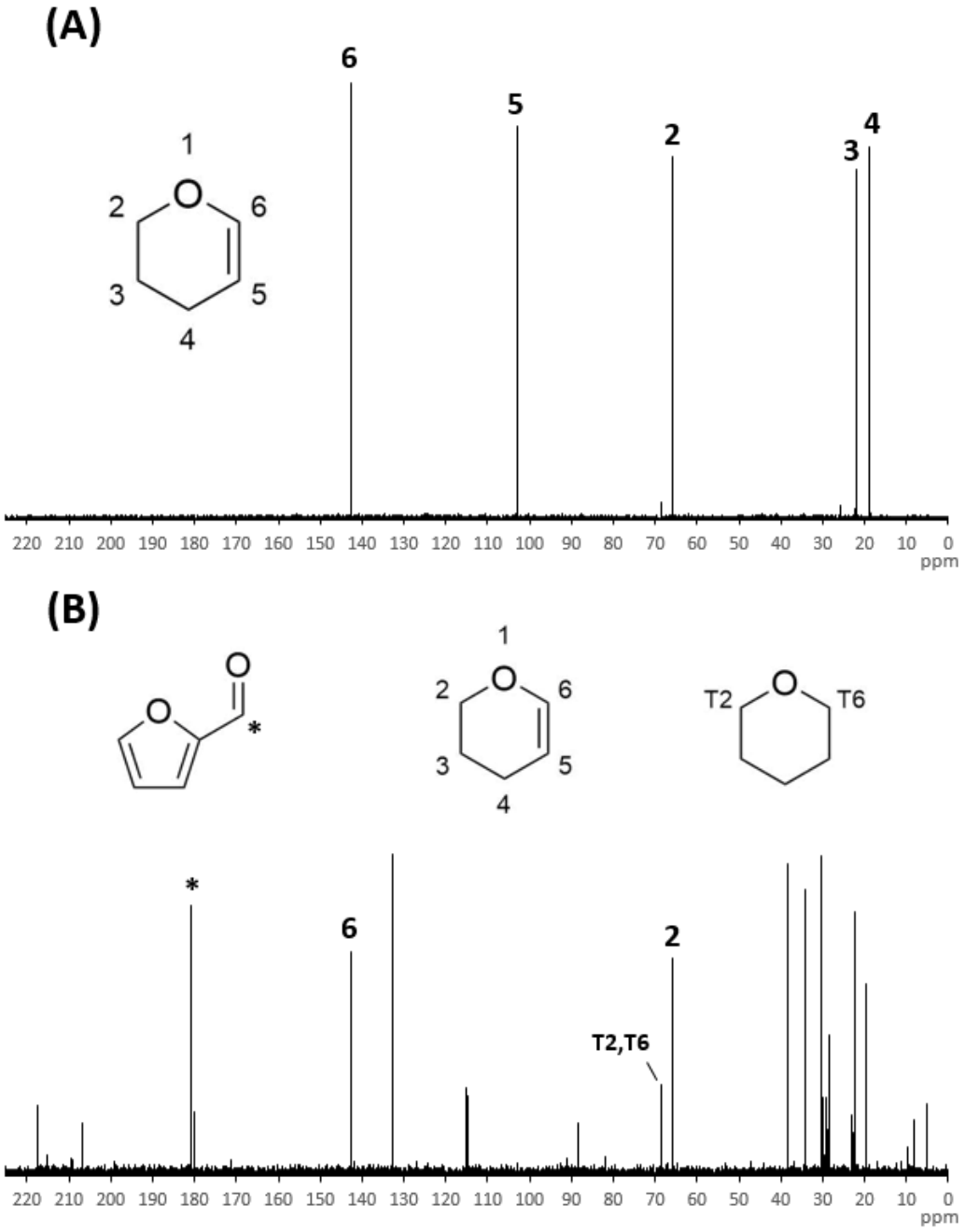

Figure 2.3 ^{13}C NMR spectrum of A) DHP standard and B) product solution of ^{13}C THFA dehydration experiment with furfural, DHP, and THP identified using standards. Reaction conditions: Catalyst: γ-Al_2O_3, Catalyst mass: 150mg, T: 375˚C, P: 1 atm, Feed Flowrate: 0.04mL/min

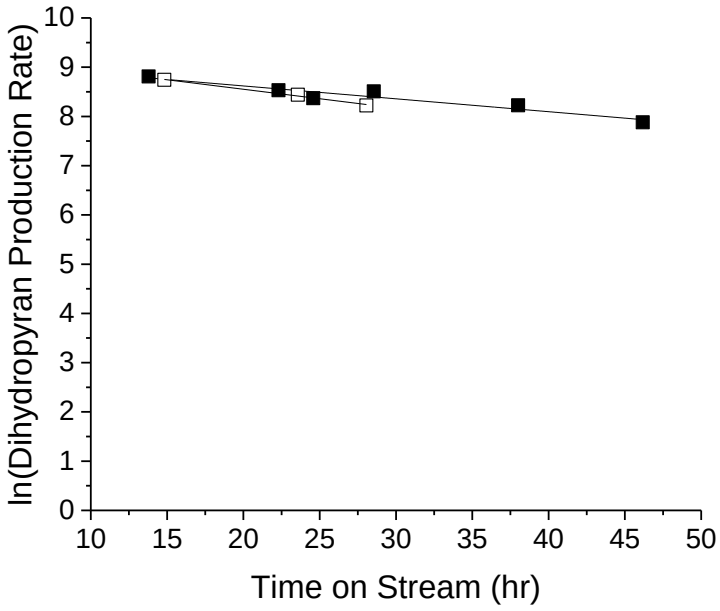

Figure 2.4 Stability versus time on stream for dehydration of THFA with γ-Al_2O_3. The reaction conditions were 375˚C, 1 atm, and a WHSV of 127 hr^{-1}. The DHP production rate has units of $\mu mol\ min^{-1}\ g_{catalyst}^{-1}$. The fresh catalyst was pretreated in flowing He at 400˚C for 1 hour (■). The catalyst was regenerated by calcination in air at 400˚C for 3 hours (□).

DHP can be hydrated in water at temperatures from 70 to 160˚C. Yields of 2-HTHP ranged from 90-92% at temperatures of 100 and 130˚C in one hour of reaction time (Table 2.1). Two dimer products were also detected, 2-tetrahydropyranyl ether (2,2'-HTHP) and 5-tetrahydropyran-2-yloxypentanal (THP-oxypentanal), as portrayed in Figure 2.1. These dimers are also precursors to 1,5-PD since they can undergo reversible hydrolysis back to monomers at the reaction conditions.[31] Thus, the yield of 1,5-PD precursors (2-HTHP and etherified dimers) is approximately 100%. Similar yields can be obtained at 70˚C with longer residence times (e.g., 12 h). At elevated temperature, 160˚C, conversion of DHP resulted in the formation of solid polymers in the reactor and lower yields to 2-HTHP and upgradable dimers (~71%). More detailed information on the DHP hydration step is provided in Chapters 4 and 5.

Table 2.1 Hydration of DHP at varying temperatures and reaction times

Temp. (˚C)	Reaction Time (h)	2-HTHP Yield[a]	THP-oxypentanal Yield[a]	2-Tetrahydropyranyl Ether Yield[a]	Overall Yield[a]	Aqueous-Phase Carbon Balance[b]
70	4	84.5%	5.3%	1.9%	91.7%	90.8%
70	12	92.7%	5.5%	1.8%	100.0%	99.3%
100	1	91.5%	6.7%	1.2%	99.4%	98.7%
100	2	89.9%	7.3%	1.9%	99.1%	100.0%
100	4	92.0%	6.6%	1.2%	99.8%	96.7%
130	1	90.3%	6.3%	1.4%	97.9%	95.1%
130	2	91.4%	7.3%	1.3%	100.0%	100.0%
130	4	89.5%	6.4%	1.0%	96.9%	99.5%
160	4	65.4%	4.2%	1.3%	70.9%	94.5%

[a] Carbon yield quantified by gas chromatogram
[b] Quantified by total-organic carbon (TOC) analyzer

The rate of 1,5-PD production from 2-HTHP with a Rh-Re/Carbon catalyst is 80 times faster than the rate from THFA over the same catalyst. This high reactivity of 2-HTHP is related to its ring-opening tautomerization to 5HVal, as shown by ^{13}C variable temperature NMR experiments (Figure 2.5), because the rate of hydrogenation of an aldehyde group is typically higher than the rate of hydrogenolysis of a cyclic ether linkage.[12,32] The ring-opening tautomerization is an endothermic reaction; therefore, the equilibrium composition of 5HVal increases with temperature (from 2.4% at 24˚C to 19.2 % at 80˚C), as shown in Figure 2.5. At the hydrogenation temperatures of 110 and 120˚C used in this study, the equilibrium concentrations of 5HVal are 47 and 58%, respectively.

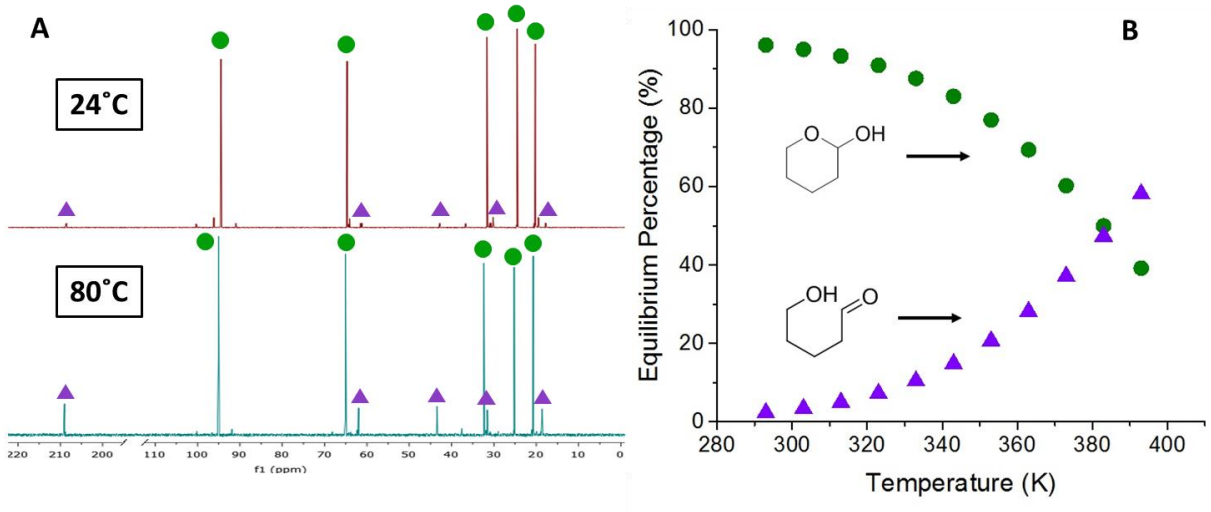

Figure 2.5 (A) Quantitative 13C NMR spectra of 10 wt% 2-hydroxytetrahydropyran (2-HTHP) in D2O at 24 and 80˚C. (B) Equilibrium percentage of 2-HTHP and 5-hydroxyvaleraldehyde (5HVal) from 24 to 80˚C based on quantitative 13C variable temperature NMR results in Figure 2.5A. (Adapted from ref. 33 with permission of the Royal Society of Chemistry)[33].

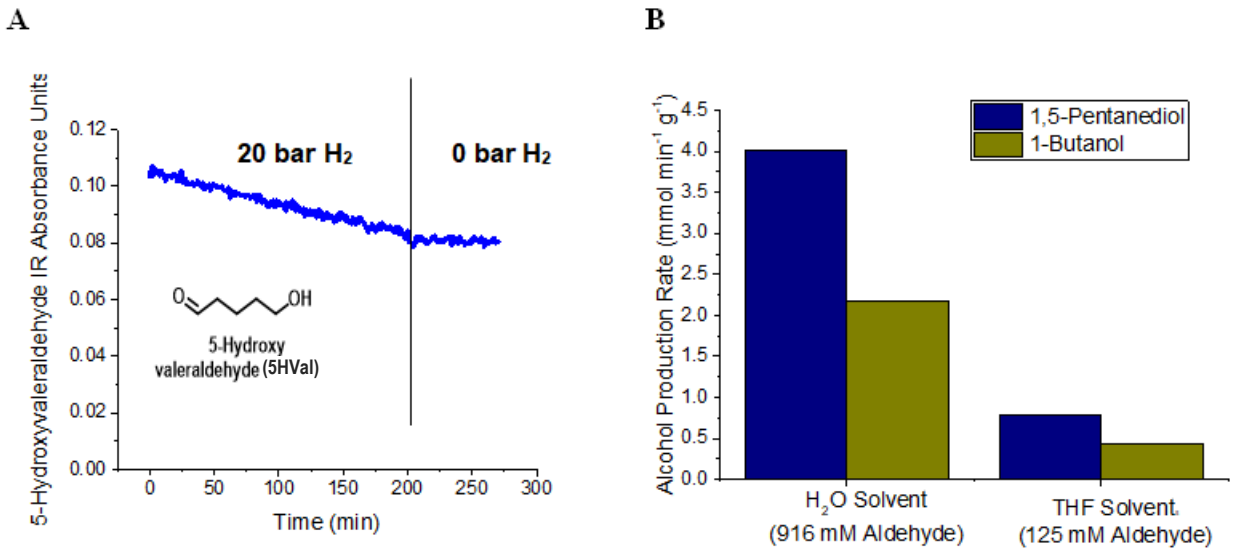

Figure 2.6 Results from *in situ* infrared spectroscopy and reactivity experiments. (A) 5-Hydroxyvaleraldehyde (5HVal) carbonyl absorbance from *in situ* ATR-FTIR spectroscopy of the ring-opening tautomerization and hydrogenation of 20 wt% 2-hydroxytetratropyran (2-HTHP) in water using 1 wt % Ru/TiO_2 at 110˚C and 20 bar H_2. (**B**) Comparison of the alcohol production rates over 1 wt % Ru/TiO_2 at 110˚C and 20 bar H_2.

Further experiments were performed to confirm that the reaction mechanism is a ring-opening and subsequent hydrogenation rather than direct hydrogenolysis of 2-HTHP. Butanal hydrogenation was used as a probe reaction to compare with respect to the rate of ring-opening and hydrogenation of 2-HTHP. Butanal concentrations were chosen based on the calculated 5HVal concentrations determined from ^{13}C variable temperature NMR of 2-HTHP in H_2O and THF solvents. In each solvent system, the rate of butanol production was proportional to the rate of 1,5-PD production (Figure 2.6B), indicating that the rate of production of 1,5-PD is proportional to the concentration of aldehyde present in solution. Under the same reaction conditions, Ru/TiO_2 was not active for the hydrogenolysis of a probe acetal molecule, 2-methoxytetrahydropyran, in a THF solvent. In water, however, the acetal was hydrolyzed to 2-HTHP and methanol, leading to high activity for production of 1,5-PD. Accordingly, results from variable temperature NMR, ATR-FTIR, and reaction kinetics measurements in different solvents demonstrate that the high reactivity of 2-HTHP compared to THFA is caused by ring-opening tautomerization of 2-HTHP followed by hydrogenation of the aldehyde intermediate, which is faster than hydrogenolysis of the α-alcohol ether linkage in THFA.

The conversion of 2-HTHP over the Ru/TiO_2 catalyst was studied at various weight hourly space velocities (WHSV) in a continuous flow reactor to determine product selectivities as a function of conversion. The selectivity for production of 1,5-PD from 2-HTHP is 96.5% from 1,5-PD precursors at full conversion and decreases as the conversion decreases (Figure 2.7). The lower 1,5-PD selectivity at high WHSVs is offset by an increase in the extent of dimer formation, most notably THP-oxypentanal and 5-tetrahydropyran-2-yloxypentanol (THP-oxypentanol). THP-oxypentanal is formed from the etherification of 5HVal and 2-HTHP. THP-oxypentanol is the hydrogenation product of THP-oxypentanal. These data suggest that the feed monomers undergo

parallel reactions: i) hydrogenation to 1,5-PD and ii) etherification to THP-oxypentanal and 2,2'-HTHP. The hydrolysis of these dimers results in 1,5-PD formation and is responsible for the high 1,5-PD yields at low space velocities.

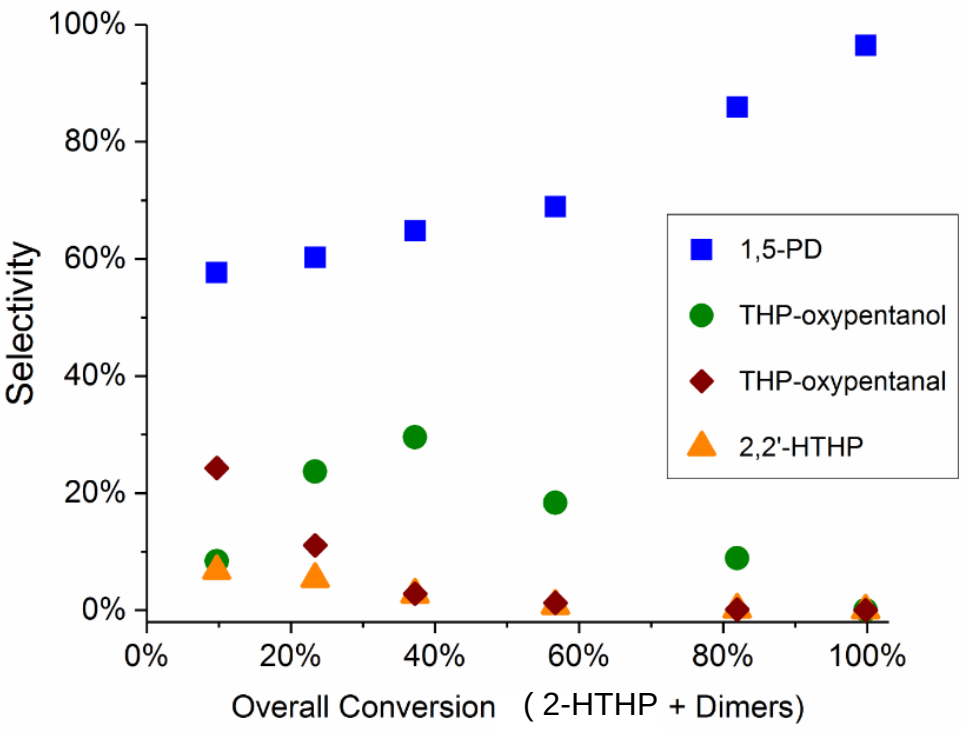

Figure 2.7 Selectivity to 1,5-pentanediol (1,5-PD) and dimers from 2-hydroxytetrahydropyran (2-HTHP) at varying weight hourly space velocities. The following plot displays the selectivities to 1,5-PD (□), THP-oxypentanal (△), THP-oxypentanol (○), and 2-tetrahydropyranyl ether (2,2'-HTHP) (◇) over 1%Ru/TiO_2 in a continuous flow reactor (40 mg Ru-TiO_2 diluted 10x in silica gel, T = 120˚C, P = 45 bar H_2, H_2 Flowrate = 40 mL/min). (Adapted from ref. 33 with permission from the Royal Society of Chemistry)[33]

The stabilities with respect to time on stream of Ru/TiO_2 and Ru/C catalysts were studied for the conversion of 2-HTHP in continuous flow reactors (Figure 2.8). These reaction kinetics studies were performed using 2-HTHP feeds formed from DHP hydration at high feed concentrations (> 20 wt%). At both 70 and 120˚C, the Ru/TiO_2 catalyst displayed more than 50% loss of activity in less than 24 hours. At 70˚C, after an initial 35 hour period of rapid deactivation, the catalyst displayed more gradual deactivation with a first order deactivation constant of 0.0086

hr^{-1}. The Ru/TiO_2 catalyst was not fully regenerable by either re-reduction at 300˚C for 2 hours or calcination at 330˚C for 30 minutes and reduction at 300˚C for 2 hours. The Ru/C catalyst was more stable than the Ru/TiO_2 catalyst, with a deactivation rate constant of 0.0020 hr^{-1} for 500 hours of time on stream. Re-reduction of the Ru/C catalyst at 300˚C for 2 hours regenerated the activity from 38% back to 65% of the initial activity. The deactivation rate constant for the regenerated catalyst was 0.0037 hr^{-1}. Prior studies with glucose hydrogenation over Ru catalysts demonstrated similar findings, i.e., the oxide-supported catalyst, Ru/Al_2O_3, displayed deactivation as a result of support restructuring under hydrothermal conditions,[34] while the carbon-supported catalyst did not deactivate since there were no morphological changes to the support.[35]

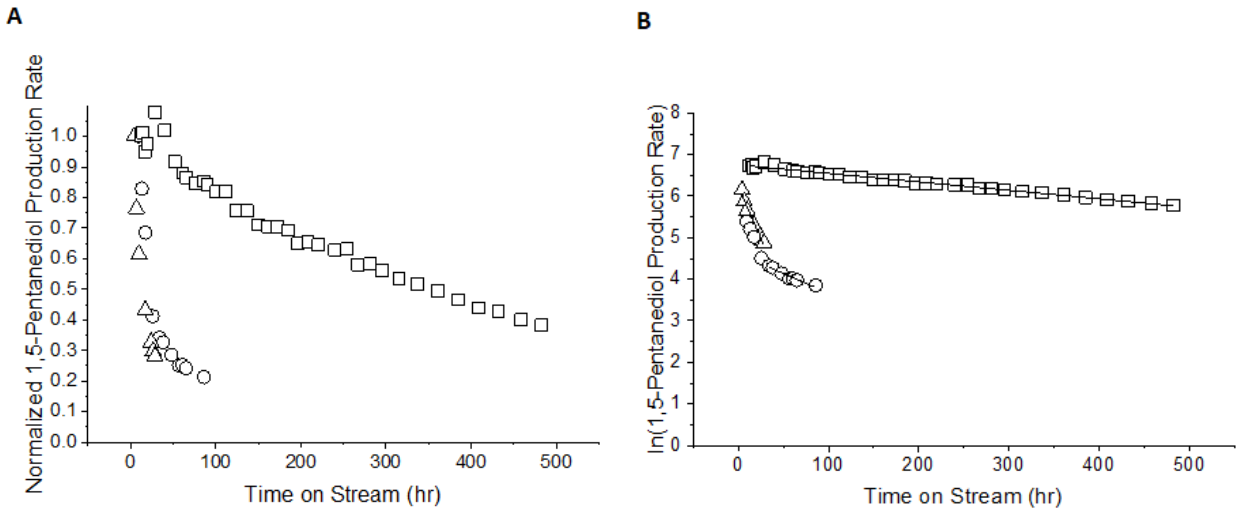

Figure 2.8 Stability versus time on stream of supported Ru catalysts. (A) Normalized 1,5-pentanediol production rates and (B) natural logarithm of the 1,5-pentanediol production rates for 5% Ru/C at 120˚C (□),1% Ru/TiO_2 at 70˚C (○), and 1% Ru/TiO_2 at 120˚C (△). The reaction conditions were 70 or 120˚C, 45 bar H_2, and WHSVs between 8 and 48 hr^{-1}. The 1,5-pentanediol production rate has units of μmol min^{-1} $g_{catalyst}^{-1}$.

2.3.2 Technoeconomic Analysis

Rigorous technoeconomic analyses were carried out using the product yields obtained in the experiments outlined above and using neat THFA as a feedstock. Our technoeconomic analyses of the two approaches for 1,5-PD from THFA follow six steps. Data for 1,5-PD production using the direct hydrogenolysis pathway are taken from the work of Chia et al.[10] Data for the DHH pathway come directly from this report. First, a process flow diagram of the DHH process was developed, as shown in Figure 2.9. The corresponding process models were developed using Aspen Plus Process Simulator (V8.6 Aspen Technology) based on the experimental data (Table 2.2). The 99.0 wt% THFA feed (Stream 1) is first heated to reaction temperature via a preheater (E-1) and then supplied to the dehydration reactor (R-1), in which complete conversion of THFA occurs with 86.8% selectivity to DHP over γ-Al_2O_3 catalyst. The DHP product is then mixed with fresh makeup water (Stream 2) and recycle water (Stream 18) and sent into the hydration reactor (R-2). According to the experimental results, 20.0 wt% DHP in water is subsequently hydrated to 2-HTHP with 98.6% conversion and 96.6% selectivity. The resulting water-rich stream (Stream 4) is sent to the hydrogenation reactor (R-3) for converting 2-HTHP to 1,5-PD in a H_2-rich environment over Ru/C catalyst at 100% conversion and 97.5% selectivity. The reactor product (Stream 6) is then split into a gas stream (Stream 7) and a liquid stream (Stream 8) in a flash drum (S-1). The gas stream is cooled and again split to a gas recycle stream (Stream 9) and a produced water stream in a subsequent flash drum (S-2). A fraction (5.0%) of the recycle gas is purged to mitigate buildup of impurities and to produce process heat and electricity in the boiler/turbogenerator if necessary. The liquid stream (Stream 8) is further split into two flash drums (S-3 and S-4) after expansion via a valve. The vapor fraction (Stream 11) is then cooled to purge the vapor fraction to boiler and liquid fraction to wastewater treatment.

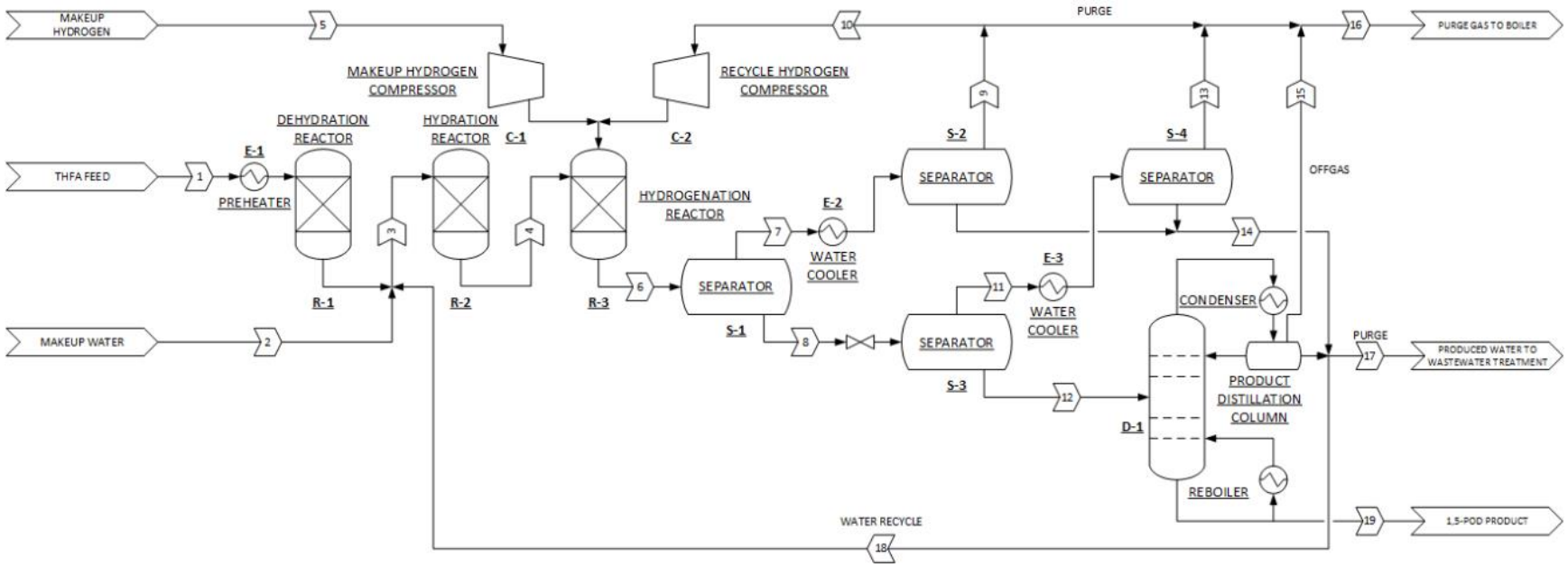

Figure 2.9 Process flow diagram for the Dehydration-Hydration-Hydrogenation (DHH) pathway.

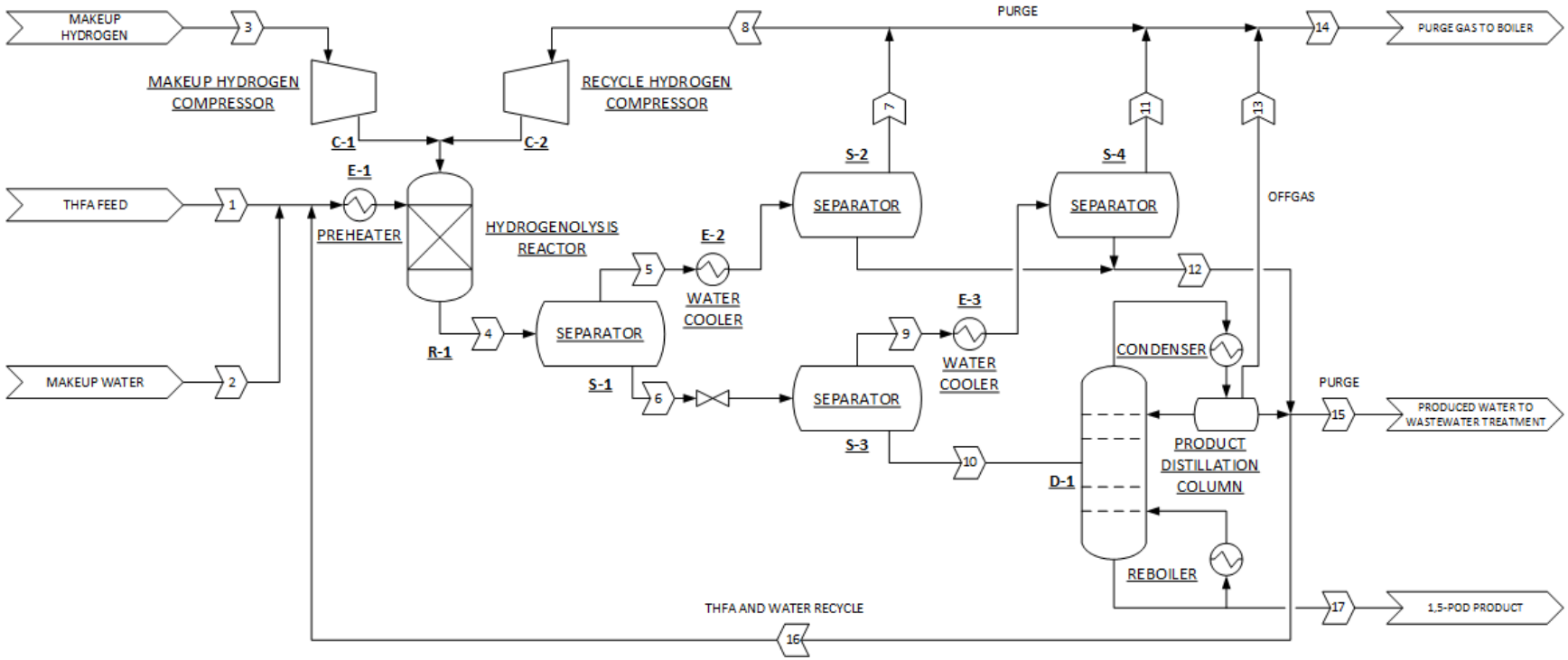

Figure 2.10 Process flow diagram for the direct hydrogenolysis pathway.

The liquid product stream (Stream 12) from Stream 8 forms the feed to the product distillation column (D-1), where a 99.0 wt% 1,5-PD stream is obtained at the bottom with over 99.9% recovery (Stream 19). According to the current process configuration, the top product contains 92.4 wt% water. Therefore, a fraction (90.0%) of the condensed water is split as a recycle to hydration reactor (Stream 18), while the remaining process water is sent to wastewater treatment.

Table 2.2 Process operating data for 1,5-PD production from THFA

Feedstock	*Purity (wt%)*
THFA	99.0
Reactions	*Conversions (%) & selectivity (%)*
THFA to DHP	100 & 86.8
DHP to 2-HTHP	98.6 & 96.6
2-HTHP to 1,5-PD	100 & 97.5
THFA to 1,5-PD [a]	47.2 & 97.2
1,5-PD Recovery	*Recovery (%) & purity (wt%)*
1,5-PD recovery from water-rich stream	99.9& 99.0

a) Taken from the work by Chia et al. [10]

Second, a process flow diagram for the direct hydrogenolysis pathway was developed using data with Rh-ReO_x/C catalyst [10] as shown in Figure 2.10. In this process, the THFA feed (Stream 1) is first diluted to 5.0 wt% by mixing with fresh makeup water (Stream 2) and recycle water containing unreacted THFA (Stream 16). This preheated water-rich stream is then fed to the hydrogenolysis reactor (R-1), in which 47.2% THFA is converted to 1,5-PD and 1-pentanol at a selectivity of 97.2% and 2.8%, respectively. Subsequently the reactor product stream (Stream 4) is passed through a separation and recovery section, which is similar to the aforementioned process in Figure 2.9, to purify and recover 1,5-PD product and recycle H_2, THFA, and water.

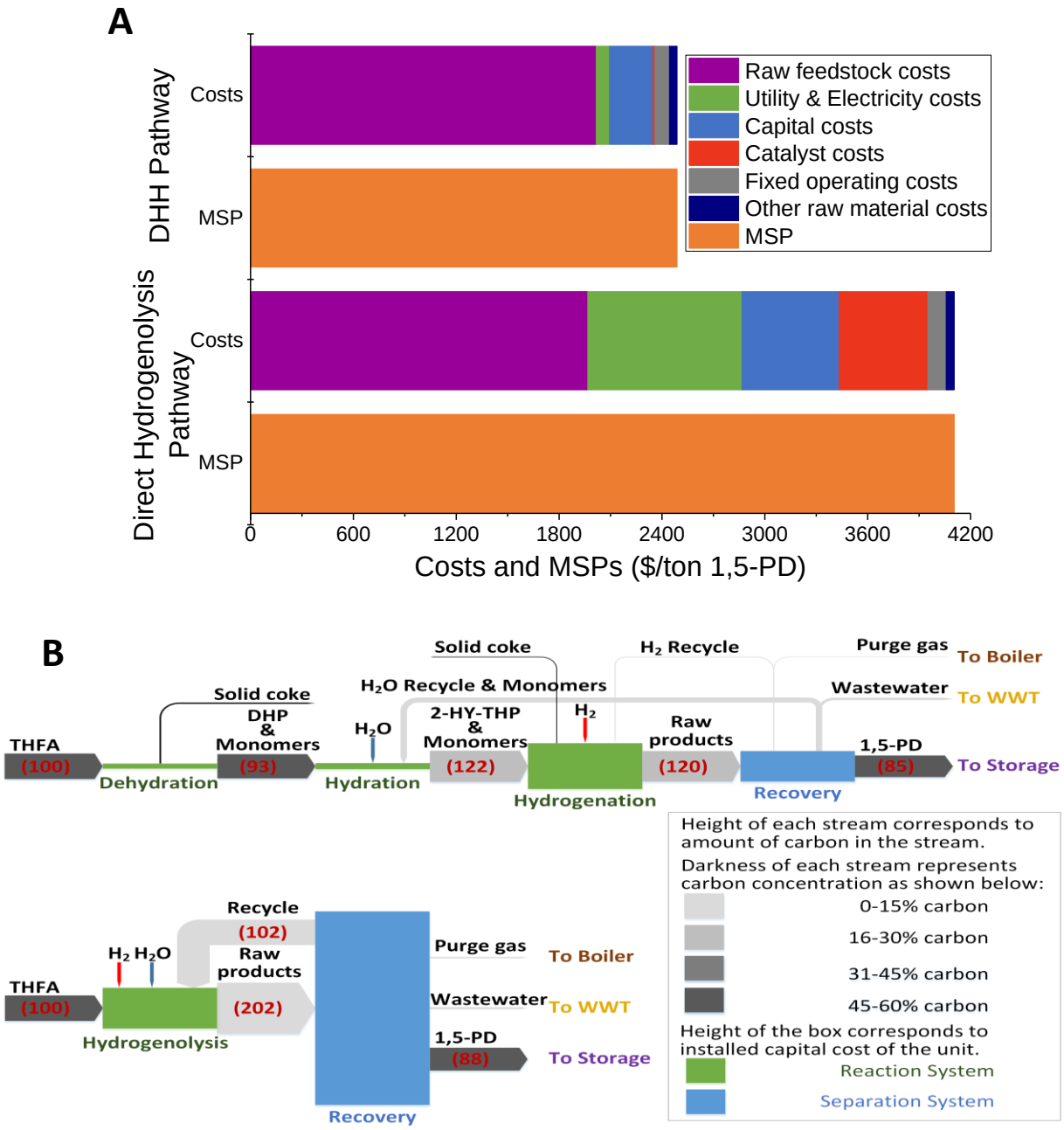

Figure 2.11 Process technoeconomics for the synthesis of 1,5-pentanediol from furfural. (A) Comparison of costs and minimum selling prices (MSPs) for the dehydration, hydration, and hydrogenation (DHH) pathway with the direct hydrogenolysis pathway. (B) Sankey diagram for the i) DHH pathway and ii) direct hydrogenolysis pathway

This technoeconomic model suggests that a pioneer plant applying the DHH pathway from THFA could produce 1,5-PD at a minimum selling price (MSP) of $2,488/ton, versus $4,105/ton for the direct hydrogenolysis pathway (Figure 2.11A). The most substantial savings come from the reduced catalyst cost and lower utility costs. Specifically, with the increase in hydrogenation activity of Ru/C compared to Rh-Re/C and the decrease in metal material costs ($31,000/kg and $1,500/kg for Rh and Ru[36], respectively) there is a 47 times decrease in catalyst cost. The Rh cost accounts for greater than 90% of the total Rh-Re/C catalyst cost. Furthermore, transitioning from a 5 to 20 wt% feed from the direct hydrogenolysis pathway to the DHH pathway decreases the utility costs for the separation and recovery of 1,5-PD product by a factor of 12. Correspondingly, the total 1,5-PD production costs (excluding the cost of the THFA feedstock) decrease from $2,137/ton for the hydrogenolysis route to $473/ton for the DHH route. In addition, the DHH pathway leads to a high overall 1,5-PD yield without requiring large recycle stream used in the hydrogenolysis pathway (Figure 2.11B), which could save over 6 times the installed capital costs on the separation and recovery systems. Using the n^{th} plant cost analysis, the MSP of 1,5-PD for the DHH pathway and the direct hydrogenolysis pathway decreases to $2,292/ton and $3,467/ton, respectively. Furfural prices have fluctuated between $500-$2,000/ton over the past 15 years.[37] An analysis on the sensitivity of the 1,5-PD MSP to the furfural and THFA feedstock costs demonstrates that the MSP of 1,5-PD can range from $1,500-$3,000 (Figure 2.12). This price is lower than the price of 1,6-hexanediol and within the same price range of 1,4-butanediol, the two largest α,ω-diols (with the exception of ethylene glycol) that are used commercially today. The technoeconomic analyses suggest that our approach can produce infrastructure compatible renewable high volume oxygenated commodity chemicals that in an economically viable way.

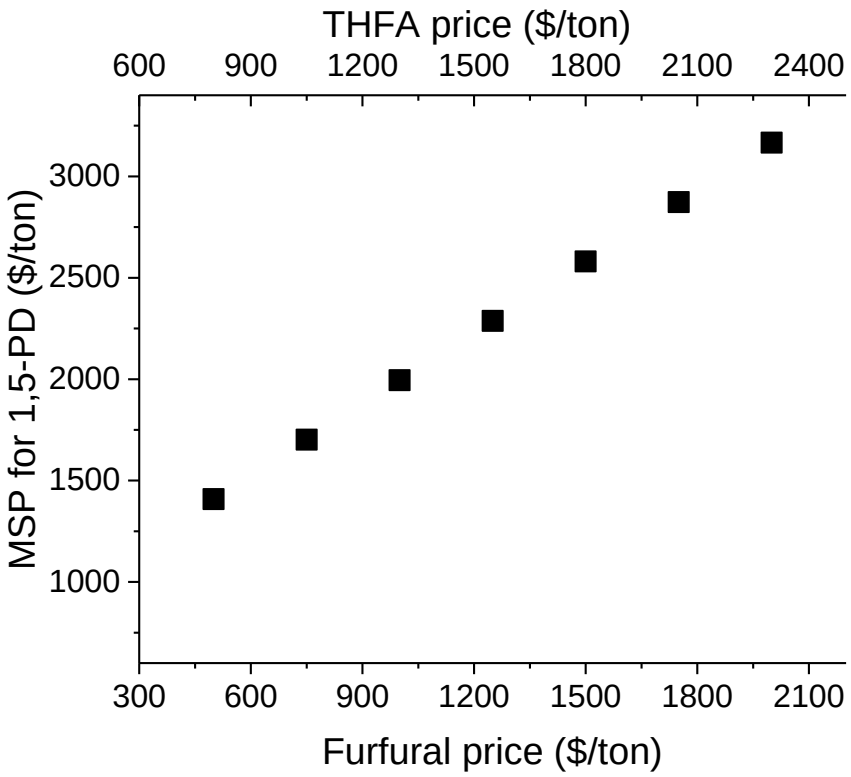

Figure 2.12 1,5-pentanediol (1,5-PD) minimum selling price (MSP) as a function of the furfural and tetrahydrofurfuryl alcohol (THFA) feedstock prices. (The THFA prices are $300/ton higher than the furfural prices because of the associated processing costs.)

2.4 Conclusions

We have demonstrated an economically feasible alternative pathway to synthesize 1,5-PD from lignocellulosic biomass. Prior approaches have focused on the direct hydrogenolysis of THFA. Technoeconomic analyses suggest that the 1,5-PD minimum selling prices for our route and the direct hydrogenolysis approach are $2,488/ton and $4,105/ton, respectively. Our pathway is also applicable to both C4 and C6 biomass-derived chemicals and allows for the ability to synthesize C4-C6 biorenewable α,ω-diols (see Chapters 3 and 5). The tautomerization-hydrogenation chemistry shown for C5 molecules in this work has been applied to C6 chemistry to produce 1,6-hexanediol from tetrahydropyran-2-methanol (see Chapter 3).[38,39] NMR results

confirmed the analogous ring-opening tautomerization chemistry, and the C6 process achieved 1,6-hexanediol yields of 34% from tetrahydropyran-2-methanol.[38]

Our approach utilizes two more reactions but no additional separation units. The vapor phase dehydration of THFA is performed with γ-Al_2O_3 and gives 87% yield to DHP. Uncatalyzed DHP hydration in water can produce up to 99% yield to 2-HTHP and its dimers. Ru catalysts are 99% selective for the hydrogenation of 2-HTHP to 1,5-PD.

The key intermediate in this alternative pathway is the cyclic hemiacetal, 2-HTHP. The cyclic hemiacetal is equilibrated with its ring-opened tautomer, 5HVal. Results from ^{13}C NMR spectroscopy measurements, ATR-FTIR spectroscopy measurements, and probe aldehyde hydrogenation reactions have demonstrated that the increased reactivity of 2-HTHP compared to THFA is a result of quasi equilibrated ring-opening and subsequent hydrogenation.

2.5 References

1. Richard, T. L. Challenges in Scaling Up Biofuels Infrastructure. *Science.* **2010**, *329*, 793–796.
2. Hoekman, S. K. Biofuels in the U.S. – Challenges and Opportunities. *Renew. Energy.* **2009**, *34*, 14–22.
3. Melero, J. A., Iglesias, J. & Garcia, A. Biomass as renewable feedstock in standard refinery units. Feasibility, opportunities and challenges. *Energy Environ. Sci.* **2012**, *5*, 7393.
4. Huber, G. W., Iborra, S. & Corma, A. Synthesis of Transportation Fuels from Biomass: Chemistry, Catalysts, and Engineering. *Chem. Rev.* **2006**, *106*, 4044–4098.
5. Werpy, T. *et al. Top Value Added Chemicals from Biomass Volume I—Results of Screening for Potential Candidates from Sugars and Synthesis Gas*. 2004.
6. Nikolau, B. J., Perera, M. A. D. N., Brachova, L. & Shanks, B. Platform biochemicals for a biorenewable chemical industry. *Plant J.* **2008**, *54*, 536–545.
7. Werle, P. *et al.* in *Ullmann's Encyclopedia of Industrial Chemistry* (Wiley-VCH Verlag GmbH & Co. KGaA, 2008).
8. Market sand Markets. *1,6-Hexanediol Market by Application (Polyurethanes, Coatings,*

Acrylates, Adhesives, Unsaturated Polyester Resins, Plasticizers, and Others) and By Geography (NA, Europe, Asia-Pacific, & ROW) - Trends and Forecasts to 2019. 2014.

9. Wolfe, A. J. Nylon: A revolution in textiles. *Chem. Herit. Found.* **2008**, *26*.

10. Chia, M. *et al.* Selective hydrogenolysis of polyols and cyclic ethers over bifunctional surface sites on rhodium-rhenium catalysts. *J. Am. Chem. Soc.* **2011**, 133, 12675–89.

11. Nakagawa, Y. & Tomishige, K. Production of 1,5-pentanediol from biomass via furfural and tetrahydrofurfuryl alcohol. *Catal. Today.* **2012**, *195*, 136–143.

12. Koso, S. *et al.* Chemoselective hydrogenolysis of tetrahydrofurfuryl alcohol to 1,5-pentanediol. *Chem. Commun.* **2009**, 2035-2037.

13. Dashtban, M., Gilbert, A. & Fatehi, P. Production of Furfural: Overview and Challenges. *J Sci Technol For. Prod Process.* **2012**, *2*, 44–53.

14. Research, G. V. *Furfural Market Analysis By Application (Furfuryl Alcohol, Solvent) And Segment Forecasts To 2020*. 2015.

15. Nakagawa, Y., Nakazawa, H., Watanabe, H. & Tomishige, K. Total Hydrogenation of Furfural over a Silica-Supported Nickel Catalyst Prepared by the Reduction of a Nickel Nitrate Precursor. *ChemCatChem.* **2012**, **4**, 1791–1797.

16. Sitthisa, S., Sooknoi, T., Ma, Y., Balbuena, P. B. & Resasco, D. E. Kinetics and mechanism of hydrogenation of furfural on Cu/SiO2 catalysts. *J. Catal.* **2011**, *277*, 1–13.

17. Sulmonetti, T. P. *et al.* Vapor phase hydrogenation of furfural over nickel mixed metal oxide catalysts derived from layered double hydroxides. *Appl. Catal. A Gen.* **2016**, *517*, 187–195 (2016).

18. Wang, Z. *et al.* Chemoselective hydrogenolysis of tetrahydrofurfuryl alcohol to 1,5-pentanediol over Ir-MoOx/SiO2 catalyst. *J. Energy Chem.* **2014**, *23*, 427–434.

19. Koso, S. *et al.* Promoting effect of Mo on the hydrogenolysis of tetrahydrofurfuryl alcohol to 1,5-pentanediol over Rh/SiO2. *J. Catal.* **2009**, *267*, 89–92.

20. Nakagawa, Y., Tamura, M. & Tomishige, K. Catalytic Conversions of Furfural to Pentanediols. *Catal. Surv. from Asia.* **2015**, *19*, 249–256.

21. Koso, S., Nakagawa, Y. & Tomishige, K. Mechanism of the hydrogenolysis of ethers over silica-supported rhodium catalyst modified with rhenium oxide. *J. Catal.* **2011**, *280*, 221–229.

22. Hurd, C. D. & Saunders, W. H. Ring-Chain Tautomerism of Hydroxy Aldehydes. *J. Am. Chem. Soc.* **1952**, *74*, 5324–5329.

23. Shono, T., Godo, M. & Shinra, K. High resolution NMR studies of ring-chain tautomerism in ω-hydroxy aldehydes. *Bunseki kagaku.* **1971**, *20*, 1183–1186.

24. Schniepp, L. E. & Geller, H. H. Preparation of Dihydropyran, δ-Hydroxyvaleraldehyde and 1,5-Pentanediol from Tetrahydrofurfuryl Alcohol. *J. Am. Chem. Soc.* **1946**, *68*, 1646–1648.

25. Sato, S., Igarashi, J. & Yamada, Y. Stable vapor-phase conversion of tetrahydrofurfuryl alcohol into 3,4-2H-dihydropyran. *Appl. Catal. A Gen.* **2013**, *453*, 213–218.

26. Butler, J. D. & Laundon, R. D. Intermediates and products in the catalytic vapour-phase dehydration and ammonolysis of 2-hydroxymethyltetrahydrofuran over alumina. *J. Chem. Soc. C Org.* **1969**, 173-176.

27. Gensler, W. J. & McLeod, G. L. Fate of the Carbinol Carbon in the Conversion of Tetrahydrofurfuryl Alcohol to Dihydropyran. *J. Org. Chem.* **1962**, *28*, 3194–3197.

28. Gensler, W. J., Ruks, I. & Marburg, S. Alumina-catalyzed rearrangements of α-methyltetrahydrofurfuryl alcohol, 5-methyltetrahydrofurfuryl alcohol, 2-methyl-2,3-dihydropyran, and 6-methyl-2,3-dihydropyran. *Chem. Commun.* **1966**, 782–783.

29. Vinueza, N. R., Kim, E. S., Gallardo, V. A., Mosier, N. S., Abu-Omar, M. M., Carpita, N. C., Kenttamaa, H. I. Tandem mass spectrometric characterization of the conversion of xylose to furfural. *Biomass and Bioenergy*. **2015**, *74*, 1-5.

30. Gensler, W. J., Manos, P. T., Ruks, I. Hydrogen and oxygen exchange in Δ^2-dihydropyran over hot alumina. *J. Org. Chem*. **1968**, *33*, 3408-3414.

31. Bell, J. M., Kubler, D. G., Sartwell, P. & Zepp, R. G. Acetal Formation for Ketones and Aromatic Aldehydes with Methanol 1. *J. Org. Chem.* **1965**, *30*, 4284–4292.

32. Ide, M. S., Hao, B., Neurock, M. & Davis, R. J. Mechanistic Insights on the Hydrogenation of α,β-Unsaturated Ketones and Aldehydes to Unsaturated Alcohols over Metal Catalysts. *ACS Catal.* **2012**, *2*, 671–683.

33. He, J.; Huang, K.; Barnett, K. J.; Krishna, S.; Martin Alonso, D.; Brentzel, Z.; Burt, S. P.; Walker, T. W.; Banholzer, W.; Maravelias, C. T.; Hermans, I.; Dumesic, J. A.; Huber, G. W. New Catalytic Strategies for Alpha-Omega Diol Production from Lignocellulosic Biomass. *Faraday Discuss.* **2017**, *202*, 247-267.

34. Arena, B. J. Deactivation of ruthenium catalysts in continuous glucose hydrogenation. *Appl. Catal. A Gen.* **1992**, *87*, 219–229.

35. Gallezot, P., Nicolaus, N., Flèche, G., Fuertes, P. & Perrard, A. Glucose Hydrogenation on Ruthenium Catalysts in a Trickle-Bed Reactor. *J. Catal.* **1998**, *180*, 51–55.

36. Survey, U. G. *Mineral Commodity Summaries 2016*. 2016.

37. Linak, E., Kishi, A., Guan, M. & Buchholz, U. *Furfural, Chemical Economics Handbook*. 2016.

38. Burt, S. P.; Barnett, K. J.; McClelland, D. J.; Wolf, P.; Dumesic, J. A.; Huber, G. W.; Hermans, I. Production of 1,6-Hexanediol from Tetrahydropyran-2-Methanol by Dehydration–hydration and Hydrogenation. *Green Chem.* **2017**, *19* (5), 1390–1398.

39. Tyssee, D. A. Preparation of 2,3,4,5-Tetrahydrooxepin. U.S. Patent, 1972.

Chapter 3. Production of 1,6-Hexanediol from Tetrahydropyran-2-methanol by Dehydration, Hydration, and Hydrogenation

3.1 Introduction

Terminal diols such as 1,4-butanediol (1,4-BD) and 1,6-hexanediol (1,6-HD) are important building-block chemicals and find application in the synthesis of specialty chemicals and a variety of polymers, primarily in polyesters and polyurethanes, and polyamides such as nylon-6,6.[1,2] Their synthesis from petro-chemical resources involves multiple reaction steps, and produces significant amounts of by-products. Therefore, sustainable catalytic systems that utilize renewable feedstocks such as biomass are desired. For short chain diols such as ethylene glycol and 1,4-BD,[3,4] renewable alternatives have recently been proposed in the literature.

Currently, 1,6-HD is produced industrially from cylohexanone/cyclohexanol (KA oil) by oxidation with nitric acid to form adipic acid, followed by hydrogenation of the dimethoxy ester to yield 1,6-HD. The attractiveness of the overall process is tempered by low conversions (4-8% for the oxidation of KA oil), difficult separations, the use of non-renewable fossil feedstocks, and emission of greenhouse gasses, namely N_2O.[5] Most recently, an alternative route to 1,6-HD *via* hydroformylation of 1,3-butadiene was proposed.[6] Although showing high yields, the use of homogeneous Rh complexes as catalyst and the multistep process hampers its industrial applicability.[6] Various attempts to synthesize 1,6-HD, as well as other α,ω-diols, from biomass resources have been reported. Using supported catalysts that contain precious metals with a

The content of this chapter is largely adapted from the following reference, Copyright (2017), reproduced by permission of the Royal Society of Chemistry:

Samuel P. Burt, Kevin J. Barnett, Daniel J. McClelland, Patrick Wolf, James A. Dumesic, George W. Huber, Ive Hermans. Production of 1,6-hexanediol from tetrahydropyran-2-methanol by dehydration-hydration and hydrogenation. *Green Chem*. **2017**. *19*, 1390-1398.

* SPB performed dehydration experiments. KJB performed hydration-hydrogenation experiments. * DJM performed NMR.

reducible metal oxide such as Pt-ReO_x,[7] Rh-ReO_x,[8-14] and Ir-ReO_x,[15,16] tetrahydropyran-2-methanol (THP2M), a biomass-derived feedstock,[17] can be converted into 1,6-HD with high selectivity. However, the high cost of the catalyst, in combination with a low productivity, limits the industrial applicability of those systems.[18]

The dehydration of THP2M to 2,3,4,5-tetrahydrooxepine (THO) over amorphous silicoaluminates was observed in the 1960s.[19,20] THO can then be re-hydrated to 2-oxepanol (OXL) and 6-hydroxyhexanal (6HHex), both of which can be subsequently hydrogenated to 1,6-HD giving an overall yield as high as 29%.[20] Slightly higher 1,6-HD yields were achieved using a copper chromite catalyst for the initial dehydration, but this introduces a toxic metal that could make this system environmentally damaging.[20-22] No time-on-stream data were reported to assess the stability of these catalysts. Moreover, only amorphous catalysts were tested for the dehydration reaction. This opens the door for a wide range of zeolites to be tested, which have been found to outperform their amorphous counterparts in many reactions.[23,24] The shape selectivity of zeolites is also ideal for biomass conversion, because the choice of framework can be used to encourage production of oxygenated products, aromatics, or larger polymers.[25]

In this study, we present a three-step approach for the synthesis of 1,6-HD from THP2M *via* THO (see Figure 3.1). In a first step, THP2M is dehydrated to THO over BEA zeolites, followed by hydration to OXL, which is in equilibrium with 6HHex. Finally, 6HHex and OXL are hydrogenated to 1,6-HD over Ru/C or Ni/C**.** In this work, we present the highest reported overall yields to 1,6-HD from THP2M using a silicoaluminate as a dehydration catalyst, and without the use of expensive metals such as Pt, Ir, and Rh. We show effects of the framework topology and exchange cation on THO yields and present a catalytic system for a renewable route to 1,6-HD.

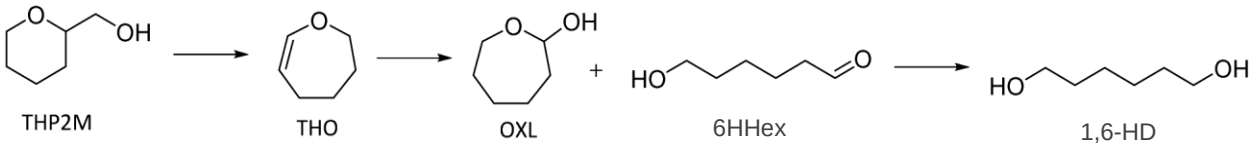

Figure 3.1 Three-step Dehydration-Hydration-Hydrogenation (DHH) route from tetrahydropyran-2-methanol (THP2M) to 1,6-hexanediol (1,6-HD).

3.2 Experimental Methods

3.2.1 Catalyst Synthesis

Amorphous SiO_2-Al_2O_3 (Sigma, grade 135) was used for comparison to zeolites in THP2M dehydration. All zeolite frameworks were purchased from Zeolyst in their hydrogen form with SiO_2:Al_2O_3 ratios of 20-30:1. All alkali exchanges were done at 80 ^oC in 1 M solutions of the corresponding nitrate in water for 8h. After exchange, the catalyst was washed with 1 L of distilled water per gram of catalyst and dried at 110 ^oC overnight. This ion-exchange was repeated two additional times, using 2 L of distilled water per gram of catalyst for the final washing. After the final drying step, the catalyst was calcined under a flow of air to 580 ^oC at a rate of 3 ^oC/min, holding at 580 ^oC for 6 hours. 5 wt% Ru/C was purchased from Sigma-Aldrich. 5 wt% Ni/C was prepared by incipient wetness impregnation of nickel nitrate hexahydrate (Sigma, >98.5% (KT)) in water onto Vulcan XC-72 (Cabot Corp.).

3.2.2 Catalyst Characterization

Exchange rates of zeolites synthesized in this study were determined by ICP-AES after digesting the solid samples in HF. NH_3-TPD measurements were carried out with a Micromeritics Autochem II Chemisorption Analyzer. Prior to NH_3-TPD analysis, samples were dehydrated at 580 ^oC for three hours (10 ^oC/min) under a flow of He. Samples were then cooled to 100 ^oC for NH_3 adsorption. Adsorption was performed for 30 min at 100 ^oC under a flow of 40 mL/min

10%NH_3-Ar (Airgas). NH_3 was desorbed under a 40 mL/min flow of He while heating at 10 ^oC/min.

FTIR experiments were performed with a Bruker Vertex 70 Fourier Transform Infrared Spectrometer equipped with an MCT detector. 32 scans were averaged to give one spectrum with a resolution of 4.00 cm^{-1}. A flow-through transmission cell was loaded with approximately 25 mg of sample that was pressed into a self-supporting wafer with a diameter of 13 mm. Samples were dehydrated at 350 ^oC (10 ^oC/min, 1h hold time) under 10^{-7} mbar. Samples were then cooled to 25 ^oC, and the time-zero spectrum was taken. Pyridine was then flowed over the catalyst for 10 min by way of a bubbler with a carrier gas of dry N_2 at atmospheric pressure. The cell was then flushed with dry N_2 for 10 min to remove physisorbed pyridine. Samples were then heated at a rate of 10 ^oC/min to 250 ^oC, and held at that temperature for 20 min while taking spectra of the catalyst. Samples were also heated to 150 ^oC and 350 ^oC with the same procedure, showing similar results. The final spectrum at 250 ^oC was used for contribution to this paper. The Opus 7.0 software package was used to analyze the data. Each spectrum was background subtracted and normalized by the intensity of silica framework signals in the range of 1800-2100 cm^{-1}. The time-zero spectrum was subtracted from each of the spectra taken at 250 ^oC so that only signals due to interaction with pyridine remained. Finally, the signals at 1540 and 1450 cm^{-1} were integrated for Brønsted and Lewis acid sites, respectively. Extinction coefficients of 1.3×10^6 cm^{-1}/mol and 1.5×10^6 cm^{-1}/mol were used to compare quantities of Brønsted and Lewis acid sites, respectively.[26]

Temperature-programmed oxidation experiments with spent catalysts were carried out with a Mettler Toledo TGA-DSC1. Samples were heated to 600 ^oC at 5 ^oC/min under a 20 mL/min flow of 20%O_2-N_2 (Airgas). Samples were then held at 600 ^oC for two hours under the same gas flow.

3.2.3 Reaction Experiments

Dehydration of THP2M was performed in a continuous flow (down-flow) reactor in the gas phase. The reactor was a quartz tube (52 cm long, 1.1 cm internal diameter) with a quartz frit in the middle to support the catalyst. The reactor was packed with 150 mg catalyst between layers of glass wool. Temperature was monitored and controlled by a thermocouple placed inside the reactor, just above the catalyst bed. The reactant was mixed with carrier gas above the furnace (Carbolite, VST12/300), and preheated in a layer of glass beads within the furnace before reaching the catalyst bed. Gas flow was controlled by mass flow controllers (Bronkhorst, EL-FLOW). Reactant flow was controlled by syringe pump (Chemyx, Fusion 200). Products were collected in a glass collection vessel inside a dry ice/acetone bath. Samples were taken at 4, 7, 10, 13, 16, and 25 hours on stream. The 4-hour sample normally showed lower carbon balances, likely due to the need to fully coat the reactor at the beginning of the reaction. That being the case, the 4-hour sample is not reported in this study, except when investigating the reaction network. The 4-hour sample is used for this purpose to minimize the effects of coking on our analysis. Products were analyzed by an Agilent gas chromatograph (HP6890) equipped with an HP-5 column and a flame ionization detector.

The organic product solution formed from THP2M dehydration over K-BEA was added dropwise to DI water up to 2wt% organic fraction in a 50mL Hastelloy Parr reactor. This was done slowly while stirring in order to prevent organic fraction loss to reactor walls and the stir bar. An insoluble organic layer was formed upon addition. The reactor was closed and pressurized to 500 psi with helium after 2 purge cycles. The reactor was heated to reaction temperature while stirring (500 rpm). An ice bath was used to quench the reaction after the desired reaction time. A single, water-soluble phase was formed after hydration. Liquid product samples were filtered with

Restek PES syringe filters prior to GC analysis (Shimadzu GC2010 equipped with a flame ionization detector and an RTX-VMS column).

The catalyst used for hydrogenation was a 5wt% Ru/C catalyst (Sigma Aldrich #206180) diluted 20x in Davisil silica gel (Sigma Aldrich #236845). The catalyst was pre-reduced in UHP H_2 (Airgas, 100 mL/min) at 300˚C (4 ˚C/min ramp rate, 1h hold time) in a glass tube reactor with Ultratorr fittings and ball valves at the inlet and outlet. Upon cooling to room temperature, the H_2 flow was stopped and the ball valves shut. The catalyst was transferred to a glove box with He atmosphere at positive pressure and stored. Prior to the hydrogenation, 130 mg of total catalyst (6.5 mg Ru/C) was added to a 75 mL Hastelloy Parr reactor equipped with a dip tub for time-on-stream sampling in the glove box. After isolating the catalyst and removing the reactor from the glove box, 40 mL of the product from the hydration step was added to the reactor with an HPLC pump after removing any residual oxygen from the lines. The reactor was pressurized to 6.4 MPa with H_2, heated to 120 ˚C, and stirred at 750 rpm. Samples were taken at desired reaction times with a dip tube and the reactor re-pressurized to 6.4 MPa after each sample. Samples were filtered with Restek PES syringe filters prior to GC analysis (Shimadzu GC2010 equipped with a flame ionization detector and an RTX-VMS column).

3.2.4 NMR Analysis

The hydration product was characterized by NMR with quantitative ^{13}C, ^{13}C DEPT-135, 2D HSQC, and 2D HMBC experiments. D_2O was added to the sample (1:9 v/v). The ^{13}C NMR experiments were acquired on a Bruker Biospin (Billerica, MA) AVANCE III 500 MHz spectrometer fitted with a DCH (^{13}C-optimized) cryoprobe. Bruker standard pulse sequence ‘zgig30’ was used for the quantitative ^{13}C experiments with the following parameters: an inter-scan relaxation delay of 40 s, a sweep width of 240 ppm centered at 110 ppm, acquiring 59,520

data points with an acquisition time of 1 s, and 256 scans. The ^{13}C DEPT-135 experiments used the Bruker standard pulse sequence 'deptsp135' with the following parameters: an inter-scan relaxation delay of 2 s, a sweep width of 240 ppm centered at 110 ppm, acquiring 59,520 data points with an acquisition time of 1 s, and 256 scans. Mestrelab Research's MestReNova software was used to process the spectra.

The 2D NMR (HSQC and HMBC) experiments were carried out on a Bruker Biospin (Billerica, MA) AVANCE III HD 600 MHz spectrometer fitted with a TCI-F cryoprobe. Bruker standard pulse sequence 'hsqcedetgpsisp2p3' was used for the HSQC experiment with the following parameters: 14 ppm sweep width in F2 (^{1}H), centered at 4.7 ppm, acquiring 3,366 data points, 240 ppm sweep width centered at 110 ppm in F1 (^{13}C) acquiring 1,309 increments, 4 scans per increment, and a 2.0 s relaxation delay. Bruker standard pulse sequence 'hmbcgplpndprqf' was used for the HMBC experiment with the following parameters: 14 ppm sweep width centered at 4.7 ppm in F2 (^{1}H) acquiring 3366 data points, 240 ppm sweep width centered at 110 ppm in F1 (^{13}C) acquiring 1309 increments, 4 scans per increment, and a 2.0 s relaxation delay. Bruker's Topspin 3.5 software was used to process spectra.

3.3 Results and Discussion

3.3.1 THP2M Dehydration

Initial experiments on the catalytic conversion of THP2M into THO were performed over Na-BEA (SiO_2/Al_2O_3 = 25) and compared with an amorphous SiO_2-Al_2O_3 (SiO_2:Al_2O_3 = 13) benchmark catalyst similar to that reported earlier[20] for this reaction (see Figure 3.2). The SiO_2-Al_2O_3 catalyst used in a previous study is no longer commercially available.[20] The SiO_2-Al_2O_3 used in this study produced low THO yields over a temperature range of 330 to 430 ^{o}C. Amorphous SiO_2 did not show any activity towards THO, and over γ-Al_2O_3 primarily

cyclopentanecarbaldehyde (CPC) was produced. Na-BEA was initially selected because sodium was previously reported to enhance the THO yield in the case of amorphous SiO_2-Al_2O_3.[20] Ion-exchange of commercial H-BEA was conducted with a 1 M aqueous $NaNO_3$ solution resulting in a Na/Al molar ratio of 0.66. Na-BEA shows higher THO yields compared to amorphous SiO_2-Al_2O_3, suggesting that the pore structure and/or Na^+ incorporation influence the catalytic performance.

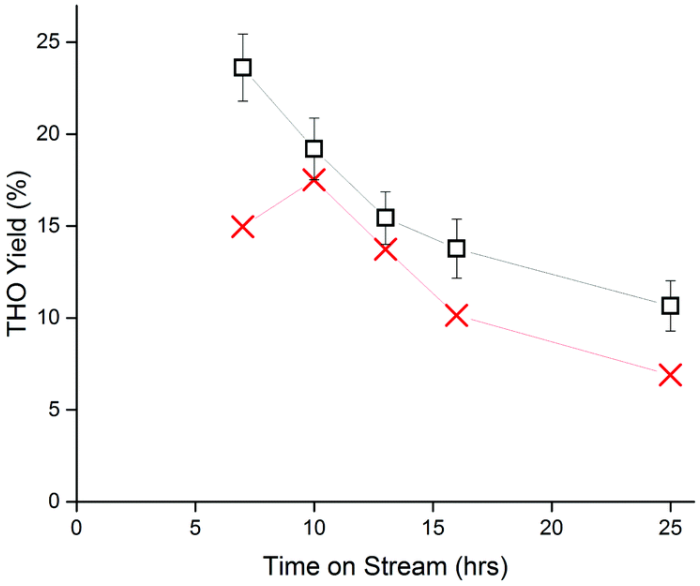

Figure 3.2 THP2M dehydration over Na-BEA (□, SiO_2:Al_2O_3 = 25) and amorphous SiO_2-Al_2O_3 (×, SiO_2:Al_2O_3 = 12). Reaction conditions: 400 °C, 0.628 mL/hr THP2M (liquid flow rate, STP), 30 mL/min (STP) H_2, 1 atm, 150 mg catalyst. Error bars shown are the result of four identical tests with Na-BEA. Error bars are assumed to be the same for each catalyst in this study.

Na-exchanged zeolites with SiO_2:Al_2O_3 ratios of 20-30 were screened for THP2M dehydration to investigate the influence of the zeolite topology on the catalytic activity. Out of the four tested framework types—MFI, MOR, FAU, BEA—the latter shows the highest yields towards THO (see Figure 3.3).

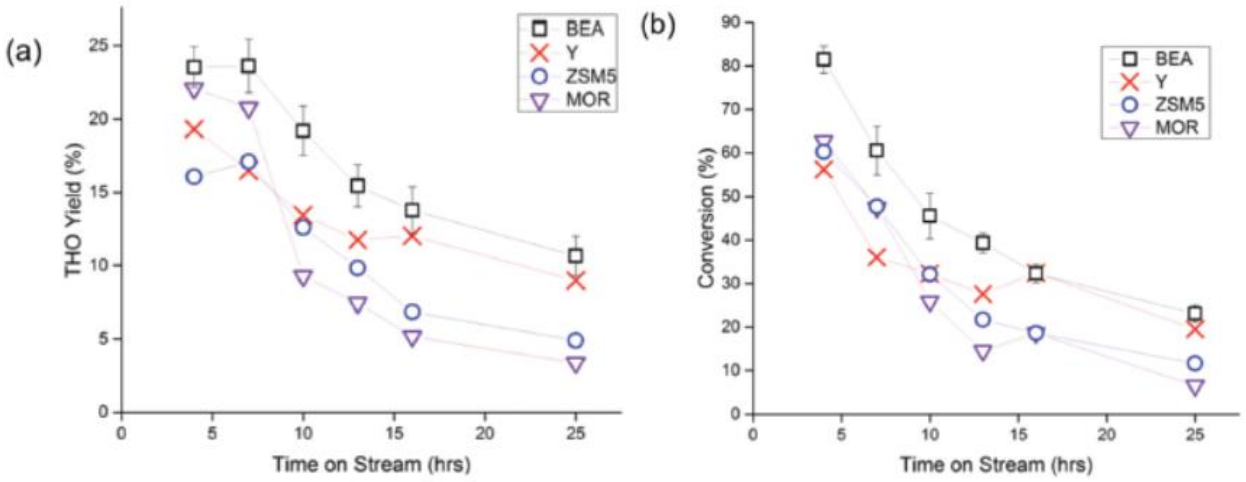

Figure 3.3 THO yields (a) and THP2M conversion (b) over Na-exchanged zeolites. Reaction conditions: 400 ^{o}C, 0.628 mL/hr THP2M (liquid flow rate, STP), 30 mL/min (STP) H_2, 1 atm, 150 mg catalyst.

As this is an acid-catalyzed dehydration, Temperature Programmed Desorption of NH_3 (NH_3-TPD) was performed (see Table 3.1) to rationalize the differences in activity between the various zeolite frameworks. The curves in the NH_3-TPD were fitted to identify individual acid sites responsible for NH_3 desorption at specific temperatures, which is displayed in Table 3.1. From this point on, all acid sites that desorb NH_3 in the range of 150-230 ^{o}C will be denoted as weak acid sites. Those that desorb NH_3 in the range of 230-350 ^{o}C will be denoted as moderate-strength acid sites, and we will not show any strong acid sites.[27] According to Table 3.1, Na-BEA, the framework with the highest yields to THO, has a weak and a moderate acid site. Na-ZSM-5 and Na-MOR also have a weak and moderate acid site (in different concentrations). The latter two catalysts produce much less THO than Na-BEA, so it is not immediately obvious which is the active site for THO production. Furthermore, Na-Y has no moderate acid site, and yet shows higher THO yields than Na-ZSM-5 and Na-MOR at nearly every time-on-stream. This would seem to indicate that the weak acid site is active for THO production, and the moderate site is not.

Table 3.1 NH_3 desorption signals fitted for weak, moderate, and strong acid sites on Na-exchanged zeolites.

Catalyst	NH_3 desorption temp. (°C)	Assignment	Quantity desorbed (μmol NH_3 per g catalyst)
Na-MOR	186	Weak acid	1080
	257	Moderate acid	264
Na-ZSM5	191	Weak acid	606
	290	Moderate acid	364
Na-Y	177	Weak acid	367
	226	Moderate acid	7.19
Na-BEA	174	Weak acid	549
	238	Moderate acid	214

Temperature programmed oxidation (TPO) experiments in a ThermoGravimetric Analyzer (TGA) were done to investigate the cause of deactivation. Spent catalysts were heated to 600 ^oC (ramp rate 5 ^oC/min) under a flow of air. Each spent catalyst shows a mass loss in the range of 16 to 37% during heating in air, due to coking over the course of the reaction. These experiments show that the less active zeolites (Na-ZSM-5 and Na-MOR) produce roughly half the amount of coke than do more active zeolites (Na-Y and Na-BEA).

BEA samples exchanged with each alkali metal were prepared to determine the effect of the exchange cation on THO yields. Moreover, the THO yields of these catalysts were compared with those of H-BEA, *i.e.* the starting material in the synthesis of all BEA zeolites in this study. The catalysts display clear differences in THO yields (see Figure 3.4), however, no clear periodic trend among the catalysts with regards to THO production is immediately observed. K- and H-BEA show the highest THO yields amongst the tested catalysts with initial yields of up to 40% for K-BEA. Furthermore, as shown in Figure 3.4b, Rb- and Cs-BEA show the lowest conversions at all times-on-stream. This will be addressed further later.

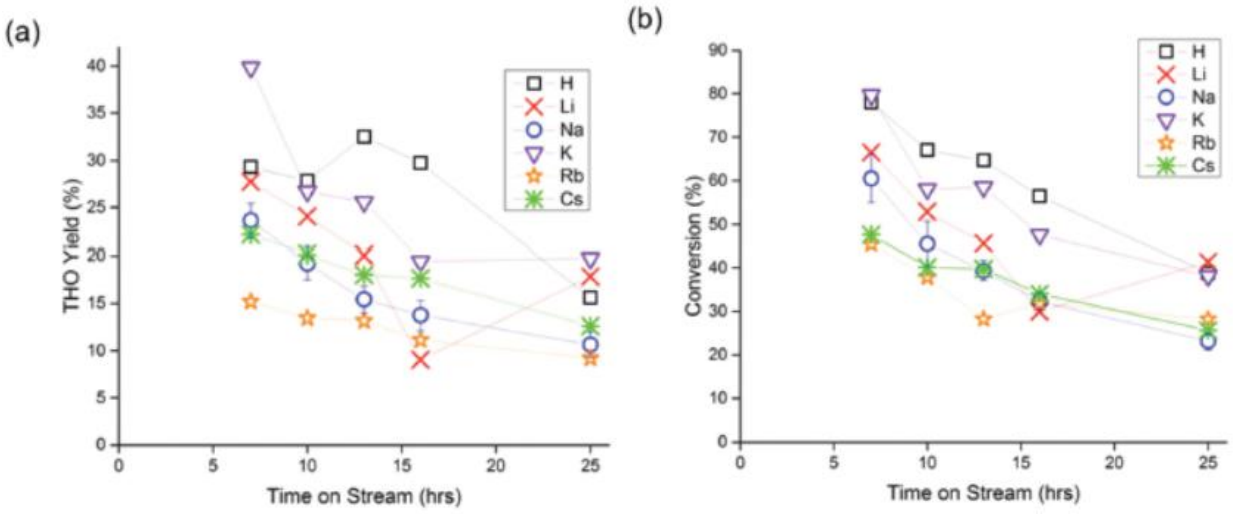

Figure 3.4 THO yields (a) and THP2M conversion (b) over alkali-exchanged BEA zeolites. Reaction conditions: 400 °C, 0.628 mL/hr THP2M (liquid flow rate, STP), 30 mL/min (STP) H_2, 1 atm, 150 mg catalyst.

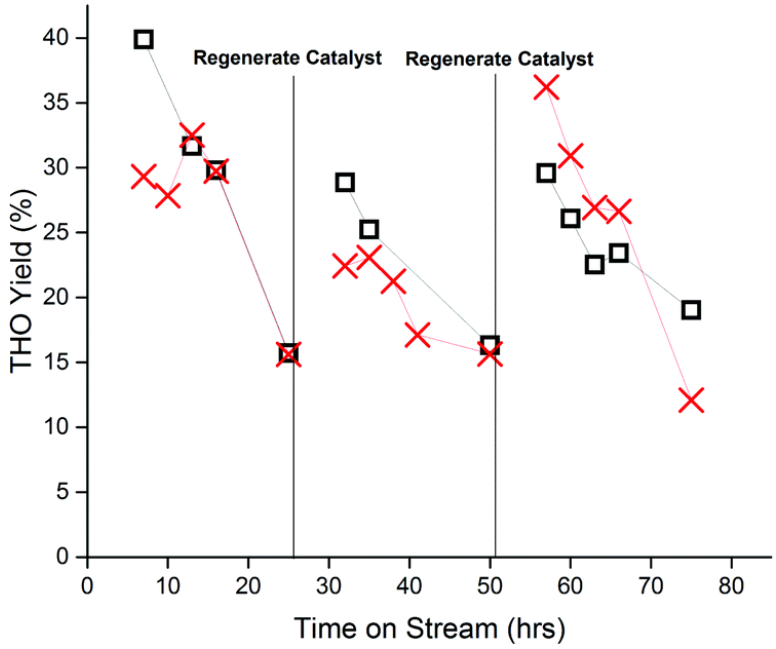

Figure 3.5 Regeneration of K-BEA (□) and H-BEA (×). Reaction conditions: 400 °C, 0.628 mL/hr THP2M (liquid flow rate, STP), 30 mL/min (STP) H_2, 1 atm, 150 mg catalyst.

We regenerated the spent K- and H-BEA catalysts under flowing air at 580 ^{o}C and then retested their catalytic activity as shown in Figure 3.5. K-BEA has the higher initial and final yields compared to H-BEA, with the highest single-point yield of 40% obtained after 7 hours on stream in the first cycle. It appears that for both catalysts the initial activity cannot be fully recovered even after regeneration. However, after the second regeneration the catalyst does not continue to lose activity.

NH_3-TPD was performed on the alkali-exchanged BEAs (see Table 3.2). NH_3 desorption below 150 ^{o}C is likely due to physisorbed NH_3, as seen previously.[28,29] It is clear that Rb- and Cs-BEA are less acidic than the other catalysts. This correlates with low conversions obtained with these catalysts. Next, Li- and Na-BEA have similar TPD profiles to each other, with large quantities of a weak acid site and comparable quantities of a moderate acid site. Figure 3.4a shows that these catalysts produce less THO than K- and H-BEA, but more than Rb- and Cs-BEA. Finally, K-BEA shows more weak acid sites than Rb- and Cs-BEA, and essentially no moderate acid sites. K-BEA is the best of all metal-exchanged catalysts in terms of THO yield, as shown by the data in Figure 3.4a. These observations are in line with our working hypothesis that the weak acid site is responsible for THO production. Furthermore, the parent catalyst, H-BEA, shows high levels of this weak acid site, along with a smaller, but still significant amount of moderate acid sites. H-BEA has a higher ratio of weak sites to moderate sites than any other catalyst except K-BEA. This, along with the fact that K- and H-BEA are the two catalysts in this study that have the highest THO yield, further supports the weak acid site being active for THO production.

Table 3.2 NH_3-desorption signals fitted for weak, moderate, and strong acid sites on alkali-exchanged BEAs. Ramp Rate = 10 °C/min

Catalyst	NH_3 desorption temp. (°C)	Assignment	Quantity desorbed (μmol NH_3 per g catalyst)
H-BEA	144	Physisorbed NH_3	150
	161	Weak acid	615
	289	Moderate acid	89.8
Li-BEA	176	Weak acid	669
	258	Moderate acid	135
Na-BEA	174	Weak acid	549
	238	Moderate acid	214
K-BEA	174	Weak acid	399
	290	Moderate acid	7.02
Rb-BEA	142	Physisorbed NH_3	74.9
	168	Weak acid	145
Cs-BEA	151	Weak acid	55.3
	244	Moderate acid	21.7

FTIR of adsorbed pyridine was performed on each catalyst to determine the Brønsted/Lewis acid nature of the active site for THO production. Pyridine was adsorbed on dehydrated samples at 25 °C, which were subsequently heated to 250 °C under a flow of dry N_2. Table 3.3 shows the Brønsted and Lewis acid concentrations for each catalyst. Concentrations were calculated by multiplying the Brønsted/Lewis acid ratios—determined by FTIR—by the overall concentration of acid sites—determined by NH_3-TPD (physisorbed NH_3 was not included in this calculation). H-BEA shows much more Brønsted acid sites (an order of magnitude in most cases) than all other catalysts. This indicates that the aqueous ion-exchange performed for the synthesis of the metal-exchanged catalysts effectively exchanges with Brønsted sites.

Table 3.3 also shows that the two catalysts that have the highest THO yield—K-BEA and H-BEA—have Brønsted acid concentrations that differ by nearly two orders of magnitude, while their Lewis acid concentrations differ by only a factor of two. This indicates that Brønsted acids are irrelevant towards THO production, and Lewis acids are the active sites. This, along with the

data from NH_3-TPD, leads us to the conclusion that THO production from THP2M is catalyzed by weak Lewis acid sites.

Table 3.3 Brønsted/Lewis acid concentrations determined by FTIR

Catalyst	Brønsted acid concentration (μmol g^{-1} catalyst)	Lewis acid concentration (μmol g^{-1} catalyst)
H-BEA	483	222
Li-BEA	322	482
Na-BEA	84.0	679
K-BEA	11.4	394
Rb-BEA	4.63	140
Cs-BEA	3.09	73.9
Na-Y	25.7	348
Na-MOR	199	1140
Na-ZSM-5	78.9	892

*Calculated by pyridine remaining on each catalyst at 250 °C after adsorption at 25 °C. 1540 cm^{-1} band used for Brønsted site, 1450 cm^{-1} band used for Lewis site.[30] Extinction coefficients shown in Experimental Section.

TPO was used to characterize the alkali-exchanged catalysts after reaction (Table 3.4). As expected, Rb- and Cs-BEA show the least amount of mass loss due to coking, as these are the least active catalysts (similar effect seen with Na-MOR and Na-ZSM-5). Furthermore, Li- and Na-BEA show 1.2-1.9 times the amount of coke that other BEA catalysts produce. In fact, Table 3.4 shows that the amount of coke formed on BEA catalysts is directly related to the concentration of moderate-strength acid sites on the catalyst. Table 3.4 also shows that this trend does not apply for other frameworks. This could be due to several reasons, such as the possibility that the frameworks with five-membered rings (MFI and MOR) are inaccessible by the reactant or certain intermediates, thus decreasing reactivity and coke formation.

Table 3.4 Fraction of mass lost in spent catalyst during TPO experiments

Catalyst	Mass Loss During Calcination of Spent Catalyst (%)
Na-MOR	16.1
Na-ZSM5	19.0
Na-Y	27.9
Na-BEA	36.5
H-BEA	30.2
Li-BEA	36.2
K-BEA	26.3
Rb-BEA	22.7
Cs-BEA	19.4

Figure 3.6 shows the major products of THP2M dehydration at four different contact times over K-BEA. Figure 3.7 shows a possible reaction pathway based on the data shown in Figure 3.6. Yields to 6,8-dioxabicyclooctane (DBO)—while relatively low at all contact times—decrease with increasing contact time, indicating it is formed early in the reaction network. Yields to tetrahydropyran-2-carbaldehyde (THP2C) stay relatively constant with contact time. However, not shown in the figures, THP2M conversion increases with increasing contact time, meaning the selectivity to THP2C drops with increasing contact time. This supports the hypothesis that THP2C is indeed formed early in the reaction sequence, as shown in Figure 3.7. The fact that yields to THO reach a maximum at an intermediate contact time indicates that it can be degraded into further reaction products, also shown in Figure 3.7. This would explain why we were unable to obtain higher THO yields with these catalysts; at low contact times, THO intermediates are formed, while at higher contact times, THO degradation occurs. Oxepane (OXE), cyclopentanecarbaldehyde (CPC), 5-hexenal, dihydromethylpyran (DMP), and 2-methylcyclopentanone (2MCP) increase in

yield with increasing contact time, indicating that they are among the degradation products formed late in the reaction network. Due to the high cost and unavailability of reaction intermediates (including THO) in their pure forms, we could not perform reactions using each intermediate as a reactant. These experiments would provide a more definitive reaction network, and should be part of the scope of future work. In our current work, Figure 3.7 represents a possible reaction pathway supported by our data and similar reactions in the literature.[31-41]

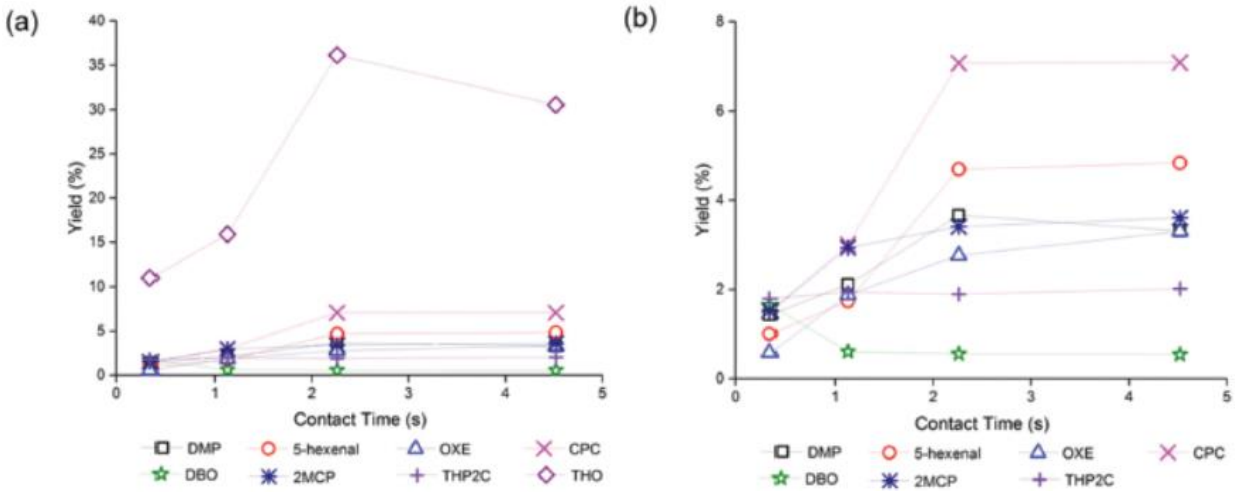

Figure 3.6 Product distribution with changing catalyst contact time (a), same data zoomed in on byproducts (b). Low time-on-stream (4 hours) was used for all measurements to minimize the effects of coking, although this led to relatively low carbon balances, in the range of 77-79% for each measurement. K-BEA was used for each test.

The final desirable step in our network, that is, the dehydration of DBO to THO, cannot be found in literature, as the mechanism of THO formation has not been studied. We have already shown that DBO is likely formed early in the reaction network, and DBO is the only product formed early in the reaction network that has a seven-membered ring. It seems likely, therefore, that THO is formed from the dehydration of DBO. The portrayal of DBO in Figure 3.7 shows that

one oxygen atom of DBO is part of a seven-membered ring, and the other (bridging) oxygen is part of a five-membered ring.

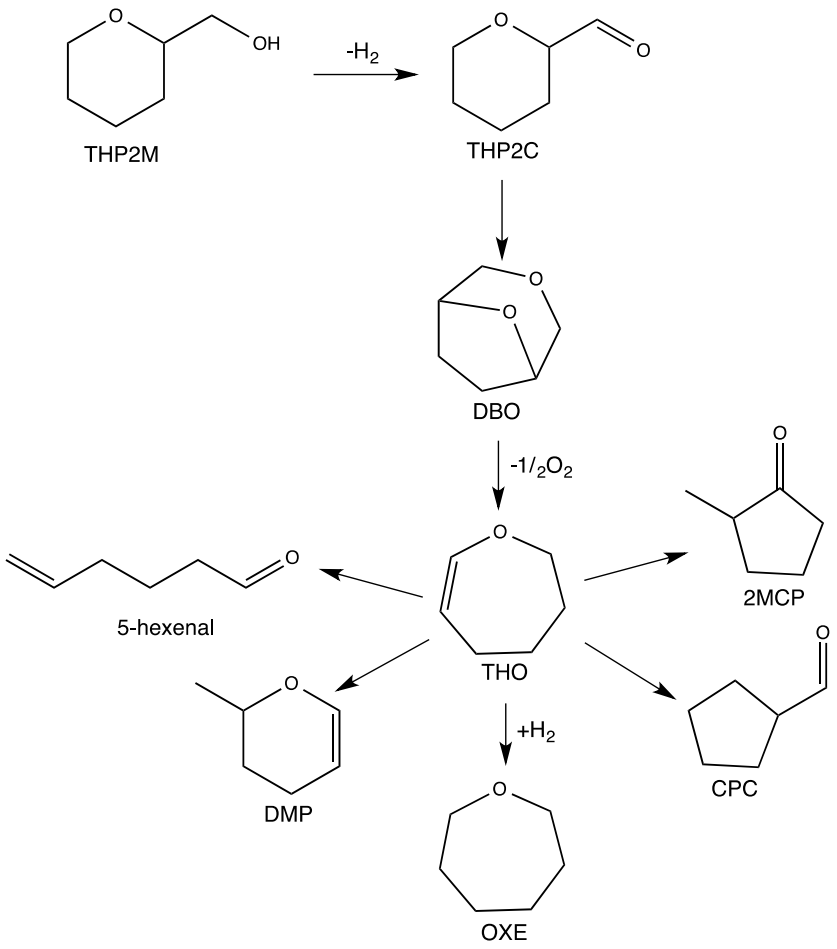

Figure 3.7 Possible reaction network for dehydration of THP2M (major products shown).

To find out which of these sites is more prone to dehydration to THO, quantum-chemical calculations were performed. The C-O-C bond angle of the oxygen in the seven- membered ring in DBO was compared to that of the same bond in OXE, the fully hydrogenated seven-membered cyclic ether (see Table 3.5). Furthermore, the C-O-C bond angle of the oxygen in the five-

membered ring of DBO was compared to that of the same bond in tetrahydrofuran (THF), the fully hydrogenated five-membered cyclic ether. Table 3.5 indicates that the C-O-C bond in the five-membered ring of DBO is more strained than that of the seven-membered ring. The C-O-C bond angle of the DBO five-membered ring is 8.0^{o} smaller than that of THF, while the C-O-C bond angle of the DBO seven-membered ring is only 2.4^{o} smaller than that of OXE. The higher strain on the oxygen atom in the five-membered ring of DBO (bridging oxygen) indicates that it is the less stable bond. Moreover, Table 3.5 shows that the C-O bonds in the five-membered ring of DBO is 0.013 Å longer than the C-O bonds in the seven-membered ring of the same compound, once again indicating that the oxygen in the five-membered ring is more reactive. If DBO dehydrates at the oxygen in the five-membered ring, it will likely form THO. Therefore, our calculations indicate that DBO could be the precursor to THO.

Table 3.5 DFT-optimized (B3LYP/G def2-SVP) C-O-C bond angles and lengths for each oxygen site in DBO, in comparison with the C-O-C bond angles of seven-membered oxepane (OXE) and five-membered tetrahydrofuran (THF).

Molecule	**C-O-C bond angle in seven-membered ring (º)**	**C-O-C bond angle in five-membered ring (º)**	**C-O bond length in seven-membered ring (Å)**	**C-O bond length in five-membered ring (Å)**
DBO	112.5	102.6	1.419	1.432
OXE	114.9	-	1.413	-
THF	-	110.6	-	1.423

* Gas phase thermochemistry values were calculated with Gaussian 09 software.
* Geometry optimizations and subsequent frequency calculations were performed using B3LYP/6-311þG(2d,p).

The 6-membered ring, THP2M, gives lower selectivity to the to the 7-membered unsaturated cyclic ether, THO, than the 5-membered ring, tetrahydrofurfuryl alcohol (THFA), gives to the 6-membered unsaturated cyclic ether, dihydropyran (DHP) (see Chapter 2). The main

side product in the C6 route is cyclopentane carboxaldehyde (CPC), as described above. This result is corroborated by the thermodynamic results for dehydration reactions of five- and six-carbon heterocyles (Table 3.6). Density functional theory calculations show that the isomerization of THO to CPC at 648 K has a Gibbs free energy change of -72.2 kJ mol^{-1}, whereas the isomerization of DHP to cyclobutane carboxaldehyde is an endergonic reaction, with a Gibbs free energy change of 15.8 kJ mol^{-1}.

Table 3.6 Thermochemistry for dehydration and isomerization reactions of five and six carbon heterocycles at 648 K.

Reaction	ΔH (kJ/mol)	ΔS (kJ/mol K)	ΔG (kJ/mol)
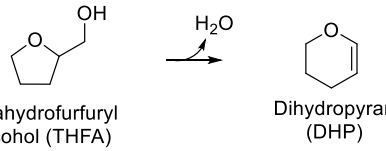	12.1	0.15	-84.2
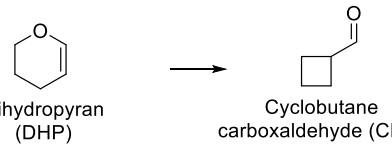	32.5	0.03	15.8
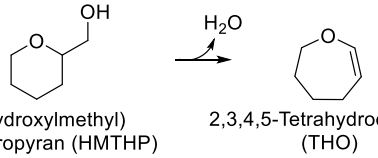	35.9	0.16	-68.6
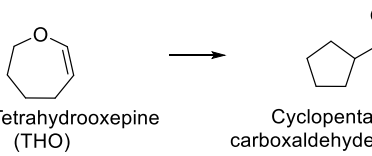	-61.0	0.02	-72.2

* Gas phase thermochemistry values were calculated with Gaussian 09 software.

* Geometry optimizations and subsequent frequency calculations were performed using B3LYP/6-311þG(2d,p).

3.3.2 THO Hydration

The product from THP2M dehydration over K-BEA was then subjected to hydration conditions to produce OXL and 6HHex from THO (see Figure 3.1). The hydration of the THO in the reaction mixture proceeded homogeneously in water at 70 °C for 5h in an autoclave. This resulted in the complete conversion of THO and the formation of one main new gas chromatogram (GC) signal. Nuclear Magnetic Resonance (NMR) spectroscopy was performed on the product mixture. As shown in the Quantitative ^{13}C NMR spectrum in Figure 3.8A, there exists two compounds that are only surpassed in intensity by unconverted THP2M from the dehydration step.[42,43]

The relative ratio of peak intensities of THP2M to the two unknown species in ^{13}C NMR matches those of THP2M to the hydration product in GC analysis, indicating these are indeed the hydration products and that their GC peaks overlap one another (or one is converted to the other in the gas phase during GC analysis). The NMR peak at 91.38 ppm is very likely the hemiacetal carbon of OXL, the direct hydration product of THO. The NMR peak at 209.31 ppm is indicative of an aldehyde, likely 6HHex, the ring-opened tautomer of OXL (see Figure 3.1). This is further evidenced by DEPT-135 NMR analysis (see Figure 3.8B),[42,43] which indicates both peaks are either primary or tertiary carbons, likely the primary carbons of OXL and 6HHex. Heteronuclear single quantum correlation (HSQC) and heteronuclear multiple bond correlation (HMBC) NMR analyses were performed and HMBC correlations confirmed the 6 carbons of each hydration product..[42,43]

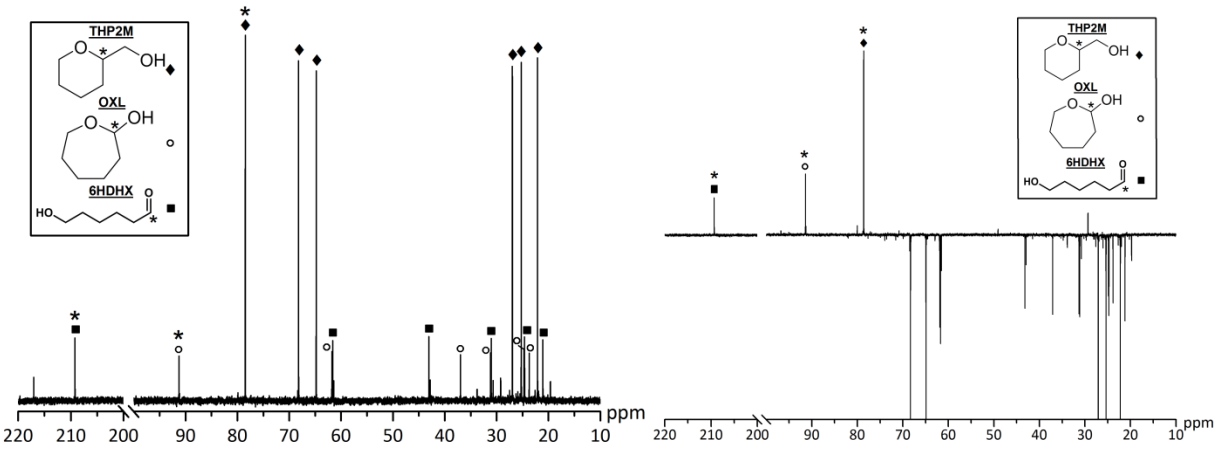

Figure 3.8 A) Quantitative ^{13}C NMR and B) ^{13}C DEPT-135 NMR spectra of reaction solution formed via hydration of THP2M dehydration product.

3.3.3 Hydrogenation to 1,6-HD

The hydration product was then hydrogenated over a pre-reduced Ru/C catalyst in a batch reactor. Prior to the reaction, Quantitative ^{13}C NMR was used to quantify the concentration of OXL and 6HHex in the feed (28.5 mM) by using the peak ratio of THP2M to the hydration products.[42,43] The hydrogenation reaction resulted in the complete conversion of the hydration products and ~98% carbon yield to 1,6-HD after 22h (see Figure 3.9). There was no appreciable side-product formation in the hydrogenation step. A maximum of 85% 1,6-HD yield from THO was achieved. Any loss in 1,6-HD yields from THO was likely the result of oligomer/polymer formation in the hydration step. In fact, hydrations at higher temperature (100 ^{o}C) resulted in the formation of solid residue in the reactor. Moreover, essentially identical results over this time scale were achieved using a Ni/C catalyst instead of Ru/C for the hydrogenation, indicating base metal catalysts can also be used for the hydrogenation step. However, Inductively Coupled Plasma (ICP) analysis of the product streams of the Ru/C and Ni/C hydrogenations displayed the instability of Ni/C catalysts, with 31% of the Ni originally present in Ni/C leached into the product stream. In

contrast, less than 1% of the Ru originally present in Ru/C leached into the product stream during its reaction.

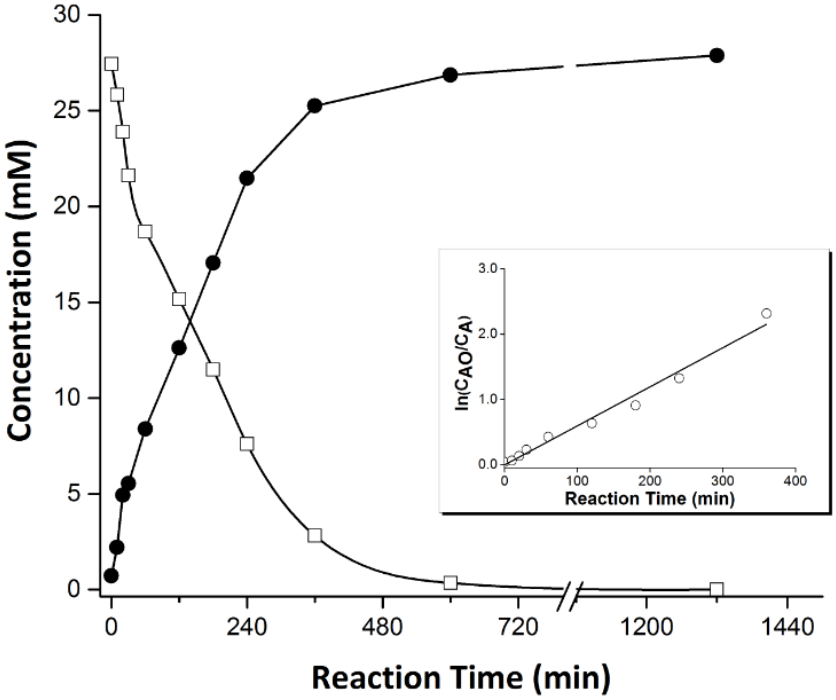

Figure 3.9 OXL + 6HHex (□) and 1,6-HD (●) concentration at various time points in a batch reactor (130 mg Ru/C diluted 20x in Silica gel [6.5 mg Ru/C], T=120 °C, P=6.4 MPa).

As the ring-opening tautomerization of OXL to 6HHex is thermodynamically favorable (as shown by gas-phase thermochemistry calculations), it is likely that 6HHex is the main product of the hydration step and was the main 1,6-HD precursor. This is further corroborated by the fact that 1,6-HD was produced via simple hydrogenation with a monometallic hydrogenation catalyst; ring-opening of OXL would require the use of a bimetallic-oxophilically promoted catalyst.[9] Additionally, the reaction was determined to be 1st order in 6HHex (see Figure 3.9 insert). The reaction rate of 994 μmol gcat^{-1} min^{-1} is an order of magnitude higher than achieved in typical C-O-C bond hydrogenolysis reactions,[9] further evidence that the hydrogenation of an aldehyde is rate determining.[44]

3.4 Conclusions

An alternative to the conventional Pt, Rh, and Ir-based catalysts for the conversion of tetrahydropyran-2-methanol (THP2M) to 1,6-hexanediol (1,6-HD) is presented. While the existence of this pathway has been known since at least the 1960s, it has essentially not been investigated over the past 40-50 years. In the first of three steps, THP2M is dehydrated to 2,3,4,5-tetrahydrooxepine (THO) in a continuous flow, gas-phase reactor over a silicoaluminate catalyst. While this study was not able to replicate THO yields over amorphous SiO_2-Al_2O_3 cited in the literature,[19,20] data from this study indicates that zeolite materials produce nearly three times higher yields of THO than amorphous SiO_2-Al_2O_3. Various zeolite frameworks, as well as various alkali metals as exchange ions were tested in this dehydration reaction. Maximum THO yields of 40% were achieved over K-BEA. THO production over K-BEA benefits from the catalyst's large quantity of weak Lewis acid sites (394 cm^3 NH_3 desorbed/g catalyst), and very few, if any, strong (Brønsted or Lewis) acid sites. Without the use of any catalyst, THO was then hydrated in 85% yields to 6-hydroxyhexanal (6HHex) and 2-oxepanol (OXL), as confirmed by NMR. 6HHex and OXL (likely through 6HHex) were then hydrogenated to 1,6-HD with Ru/C or Ni/C nearly quantitatively. Therefore, our pathway affords an overall yield of 34% to 1,6-HD from THP2M, higher than previously reported 1,6-HD yields from THP2M without using toxic metals.[20] In future research, optimizing Lewis acid strength and concentration could potentially lead to higher THO selectivity, and therefore improve the overall viability of this route.

3.5 References

1. Werle P, Morawietz M, Lundmark S, Sörensen K, Karvinen E, Lehtonen J. Alcohols, Polyhydric. In: *Ullmann's Encyclopedia of Industrial Chemistry*. Wiley-VCH Verlag GmbH & Co. KGaA; **2000**.

2. Wang T, Ide MS, Nolan MR, Davis RJ, Shanks BH. Renewable Production of Nylon-6,6 Monomers from Biomass-Derived 5-Hydroxymethylfurfural (HMF). *Energy Environ Focus*. **2016**; *5*: 13-17.

3. Angelici C., Weckhuysen B.M., Bruijnincx P.C.A. Chemocatalytic conversion of ethanol into butadiene and other bulk chemicals. *ChemSusChem*. **2013**; *6*(9): 1595-1614.

4. Wang A., Zhang T. One-Pot Conversion of Cellulose to Ethylene Glycol with Multifunctional Tungsten-Based Catalysts. *Acc Chem Res*. **2013**; *46*(7): 1377-1386.

5. Van de Vyver S. and Roman-Leshkov Y. Emerging catalytic processes for the production of adipic acid. *Catalysis Science & Technology*. **2013**; *3*: 1465–1479.

6. Mormul J., Breitenfeld J., Trapp O., Paciello R., Schaub T., and Hoffman P. Synthesis of adipic acid, 1,6-hexanediamine, and 1,6-hexanediol via double-*n*-selective hydroformylation of 1,3-butadiene. *ACS Catalysis*. **2016**, *6*, 2802–2810.

7. Allgeier A.M., De Silva W.I.N., Ekaterini K., Menning C.A., Ritter J.C., Sengupta S.K., Stauffer C.S. Process For Preparing 1,6-Hexanediol. **2014**.

8. Chia M., Pagán-Torres Y.J., Hibbitts D., Tan Q., Pham H.N., Datye A.K., Neurock M., Davis R.J., Dumesic J.A. Selective Hydrogenolysis of Polyols and Cyclic Ethers over Bifunctional Surface Sites on Rhodium–Rhenium Catalysts. *J Am Chem Soc*. **2011**; *133*(32): 12675-12689.

9. Chia M., O'Neill B.J., Alamillo R., Dietrich P.J., Ribeiro F.H., Miller J.T., Dumesic J.A. Bimetallic RhRe/C catalysts for the production of biomass-derived chemicals. *J Catal*. **2013**; *308*(0): 226-236.

10. Karanjkar P.U., Burt S.P., Chen X., Barnett K.J., Ball M.R., Kumbhalkar M.D., Wang X., Miller J.B., Hermans I., Dumesic J.A., Huber G.W. Effect of carbon supports on RhRe bifunctional catalysts for selective hydrogenolysis of tetrahydropyran-2-methanol. *Catal Sci Technol*. **2016**; *6*(21): 7841-7851.

11. Kojima Y., Kotani S., Sano M., Suzuki T., Miyake T. Hydrogenation of Dimethyl Adipate to 1,6-Hexanediol on Supported Rh–Sn Catalysts. *J Japan Pet Inst*. **2013**; *56*(3): 133-141.

12. Chen K., Koso S., Kubota T., Nakagawa Y., Tomishige K. Chemoselective Hydrogenolysis of Tetrahydropyran-2-methanol to 1,6-Hexanediol over Rhenium-Modified Carbon-Supported Rhodium Catalysts. *ChemCatChem*. **2010**; *2*(5): 547-555.

13. Nakagawa Y., Tamura M., Tomishige K. Catalytic Reduction of Biomass-Derived Furanic Compounds with Hydrogen. *ACS Catal*. **2013**; *3*(12): 2655-2668.

14. Koso S., Furikado I., Shimao A., Miyazawa T., Kunimori K., Tomishige K. Chemoselective hydrogenolysis of tetrahydrofurfuryl alcohol to 1,5-pentanediol. *Chem Commun*. **2009**;(15): 2035-2037.

15. Nakagawa Y., Shinmi Y., Koso S., Tomishige K. Direct hydrogenolysis of glycerol into 1,3-propanediol over rhenium-modified iridium catalyst. *J Catal*. **2010**; *272*(2): 191-194.

16. Xiao B., Zheng M., Li X., Pang J., Sun R., Wang H., Pang X., Wang A., Wang X., Zhang T. Synthesis of 1,6-hexanediol from HMF over double-layered catalysts of Pd/SiO2 + Ir-ReOx/SiO2 in a fixed-bed reactor. *Green Chem*. **2016**; *18*(7): 2175-2184.

17. Buntara T., Noel S., Phua P.H., Melián-Cabrera I., de Vries J.G., Heeres H.J. Caprolactam from Renewable Resources: Catalytic Conversion of 5-Hydroxymethylfurfural into Caprolactone. *Angew Chemie Int Ed*. **2011**; *50*(31): 7083-7087.

18. Brentzel Z.J., Barnett K.J., Huang K., Maravelias C.T., Dumesic J.A., Huber G.W. Chemicals from Biomass: Combining Ring-Opening Tautomerization and Hydrogenation Reactions to Produce 1,5-Pentanediol from Furfural. *ChemSusChem*. **2017**; *10*(7): 1351-1355.

19. Tysee, D. A. Preparation of 2,3,4,5-Tetrahydrooxepin. U.S. 6,636,053, 1972.

20. Misono, A.; Osa, T.; Sanami, Y. The Hydrogenation of Pyran Derivatives. IV. The Skeletal Rearrangement in the Gas-Phase Dehydration of Tetrahydropyran-2-Methanol. *Bull. Chem. Soc. Jpn.* **1968**, *41* (10), 2447–2453.

21. Dhal B., Thatoi H., Das N., Pandey B.D. Reduction of hexavalent chromium by Bacillus sp. isolated from chromite mine soils and characterization of reduced product. *J Chem Technol Biotechnol*. **2010**; *85*(11): 1471-1479.

22. Guo L., Zhou J., Mao J., Guo X., Zhang S. Supported Cu catalysts for the selective hydrogenolysis of glycerol to propanediols. *Appl Catal A Gen*. **2009**; *367*(1): 93-98.

23. Corma A., Martinez A., Martinezsoria V., Monton J.B. Hydrocracking of Vacuum Gasoil on the Novel Mesoporous MCM-41 Aluminosilicate Catalyst. *J Catal*. **1995**; *153*(1): 25-

24. Climent M.J., Corma A., Iborra S., Navarro M.C., Primo J. Use of Mesoporous MCM-41 Aluminosilicates as Catalysts in the Production of Fine Chemicals: Preparation of Dimethylacetals. *J Catal*. **1996**; *161*(2): 783-789.

25. Jae J., Tompsett G.A., Foster A.J., Hammond K.D., Auerbach S.M., Lobo R.F., Huber G.W. Investigation into the shape selectivity of zeolite catalysts for biomass conversion. *J Catal*. **2011**; *279*(2): 257-268.

26. Kiricsi I., Flego C., Pazzuconi G., Parker W.O.J., Millini R., Perego C., Bellussi G. Progress toward Understanding Zeolite .beta. Acidity: An IR and 27Al NMR Spectroscopic Study. *J Phys Chem*. **1994**; *98*(17): 4627-4634.

27. Liu D., Yuan P., Liu H., Cai J., Tan D., He H., Zhu J., Chen T. Quantitative characterization of the solid acidity of montmorillonite using combined FTIR and TPD based on the NH3 adsorption system. *Appl Clay Sci*. **2013**; *80–81*: 407-412.

28. Kumari V. D., Prasad B. P., and Rao V. V. Influence of preparative conditions on the structure, acidity and catalytic activity of dealuminated Y zeolite. *Indian Journal of Chemical Technology*. **1996**; *3*, 95-100.

29. Dima E., Rees L.V.C. Temperature-programmed desorption of ammonia from Na- and H-Y zeolites: Desorption energies derived from analyses of t.p.d. profiles by two new methods. *Zeolites*. **1990**; *10*(1): 8-15.

30. Zaki M.I., Hasan M.A., Al-Sagheer F.A., Pasupulety L. In situ FTIR spectra of pyridine adsorbed on SiO2–Al2O3, TiO2, ZrO2 and CeO2: general considerations for the identification of acid sites on surfaces of finely divided metal oxides. *Colloids Surfaces A Physicochem Eng Asp*. **2001**; *190*(3): 261-274.

31. Sushkevich V.L., Ivanova I.I., Taarning E. Mechanistic Study of Ethanol Dehydrogenation over Silica-Supported Silver. *ChemCatChem*. **2013**; *5*: 2367-2373.

32. D'Silva T.D.J., Peck D.W. Convenient Synthesis of Frontalin- 1,5-Dimethyl-6,8-dioxabicyclo[3.2.l]octane. *J Org Chem*. **1972**; *37*(11): 1828-1829.

33. Hagiwara H., Uda H. A facile synthesis of 5-methyl-6,8-dioxabicyclo[3.2.1]octan-3-ones from 4-(t-butyldimethylsiloxy)pent-3-en-2-one and protected [small alpha]-ketols. A synthesis of (+/-)-frontalin. *J Chem Soc Perkin Trans 1*. **1985**;(0): 283-287.

34. Ranney A.P., Ziemann P.J. Kinetics of Acid-Catalyzed Dehydration of Cyclic Hemiacetals in Organic Aerosol Particles in Equilibrium with Nitric Acid Vapor. *J Phys Chem A*. **2016**; *120*(16): 2561-2568.

35. Kuplenieks V.A., Kreile D.R., Slavinskaya V.A., Avots A.A. Hydrogenation of 2,3-dihydropyran to tetrahydropyran. *Chem Heterocycl Compd*. **1982**; *18*(4): 351-354.

36. Wilson C.L. Reactions of Furan Compounds. VII. Thermal Interconversion of 2,3-Dihydrofuran and Cyclopropane Aldehyde1. *J Am Chem Soc*. **1947**; *69*(12): 3002-3004.

37. Inoue Y., Matsumoto N., Hakushi T., Srinivasan R. Photochemistry of 3-oxacycloalkenes. *J Org Chem*. **1981**; *46*(11): 2267-2272.

38. Wang J., Wang M., Xiang J., Xi H., Wu A. Generation of o-quinodimethanes (o-QDMs) from benzo[c]oxepines and the synthetic application for polysubstituted tetrahydronaphthalenes. *Tetrahedron*. **2015**; *71*(40): 7687-7694.

39. Sekizawa K., Miyake T., Nakano M., Hironaka T., Fujii S., Kikuchi M. Catalytic Reactions on Zeolites Ion-Exchanged with Alkali Cations. In: Inui T, ed. *Successful Design of Catalysts: Future Requirements and Development*. New York, NY: Elsivier Science Publishers; 1989:203-217.

40. Ziólek M., Szuba D., Leksowski R. The Role of Cations in the Reaction Between Alcohols and Hydrogen Sulfide on X-Type Zeolites. In: Grobet PJ, Mortier WJ, Vansant EF, Schulz-Ekloff G, eds. *Innovation in Zeolite Materials Science*. Vol 37. Studies in Surface Science and Catalysis. Elsevier; 1988:427-434.

41. Jacobs P.A., Tielen M., Uytterhoeven J.B. Active sites in zeolites: Part 6. Alcohol dehydration over alkali cation-exchanged X and Y zeolites. *J Catal*. **1977**; *50*(1): 98-108.

42. Silverstein R.M., Webster F.X., Kiemle D. *Spectrometric Identification of Organic Compounds*. 7th edition. Wiley; **2005**.

43. Fisher J. *Modern NMR Techniques for Synthetic Chemistry*. Taylor & Francis; **2014**.

44. Falcone D.D., Hack J.H., Davis R.J. Aqueous-Phase Hydrogenation of Saturated and Unsaturated Ketones and Aldehydes over Supported Platinum–Rhenium Catalysts. *ChemCatChem*. **2016**; *8*(6): 1074-1083.

Chapter 4. Auto-catalytic Hydration of Dihydropyran to 1,5-Pentanediol Precursors via in situ Formation of Liquid- and Solid-phase Acids

4.1 Introduction

Lignocellulosic biomass has great potential as a renewable feedstock for the production of fuels[1–3] and chemicals[4–7] due to its relative abundance and low cost.[8] Synthesis of high-value commodity chemicals from lignocellulosic biomass improves the economics of biomass conversion technologies, including biofuel production. One class of value-added chemicals are α,ω-diols, such as 1,5-pentanediol (1,5-PD) and 1,6-hexanediol (1,6-HD). α,ω-diols are utilized as monomers for polyurethane and polyester production. Due to the lack of readily available C5 streams from petroleum, 1,5-PD is currently only produced at 3,000 tons/year, mainly as a byproduct of 1,6-HD synthesis from adipic acid.[9] Alternatively, biomass feedstocks are capable of forming large amounts of C5 chemicals from the hemicellulose fraction, which can be hydrolyzed to xylose and further dehydrated to the platform chemical furfural.[10,11]

We recently demonstrated a 3-step process for the production of 1,5-PD from furfural-derived tetrahydrofurfuryl alcohol (THFA) as shown in Figure 4.1.[12,13] In the first reaction step, THFA is dehydrated in the gas phase over γ-Al_2O_3 to dihydropyran (DHP).[14,15] The DHP is then hydrated with H_2O in the liquid phase to form 2-hydroxytetrahydropyran (2-HTHP) without the addition of any external catalyst.[12] The 2-HTHP undergoes ring-opening tautomerization to form 5-hydroxyvaleraldehyde (5HVal), which can be hydrogenated into 1,5 PD over Ru catalysts. The

The content of this chapter is largely adapted from the following reference, Copyright (2017), reproduced by permission of the American Chemical Society:

Kevin J. Barnett, Daniel J. McClelland, George W. Huber. Autocatalytic hydration of dihydropyran to 1,5-pentanediol precursors via in situ formation of liquid- and solid-phase acids.. *ACS Sust. Chem. & Engr*. **2017**. *5* (11), 10233-10230.

* KJB performed experiments. DJM performed NMR. *

overall yield of all reaction steps is 90% and we have previously reported a rigorous technoeconomic model for large scale production of 1,5 PD.[12] The current paper focuses on the reaction chemistry and kinetics of the DHP hydration step.

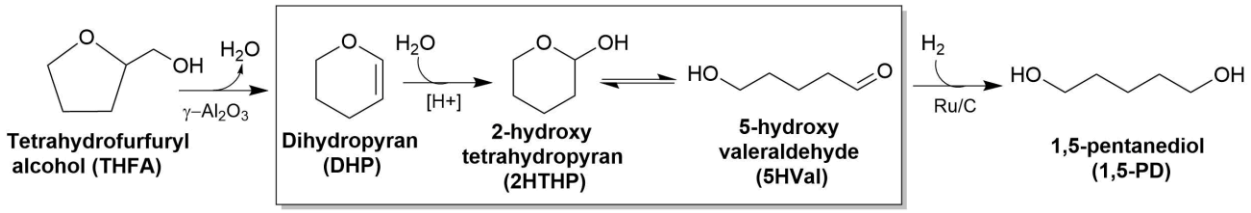

Figure 4.1 Dehydration-hydration-hydrogenation (DHH) pathway for conversion of tetrahydrofurfuryl alcohol (THFA) into 1,5-pentanediol (1,5-PD).

DHP hydration is auto-catalyzed by carboxylic acids formed *in situ* during the reaction. Acid-catalyzed reactions can be auto-catalyzed by acidic reactants or reaction products. One example is the esterification of organic acids with alcohols in the absence of water.[16–18] In this reaction, esterification is catalyzed by the carboxylic acid reactant without the addition of any acid catalyst at elevated temperatures. Another class of auto-catalyzed reactions is the hydrolysis of polymer chains containing acid functionality. In these reactions, acidic monomers such as lactic acid,[19,20] malic acid,[21] or terephthalic acid[22] are produced during hydrolysis and re-catalyze cleavage of the polymer chain. Organosolv delignification of raw biomass feedstocks is another example of auto-catalytic hydrolysis.[23–27] Here, raw biomass is subjected to elevated temperatures in an ethanol-water solvent mixture with no catalyst added. Acetic acid formed via the cleavage of the acetyl groups of xylans provides acid character which catalyzes further hydrolysis.[28] In the present work, we report the auto-catalytic hydration of DHP by carboxylic acids formed at the reaction onset. While carboxylic acids have been shown to catalyze hydration reactions in limited

cases,[29] to our knowledge the present work is the first to report an auto-catalyzed hydration reaction.

Hydration of DHP in water without any added catalyst is contrary to most early works which employed HCl as a catalyst.[14,30,31] Eliminating HCl represents a large improvement from a process perspective, as the neutralization and separation of homogeneous acids from solution adds to the processing costs.[32,33] However, little is known mechanistically as to why HCl is not required to catalyze DHP hydration. Additionally, while the etherification of the 2-HTHP has been briefly studied in the literature,[34,35] no analysis of the dimers formed in the context of DHP hydration has been performed. This is an important consideration, as the dimers form in considerable amounts at all reaction conditions tested and the identity of which are critical for the subsequent upgrading to 1,5-PD. The objective of this paper is to study the kinetics of the auto-catalytic hydration of DHP and to study in more depth the by-products that are formed in this reaction.

4.2 Experimental Methods

DHP (95%, AK Scientific) was used as received. Argon (Airgas, Industrial Grade) and UHP Helium (Airgas, 99.999%) were used as inert gases for reaction studies.

4.2.1 Batch Reaction Studies

Batch reactor experiments were performed in 45mL or 75mL Parr Hastelloy autoclaves. After adding a magnetic stir bar (1" (2.54cm) length; $^{5}/_{16}$" (0.79cm) diameter), DHP was added to DI water up to 20wt% in all experiments. All experiments in which kinetic data were obtained were carried out in a 75mL Parr reactor with 30g of feedstock (6g DHP/24g DI water) due to better mixing conditions. Liquid feed volume and reactor geometry are important considerations for the proper mixing of the organic and aqueous phases in batch mode. The 75mL reactor with 30g of feedstock resulted in a reactor H/D ratio and liquid feed H/D ratio of 1.83 and 0.83, respectively.

Stir rate did not affect hydration rates at these conditions (see Figure 4.3). The temperature effects and pH value experiments (see Table 4.1 and Figure 4.9) were performed in a 45mL Parr reactor with 20g of feedstock (4g DHP/16g DI water) and a stir rate of 800 rpm. In all batch reactions, the reactor was purged with Ar or He two times before pressurizing the reactor to 20.7-34.5 bar, pressures at which issues related to the high volatility of DHP were avoided. Reactors were heated to the reaction temperature at 4˚C/min. Zero time was defined as the point at which the reactor reached the final reaction temperature. Due to the fast temperature ramp and low reaction temperatures used, the heat up time was determined to have a negligible effect on the overall reaction rate and was not considered in the kinetic analyses. After holding for the desired reaction time, reactors were quenched in an ice water bath. The procedure for the experiment probing the reactivity of the 200˚C product filtrate (see Figure 4.9B) was identical to that above with the exception that the solvent was comprised of a 50:50 volume ratio of DI water and the 200˚C reaction filtrate after vacuum filtration to remove all solid matter.

Product carbon yields were calculated on a total mol C basis according to Equation 1. Product concentrations (mol/L) were measured by GC, "A" stands for the aqueous-phase, and the Volume_A (L) is the aqueous-phase volume of the product. The 2-HTHP production rate was calculated according to Equation 2.

$$Yield\ (C\%) = \frac{mol\ C\ product}{mol\ C\ DHP\ feed} = \frac{(\frac{mol\ product}{L})_A \cdot Volume_A(L) \cdot \left(\frac{mol\ C\ product}{mol\ product}\right)}{mol\ C\ DHP\ feed} \quad (1)$$

$$Reaction\ Rate\ \left(\frac{\mu mol}{min \cdot L}\right) = \frac{(\frac{mol\ 2HYTHP\ product}{L})_A \cdot Volume_A(L) \cdot \left(\frac{1E6\ \mu mol}{mol}\right)}{Reaction\ time\ (\text{min}) \cdot Feed\ Volume\ (L)} \quad (2)$$

4.2.2 Continuous Flow Reactor Setup

The continuous reactor setup is displayed in Figure 4.2. A 24 inch (61cm) long reactor tube (316SS, 1/4 inch (0.635cm) O.D., 0.18 inch (0.457cm) I.D.) was filled with inert glass beads (Sigma Aldrich, unwashed, 30-40 US sieve), held at each end by quartz wool (Leco, fine). The reactor tube was contained inside a tube furnace equipped with aluminum filler rods for uniform heat distribution. Both ends of the furnace were sealed with quartz wool. The reactor was pressurized with Ar gas to 34.5 bar. A back-pressure regulator at the reactor system outlet was set at 34.5 bar to hold at pressure while allowing gas flow through the system. The reactor furnace controller was set to the desired reaction temperature. Two separate liquid HPLC pumps (Varian ProStar 210 Series) were used due to the immiscibility of DHP in water. DHP and DI water were flowed separately at a 1:4 mass ratio (20wt% DHP) into a 1/4 inch (0.635cm) tee junction where they mixed. The DHP:H_2O mixture flowed upwards where it was combined with Ar flow at 40 mL/min sccm. Inert Ar was flowed for gas phase analysis; an experiment with no Ar flow confirmed that the gas flow did not have any noticeable effects on the DHP hydration rate (i.e. improved mixing). Liquid products accumulated in a stainless-steel gas–liquid separator (300 mL) at the top of the reactor. Liquid samples were collected by first closing the inlet and outlet ball valves of the reactor to isolate the system. The outlet needle valve at the bottom of the liquid collection vessel was opened to collect liquid product into a container for filtration and analysis. Inlet and outlet ball valves were re-opened to continue flow through the reactor.

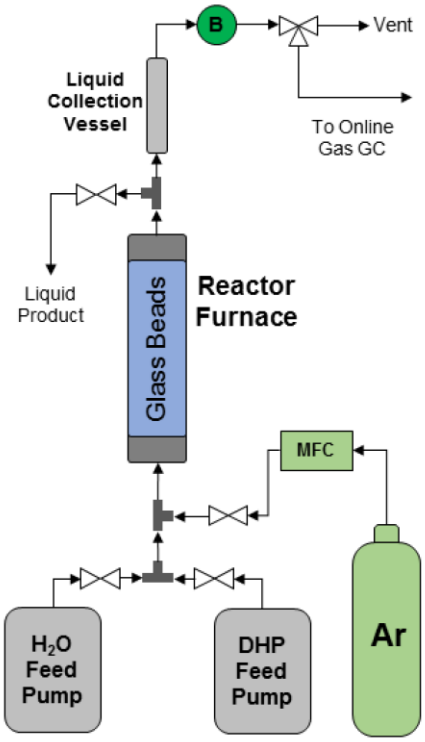

Figure 4.2 Schematic of dual-pump continuous flow reactor employed for DHP hydration flow studies. MFC: Mass-flow controller, B: Back-pressure regulator.

4.2.3 Continuous Reaction Studies

A dual-pump upflow reactor was employed for continuous flow reaction studies (Figure 4.2). DHP and DI water were flowed in a 1:4 mass ratio (20wt% DHP) through the reactor tube filled with inert glass beads (Sigma Aldrich, unwashed, 30-40 US sieve). The glass beads filled a reactor length of 19 3/4 (50.2cm), with a measured void volume of 3.3 cm^3 [void fraction(ε) = 0.40].

In the continuous flow reactor system, the initial time-on-stream (TOS = 0) is defined as the first steady state data point for activation rate experiments (see Figure 4.12). This was normally taken after 8-14h of operation. For acidic coke activation experiments (see Figure 4.13), the total liquid flowrate was 0.037mL/min. Coke was formed by flowing 20wt% DHP/H_2O at 0.23 mL/min

at 140˚C and 34.5 bar for 20-24h while flowing Ar at 40 mL/min. For experiments employing a drying step, the reactor was depressurized to 1 atm and held at 140˚C in 100 mL/min Ar flow for >4h. Prior to restarting the reaction, the reactor was repressurized to 34.5 bar Ar and cooled to the desired reaction temperature. The coke formation experiment at 180˚C resulting in 28x hydration rate increase underwent three 180˚C coke formation treatments at 50wt%DHP/H_2O (0.083 mL/min) for >6h each interspersed with three 140˚C drying steps identical to those described above.

Product carbon yields were calculated on a total mol C basis as shown in Equation 3. The product concentration (mol/L) was measured by GC. The reaction rate was calculated according to Equation 4.

$$Yield\ (C\%) = \frac{mol\ C\ product}{mol\ C\ DHP\ fed} = \frac{(\frac{mol\ product}{L})_A \cdot Volume_A(L) \cdot \left(\frac{mol\ C\ product}{mol\ product}\right)}{DHP\ flowrate\left(\frac{mol\ C}{min}\right) \cdot Total\ sample\ time\ (min)} \quad (3)$$

$$Reaction\ Rate\ \left(\frac{\mu mol}{min \cdot L}\right) = \frac{(\frac{mol\ 2HYTHP\ product}{L})_A \cdot Volume_A(L) \cdot \left(\frac{1E6\ \mu mol}{mol}\right)}{Total\ sample\ time\ (\text{min}) \cdot Void\ Volume\ (L)} \quad (4)$$

4.2.4 Product Analysis

GC. Reaction product solutions were placed in a separation funnel for 10 minutes. The volumes of the organic and aqueous phases were recorded by funneling each phase into a graduated cylinder. The aqueous and organic products were filtered with 0.22µm polyethersulfone and polytetrafluoroethelyne filter membranes, respectively, before analysis. Liquid products were injected into a Shimadzu Gas Chromatograph with a Flame Ionization Detector (FID). The FID and injection port temperatures were 240 °C. The injection volume was 1 µL and a split ratio of 100 was used. The GC column was a Restek RTX-VMS capillary column (length: 30 m, ID: 0.25

mm, film thickness: 1.4 μm). The column temperature was held at 40°C for 1 min, ramped at 20°C/min to 240°C, and held at 240 °C for 13 min.

GC-MS. Mass spectrometry of product solutions was performed on a two-dimensional (2D) gas chromatography–mass spectroscopy (GC×GC–MS) with both a FID (Agilent, 7890B) and a mass selective detector (MSD; Agilent, 5977A). A flow modulator (CFP; Agilent, G3487A) was installed to make a GC×GC system. Two capillary columns, DB-17 (Agilent, Catalog No. 121-1723) and CP-Sil 5 CB (Agilent, Catalog No. CP7700), were set up in series with the CFP for 2D separation. H_2 carrier gas was flowed at 0.7 mL/min and 25 mL/min through the first and second dimension columns, respectively. In all experiments, both the first and second dimensions were operated in constant flow mode. Ion fragment patterns were compared to known patterns in the NIST mass spectrometry database for product identification.

NMR. The 200˚C hydration product was characterized by NMR with quantitative ^{13}C, ^{13}C DEPT-135, 2D HSQC, and 2D HMBC experiments. D_2O was added to the sample (1:9 v/v). The ^{13}C NMR experiments were acquired on a Bruker Biospin (BFillerica, MA) AVANCE III 500 MHz spectrometer fitted with a DCH (^{13}C-optimized) cryoprobe.

Bruker standard pulse sequence ‘zgig30’ was used for the quantitative ^{13}C experiments with the following parameters: an inter-scan relaxation delay of 12 s, a sweep width of 240 ppm centered at 110 ppm, acquiring 59,520 data points with an acquisition time of 1 s, and 128 scans. The ^{13}C DEPT-135 experiments used the Bruker standard pulse sequence ‘deptsp135’ with the following parameters: an inter-scan relaxation delay of 2 s, a sweep width of 240 ppm centered at 110 ppm, acquiring 59,520 data points with an acquisition time of 1 s, and 128 scans. Mestrelab Research’s MestReNova software was used to process the spectra and the spectra were referenced to a TMS internal standard at 0 ppm.

The 2D NMR (HSQC and HMBC) experiments were carried out on a Bruker Biospin (Billerica, MA) AVANCE III HD 600 MHz spectrometer fitted with a TCI-F cryoprobe. Bruker standard pulse sequence 'hsqcedetgpsisp2p3' was used for the HSQC experiment with the following parameters: 14 ppm sweep width in F2 (^{1}H), centered at 4.7 ppm, acquiring 3,366 data points, 240 ppm sweep width centered at 110 ppm in F1 (^{13}C) acquiring 1,309 increments, 4 scans per increment, and a 2.0 s relaxation delay. Bruker standard pulse sequence 'hmbcgplpndprqf' was used for the HMBC experiment with the following parameters: 14 ppm sweep width centered at 4.7 ppm in F2 (^{1}H) acquiring 3366 data points, 240 ppm sweep width centered at 110 ppm in F1 (^{13}C) acquiring 1309 increments, 4 scans per increment, and a 2.0 s relaxation delay. Bruker's Topspin 3.5 software was used to process spectra.

pH Meter. For reactions in which the aqueous phase pH was tested, products were syringe filtered until completely clear to negate any effects of solid material on the pH. A pH meter (Ohaus ST20) was calibrated immediately before each analysis. pH values were evaluated directly after the completion of each reaction. Product solutions were stirred at 125 rpm on a stir plate with the pH probe slightly submerged in the solution. pH values were given 5 minutes to equilibrate before recording the final value.

TOC. A total organic carbon analyzer (TOC; Shimadzu TOC-V_{CPH}) with a solid sample module (Shimadzu SSM-5000A) was used to quantify the total carbon content of the spent glass beads (see Table 4.3). Spent beads (2.5g) were heated to 900°C to combust all carbonaceous material, which was catalytically oxidized to CO_2 and quantified with an online non-dispersive infrared (NDIR) detector. Spent beads were taken from the center 6 inches (15.2cm) of tubing surrounding the furnace thermocouple, where the highest degrees of coke formation likely occurred.

4.3 Results and Discussion

4.3.1 Batch Reactor Studies

DHP was hydrated in a batch reactor at 20 wt% DHP without the addition of any catalyst. Due to its limited solubility in water (<1wt%), DHP forms an insoluble layer on top of water. The products formed in the reaction (primarily 2-HTHP) enter the aqueous phase until there is a single aqueous phase at total DHP conversion. Figure 4.3 shows the rate of 2-HTHP formation as a function of stirring speed. As can be seen, the rate of 2-HTHP formation is not dependent on stirring speeds ranging from 250-1000 rpm, indicating that no transport restrictions exist at these conditions. The pressure of the inert Ar gas was also shown to have a negligible effect on the DHP hydration rate.

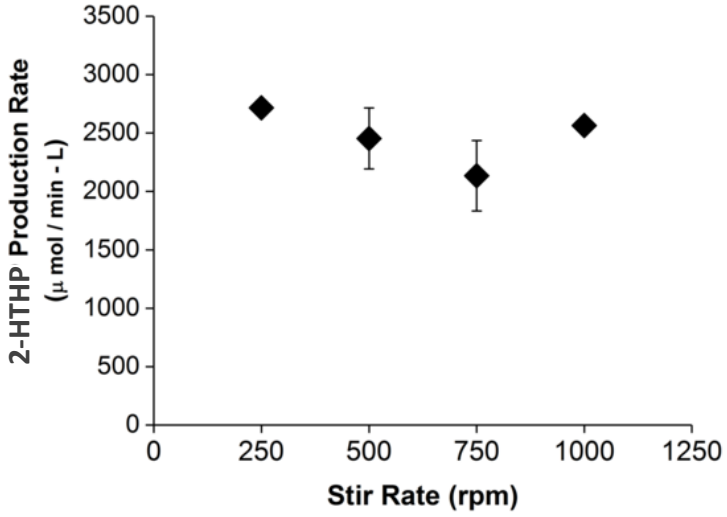

Figure 4.3 2-HTHP production rate vs. stir rate for 20wt% DHP hydration in DI water in a batch reactor (T: 50˚C, P: 34.5 bar Ar, t: 2h)

The rate of 2-HTHP formation from 25 to 62.5˚C was obtained for the hydration of 20wt% DHP in water in the batch reactor with no catalyst addition. Kinetic data could not be obtained above 62.5˚C due to high reaction rates and conversions outside the kinetic regime (>30%). Figure

4.4 shows the 2-HTHP production rate in an Arrhenius plot. The apparent activation energy for DHP hydration is 78.8 kJ/mol (standard deviation = 1.5 kJ/mol). The linearity of the Arrhenius plot suggests the same type of active site is catalyzing the reaction over the range of temperatures tested.

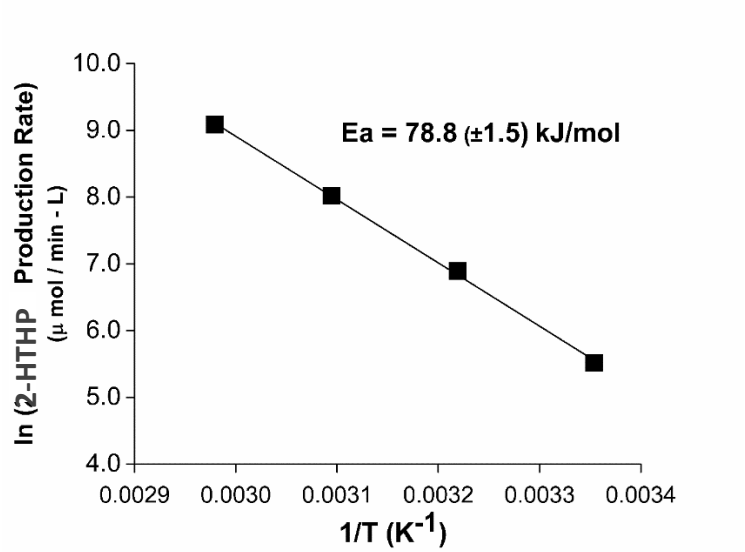

Figure 4.4 Auto-catalytic hydration of 20wt% DHP in DI water in a batch reactor (T: 25-62.5˚C, P: 34.5 bar Ar, stir rate: 750rpm).

Table 4.1 shows the effect of temperature on the product distribution and Figure 4.5 shows the proposed reaction pathway. 2-HTHP, 2-tetrahydropyranyl ether (2,2'-HTHP), and 5-tetrahydropyran-2-yloxypentanal (THP-oxypentanal) were previously shown to convert to 1,5-PD in 97% yields during subsequent hydrogenation and are reported as 1,5-PD precursors.[12] 2,2'-HTHP and THP-oxypentanal were identified by GC-MS. These product yields were calculated using a GC response factor (M/Area) half that of 2-HTHP, due to the lack of standards for these molecules. The carbon balance is defined as the total carbon accounted for in the GC, including estimated carbon yields of unidentified byproducts, divided by the feed carbon content. Unidentified byproducts comprised less than 3C% for all reactions presented. All reactions were run to complete DHP conversion except the 60˚C reaction for 2h (Entry 1). At temperatures

≤100˚C the 1,5-PD precursor selectivity was near quantitative with 2-HTHP and C10 dimers (2,2'-HTHP and THP-oxypentanal) formed at roughly a 12:1 ratio. The C10 dimers are made via etherification of the 2-HTHP and 5-hydroxyvaleraldehye (5HVal) monomers (see Figure 4.5).[34]

Table 4.1 Temperature effects on product carbon yields for DHP hydration in DI H_2O in a batch reactor.

Temperature (°C)	Reaction Time (h)	2-HTHP	2,2'-HTHP	THP-oxypentanal	Total 1,5-PD Precursors	High T Dimer	Carbon Balance
60[a]	2[a]	21.1%	0.3%	0.4%	**21.8%**	0.0%	-
60	12	90.6%	2.5%	5.2%	**98.3%**	0.0%	100.0%
100	2	92.2%	2.3%	3.8%	**98.3%**	0.0%	99.9%
140	2	84.3%	1.1%	5.2%	**90.6%**	1.8%	94.3%
180	2	59.5%	0.6%	1.9%	**62.0%**	7.0%	70.8%
200	2	14.8%	0.1%	0.3%	**15.1%**	1.8%	19.2%

* DHP Concentration: 20wt%, P: 20.7 bar Ar, Stir rate: 800rpm [a] Total yield = 24.4%

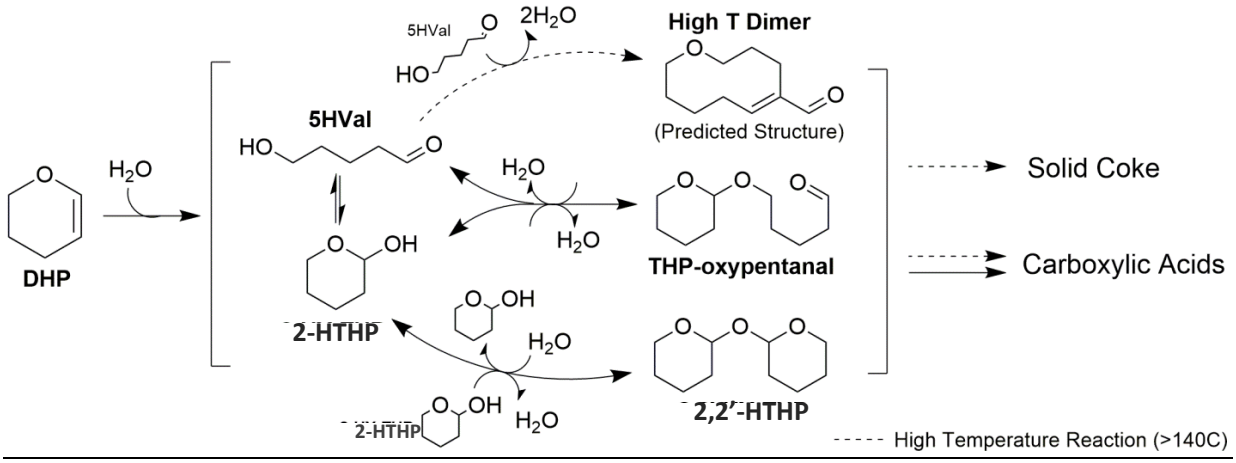

Figure 4.5 Proposed reaction pathway of auto-catalytic hydration of DHP. DHP: dihydropyran, 2-HTHP: 2-hydroxytetrahydropyran, 5HVal: 5-hydroxyvaleraldehyde, 2,2'-HTHP: 2-tetrahydropyranyl ether, THP-oxypentanal: 5-tetrahydropyran-2-yloxypentanal.

Both dimers formed at low temperatures (2,2'-HTHP and THP—oxypentanal) comprise a tetrahydropyranyl ring. We hypothesize that the tetrahydropyranyl ring functionality is necessary for etherification at low temperatures. This is due to the stability of the oxocarbenium transition state formed by the dehydration of 2-HTHP prior to SN1 substitution to the ether product (Figure 4.6).[35] The result is the more facile etherification at the hemiacetal -OH position of 2-HTHP than the unfavorable etherification at the terminal -OH group of 5HVal (Figure 4.6). This hypothesis also explains why 2,2'-HTHP is produced in lower amounts than THP-oxypentanal: 2,2'-HTHP contains two of the weaker hemiacetal bonds versus the one hemiacetal bond in THP-oxypentanal and is more easily hydrolyzed into its monomers. It should be noted that increased concentration of organics in water (e.g. 50wt% DHP) greatly increases the amount of dimer formation. This is due to a shift in equilibrium towards the dimers as there is less water available for hydrolysis of the ether bond (Figure 4.5).

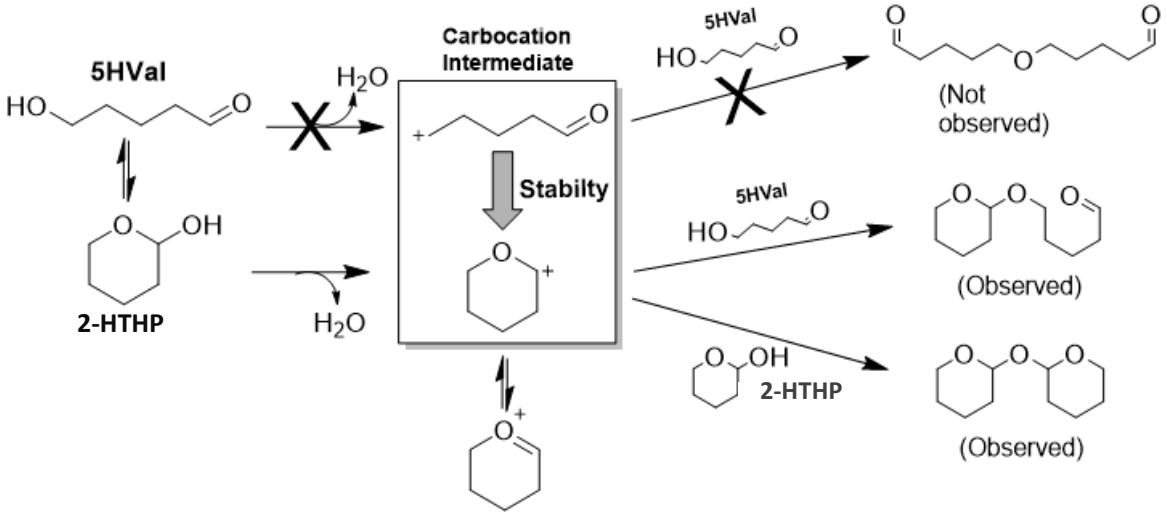

Figure 4.6 Effect of carbocation stability on etherification product distribution.

At temperatures above 140˚C, higher amounts of undesired byproducts are formed. At 140˚C, the carbon balance decreases to 94.3% and a C10 species - termed "High T Dimer"- begins

to appear in the GC. Product yields further decrease at temperatures above 180˚C, with a further decrease in yields and a large amount of visible solid coke formed in the reactor at 200˚C. The identity of the dimer formed at high temperatures was probed using quantitative ^{13}C NMR spectroscopy. The 200˚C DHP hydration product (Table 4.1, Entry 6) was vacuum filtered to remove any solid matter before performing NMR analysis (Figure 4.7). The 2-HTHP and dimer NMR peak locations were confirmed by comparing the relative peak areas of the quantitative ^{13}C NMR spectrum to the GC peak areas of the same sample. Ten dimer peaks were observed in the NMR, corresponding to all ten carbon atoms in the dimer molecule. Noteworthy carbon peaks include an aldehyde carbon (199.17 ppm), two alkene carbons (142.39 ppm and 160.47 ppm), and two ether carbons (61.37 and 61.51 ppm) with the other five being aliphatic carbons. DEPT-135 (Figure 4.7B), HSQC, and HMBC NMR analyses were performed on the sample to help determine the C-C bond coordination and the relative location of specific carbon atoms within the molecule.

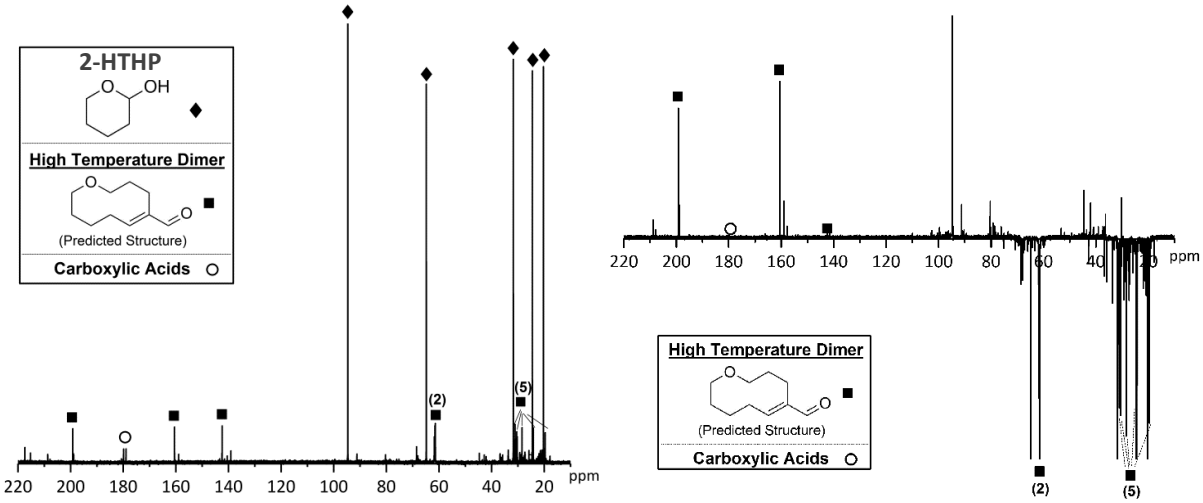

Figure 4.7 A) Quantitative ^{13}C and B) DEPT-135 ^{13}C NMR spectra of product solution from 20wt% DHP hydration in DI water at 200˚C (Table 4.1, Entry 6).

NMR analyses suggest the molecule contains alkene and ether functionality inside a 10-member ring with an aldehyde substituent group. Additionally, GC-MS analysis shows the dimer has a molecular weight of 168 g/mol. The predicted dimer species portrayed in Figure 4.8 has this exact mass and structure. This molecule can be formed via the aldol condensation of two 5HVal molecules, followed by cyclodehydration of the terminal alcohol groups (Figure 4.8). In fact, aldol condensation[36] and cyclodehydration[37] reactions can both occur at these reaction conditions.

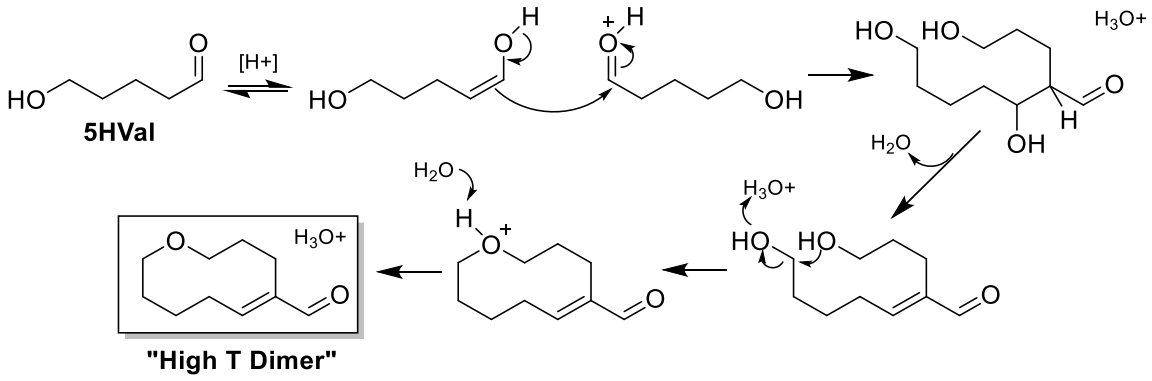

Figure 4.8 Proposed mechanism of "High T Dimer" formation via aldol condensation-cyclodehydration of 5-hydroxyvaleraldehyde (5HVal).

The pH values of the batch hydration products shown in Table 4.1 were tested to quantify any change in the solution acidity during the reaction. From Figure 4.9A it can be seen that the pH values for all reactions from 60-180˚C resulted in a product pH value near 3.4. This is compared to a pH value of 7.01 found for a blank reaction with DI water at 60˚C for 2h, ruling out any reactor effects on the acidity. A reaction with pure DHP (no water) at 60˚C for 2h also showed no pH change or product formation, demonstrating water is required for any DHP conversion and subsequent drop in pH. A pH of ~3.4 is indicative of carboxylic acid formation based on the pKa of carboxylic acids (e.g. acetic acid = 4.76) and the estimated concentration range for acids formed in the reaction. NMR analysis of the 200˚C reaction product shows two smaller carbon peaks at

178.94 and 179.85 ppm, indicative of carboxylic acids (Figure 4.7A). Thus, from the pH values and NMR spectrum, it can be concluded that the high temperature dimer contains only aldehyde functionality and is an inert byproduct of DHP hydration at high temperatures, while carboxylic acids formed in smaller amounts are responsible for the increase in acidity during the reaction. Therefore, DHP hydration in water without an added catalyst is not a homogeneous reaction, but a self-catalyzed reaction utilizing carboxylic acids. To test this hypothesis, the 200˚C product solution (Table 4.1, Entry 6) was added to DI water in a 50:50 volume ratio and used as the solvent for hydration of 20wt% DHP in a batch reactor. Figure 4.9B shows that the 2-HTHP yield with the 200˚C product added to the reaction solvent was 4 times higher than with the same reaction conditions in pure DI water.

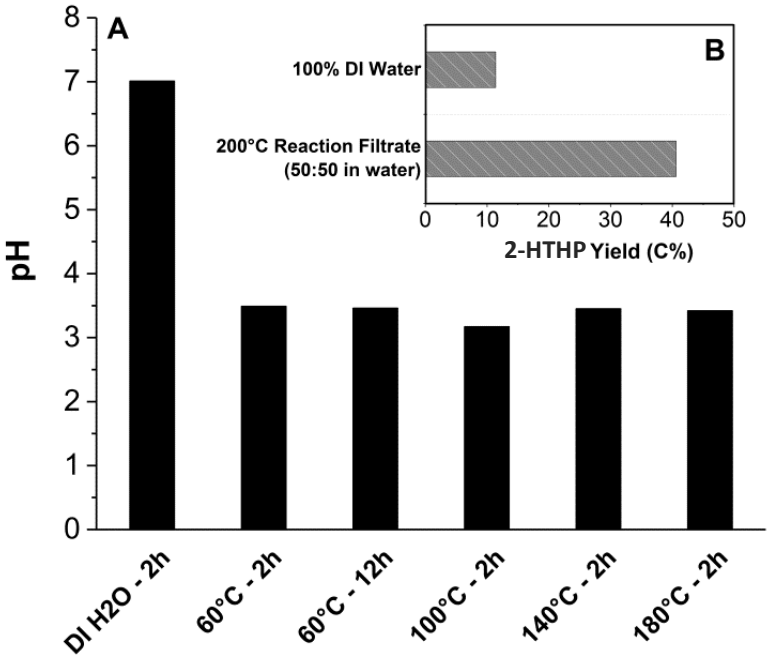

Figure 4.9 A) pH measured after batch hydration of 20wt% DHP in DI water at 20.7 bar He and 800 rpm stir rate at different temperatures and reaction times and B) 2-HTHP yields after batch reactions (20wt% DHP/H_2O, 2h, 50˚C, 34.5 bar Ar, 750 rpm) with a pure DI water solvent and a 50:50 vol% mixture of DI water and product filtrate from the 200˚C batch reaction (Table 4.1, Entry 6).

The increase in solution acidity due to the formation of carboxylic acids increases the rate of DHP hydration, creating an auto-catalytic reaction. The pH values of all batch reactions in Table 1 were nearly identical, even for the 2h reaction at 60˚C which only went to ~25% conversion (Figure 4.9). Together these observations suggest the carboxylic acid concentration in solution does not greatly increase with increasing temperature and, more importantly, carboxylic acids are present over the whole range of reaction conditions tested, even near the reaction onset.

The initiation period of the reaction was studied in more detail in an attempt to probe the time scale, quantity, and identity of any carboxylic acids formed. In this vein, several DHP hydration reactions were performed at 25˚C; a temperature at which low hydration rates allowed for a closer observation of the initiation period. The pH was tested for each reaction product. From Figure 4.10, it can be seen that there is an initiation period of ~4h in which the hydration rate is low, after which the hydration rate increases by roughly 2x (shown in the form of 2-HTHP concentration). The hydration rate increase correlates with the rise in hydronium ion concentration demonstrating that DHP hydration is an auto-catalytic, acid-catalyzed reaction.

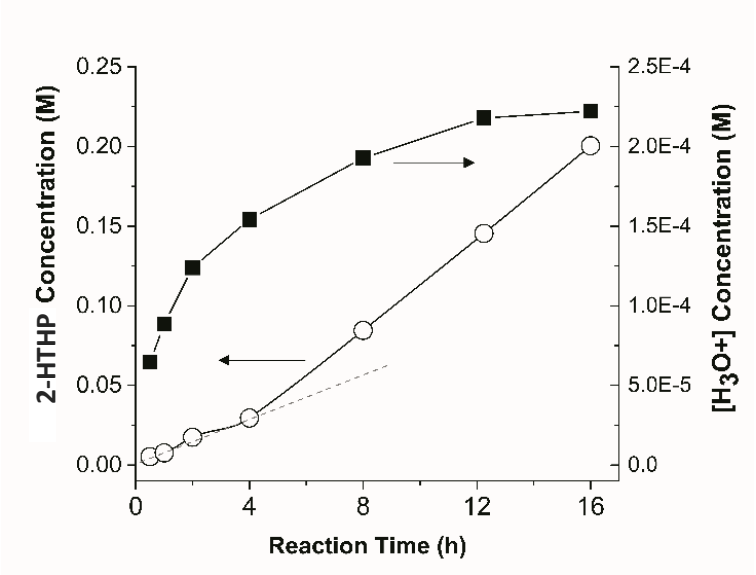

Figure 4.10 2-HTHP (○) and H_3O+ concentrations (■) as a function of reaction time for separate batch hydrations of 20wt% DHP in DI water (T: 25˚C, P: 34.5 bar Ar, stir rate: 750 rpm).

The increase in solution acidity tracked with the formation of a small amount of byproducts. GC-MS analysis and a GC standard were able to show that two of these byproducts were likely 5-hydroxy-valeric acid (5-HY-VA) and delta-valerolactone (DVL). The 5-HY-VA and DVL species could not be quantified as they are in equilibrium in water at these conditions, but their respective GC retention times were confirmed by using standards (Figure 4.11). Because the decrease in solution pH correlated with the formation of these species, the increase in solution acidity could likely be attributed to the formation of 5-HY-VA. While only a very small amount of 5-HY-VA is likely produced (<0.2C% yields), enough forms to lower the solution pH and drive the hydration of DHP. The hydronium ion concentrations level off as 2-HTHP yields continue to increase, explaining the consistent pH values at higher temperatures and DHP conversions (Figure 4.9A). Although the initiation period lasts up to 4h at 25°C, 2-HTHP yields never exceed 1C% throughout this period. Thus, the initiation period likely occurs at very small time scales at higher reaction temperatures.

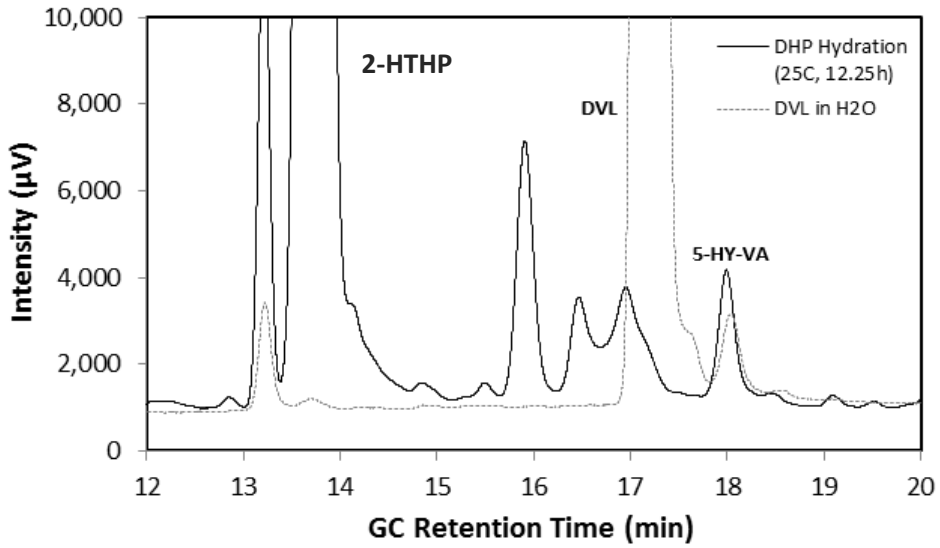

Figure 4.11 Gas chromatogram of a DVL standard in water (dashed lines) and the product of 20wt%DHP/H_2O hydration at 25°C for 12.25h (see Figure 4.10). The DVL and 5-HY-VA are in equilibrium at these conditions. Other hydration byproducts can be seen at retention times between 16 and 17 minutes.

4.3.2 Continuous Flow Reactor Studies

Figure 4.12 shows the 2-HTHP yields as a function of TOS for 20wt% DHP hydration in a continuous flow reactor. The 2-HTHP yields increased with TOS for all reaction temperatures tested. This is due to the formation of acidic humins in the reactor, of which even a small amount (as low as 0.05-0.25wt% from Table 4.3) deposited on the inert glass beads can have a large effect on the hydration rate. The activation rate of DHP hydration increased with reaction temperature.

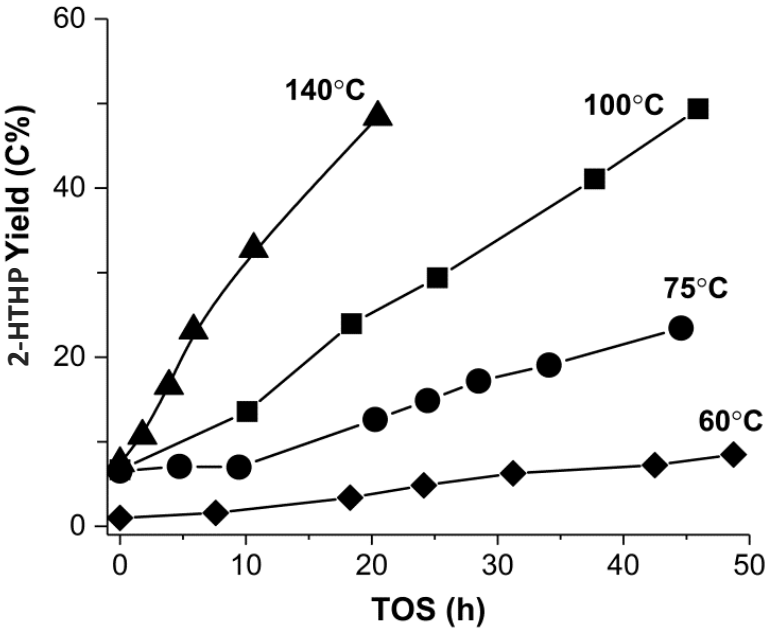

Figure 4.12 2-HTHP yields vs. time-on-stream (TOS) for the auto-catalytic hydration of DHP in a continuous flow reactor packed with inert glass beads at various reaction temperatures. Feed: 20wt% DHP/H_2O, P: 34.5 bar, Ar flowrate: 40mL/min. Total feed flowrates: 60°C reaction = 0.037 mL/min ; 75°C reaction = 0.037mL/min ; 100°C reaction = 0.071mL/min ; 140°C reaction = 0.229mL/min.

Activation rates for each reaction were found by fitting the first 3-4 data points with 1st and 2nd order activation models (Equations 5 and 6), with 'a' defined as the ratio of the rate at reaction time 't' to the initial rate.[38] The data fit the 1st order activation model better than the 2nd order model (R^2 = 0.989 and R^2 = 0.967, respectively). 1st order activation constants and the percent

rate increase per hour for each reaction temperature are displayed in Table 4.2. The activation rate increases with temperature, with the exception of the rate at 60˚C being higher than that at 75˚C. A large increase in activation rate was observed from 100˚C to 140˚C. This is the temperature range in which coke formation was observed in the batch experiments as seen by a decreased carbon balance (Table 4.1). In the continuous flow reactor the solid coke adsorbs on the surface of the glass beads and stays in the reactor, further increasing the hydration rates at high temperatures.

$$\frac{da}{dt} = \beta_1 \cdot a \quad ; \quad a = e^{\beta_1 \cdot t} \tag{5}$$

$$\frac{da}{dt} = \beta_2 \cdot a^2 \quad ; \quad \frac{1}{a} = 1 + \beta_2 \cdot t \tag{6}$$

Table 4.2 Initial rate of activation vs. temperature for 20wt% DHP hydration in a flow reactor

Temperature (˚C)	1st Order Activation Rate (β_1)	Rate increase per hour (%/h)
60	0.067	6.8%
75	0.056	5.6%
100	0.070	7.2%
140	0.196	21.7%

The activity of the solid coke formed at high temperatures was tested for DHP hydration. 20wt% DHP/H_2O was flowed through the continuous reactor at 75˚C to establish a baseline hydration rate (Figure 4.13A). The reactor was then brought to 140˚C for 20h while continuously flowing 20wt% DHP in water to form solid coke in the reactor bed. The 2-HTHP yields increased 6.5 times during the 20h hold at 140˚C – indicative of an active coke formation. Upon returning the reaction temperature to 75˚C without any reactor drying step, the 2-HTHP yields increased by

37% (Figure 4.13A). This increase in activity was much lower than the increase while holding at 140˚C, meaning that much of the activity gain during the high temperature treatment was not retained upon lowering the temperature. In Figure 4.13B, it can be seen that employing a drying step led to a 144% increase in 2-HTHP yields. Drying the reactor before lowering the temperature helped to retain more of the active coke formed at 140˚C. This same procedure was applied to a 100˚C reaction but with two high temperature treatment/drying steps. This led to an increase in 2-HTHP + dimer yields from 15.6C% to >98C% (Figure 4.13C). In addition to showing a hydration rate increase of at least 650%, this also demonstrates the ability of the solid coke-catalyzed hydration to give near 100% yields to 1,5-PD precursors. In a separate experiment, a 180˚C high temperature treatment with 50wt% DHP/H_2O was shown to increase the hydration rate by 28x for a 50˚C reaction.

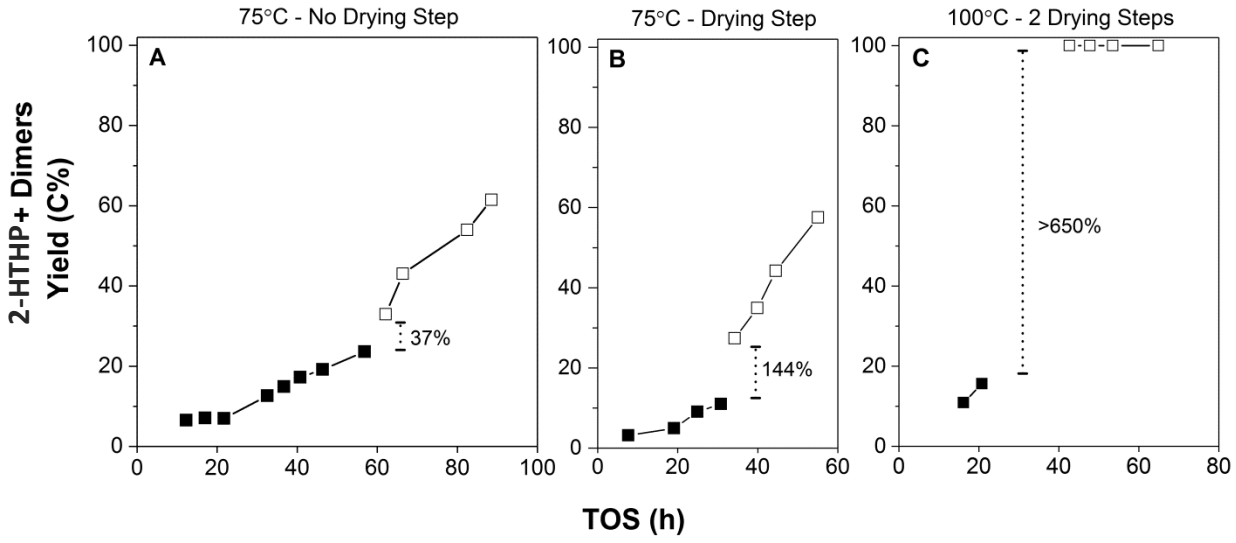

Figure 4.13 2-HTHP plus dimers (2,2'-HTHP and THP-oxypentanal) yield versus TOS in a continuous flow reactor packed with inert glass beads before (solid squares) and after (open squares) subjecting reactor to 20% DHP/H_2O flow at 140˚C and 34.5 bar Ar for >20h: A) 75˚C reaction with no drying step, B) 75˚C reaction with one drying step, and C) 100˚C reaction with two drying steps. Total liquid flowrate for reaction data portrayed in Figures 4.13A-C was 0.037mL/min. Reactor drying conditions were T: 140˚C, Ar flow: 100mL/min, t:>4h.

Table 4.3 Solid total-organic-carbon (TOC) analysis of glass beads after high temperature coking treatments and after 50°C DHP hydrations in continuous flow reactors

Sample	wt% Carbon
180°C Coked Beads[a]	0.056%
180°C Coked Beads - 50°C DHP Hydration[b]	0.049%
200°C Coked Beads[c]	0.249%
200°C Coked Beads - 50°C DHP Hydration[d]	0.011%

* All runs were at 34.5 bar with an Ar flow of 40mL/min. Beads were dried >140°C after each run.

[a] DHP Concentration: 50wt%, Flowrate: 0.084mL/min, Coked for 24h - dried

[b] Procedure [a] followed by 50°C reaction (DHP Concentration: 20wt%, Flowrate: 0.042mL/min, TOS: 22h)

[c] DHP Concentration: 50wt%, Flowrate: 0.031mL/min, Coked 4h - dried - coked 11h -dried

[d] Procedure [c] followed by 50°C reaction (DHP Concentration: 20wt%, Flowrate: 0.042mL/min, TOS: 22h)

The results of the continuous flow coke activation studies are further evidence for the formation of soluble and insoluble acidic humins. After catalyzing DHP hydration in the continuous reactor, the soluble humins exit the reactor with the product stream. Conversely, in the batch reactor all acidic species formed are retained in the reactor over the course of the reaction. This is evidenced by the higher reaction rates in batch mode than continuous mode – 3036 and 219 μmol/min-L, respectively, at 50˚C. However, as the temperature increases the soluble humins are more likely to polymerize and physically adsorb on the inert glass beads. In fact, the temperature gradient in the reactor tube led to increased coke adsorption on the glass beads in the reactor center with less coke at the inlet and outlet: further evidence for the large effect temperature has on the solids formation. The reactive solid coke formed is not permanent, though, as much of the activity gained while holding at high temperatures is not maintained after lowering the temperature (Figure 4.13A). In fact, solid TOC analysis of glass beads coked at high temperatures (180-200°C) showed a decrease in carbon content after subjecting the coked beads to a lower temperature (50°C) DHP hydration reaction (Table 4.3). This confirms the acidic coke is soluble in water and its formation is reversible. Humin polymerization is favored at higher temperatures and solubilization favored

at lower temperatures, with the coke formation becoming favorable at ~140˚C. Practically, this means that high temperatures (>140˚C) must be retained in order to keep active coke in the reactor in high quantities; otherwise, some of the coke will resolubilize into solution.

4.4 Conclusions

Dihydropyran (DHP) was hydrated to 1,5-pentanediol (1,5-PD) precursors in the absence of an added catalyst in batch and continuous flow reactors. Yields to 1,5-PD precursors are maximized at low temperatures (≤100˚C), with insoluble humins and undesired (non 1,5-PD precursors) dimers forming at high temperatures (≥140˚C). The C10 dimer formed at high temperatures was likely formed via aldol condensation of two 5-hydroxyvaleraldehyde (5HVal) molecules. Both soluble and insoluble humins were shown to be catalytically active for DHP hydration. The carboxylic acid, 5-hydroxy-valeric acid (5-HY-VA), is suspected to form as low as 25˚C at <1C% 2-HTHP yields, increasing solution acidity and catalyzing the hydration of DHP. Thus, DHP hydration is an auto-catalyzed reaction over a large spectrum of operating conditions.

Acidic coke was formed in a continuous reactor, increasing 2-HTHP yields with time-on-stream. Hydration activation rates increased with increasing temperature. Coke formation is reversible, with polymerization favored over solubilization at high temperatures (≥140˚C). Solid coke formed at high temperatures was shown to greatly increase the DHP hydration rate – up to 28x – as compared to the fresh reactor bed. This suggests a possible DHP upgrading strategy consisting of the formation of the highly active coke species *in situ* without the need to load any *ex situ* synthesized solid acid catalyst. Furthermore, the active coke species can be regenerated at any point in the reaction with a simple high temperature heat treatment.

4.5 References

1. Routray, K.; Barnett, K. J.; Huber, G. W. Hydrodeoxygenation of Pyrolysis Oils. *Energy Technol.* **2017**, *5*, 80–93.

2. Bond, J. Q.; Upadhye, A. A.; Olcay, H.; Tompsett, G. A.; Jae, J.; Xing, R.; Alonso, D. M.; Wang, D.; Zhang, T.; Kumar, R.; Foster, A.; Sen, S. M.; Maravelias, C. T.; Malina, R.; Barrett, S. R. H.; Lobo, R.; Wyman, C. E.; Dumesic, J. A.; Huber, G. W. Production of Renewable Jet Fuel Range Alkanes and Commodity Chemicals from Integrated Catalytic Processing of Biomass. *Energy Environ. Sci.* **2014**, *7* (4), 1500–1523.

3. Kunkes, E. L.; Simonetti, D. A; West, R. M.; Serrano-Ruiz, J. C.; Gärtner, C. A; Dumesic, J. A. Catalytic Conversion of Biomass to Monofunctional Hydrocarbons and Targeted Liquid-Fuel Classes. *Science* **2008**, *322*, 417–421.

4. Besson, M.; Gallezot, P.; Pinel, C. Conversion of Biomass into Chemicals over Metal Catalysts. *Chem. Rev.* **2014**, *114*, 1827–1870.

5. Chatterjee, C.; Pong, F.; Sen, A. Chemical Conversion Pathways for Carbohydrates. *Green Chem.* **2015**, *17*, 40–71.

6. Vispute, T. P.; Zhang, H.; Sanna, A.; Xiao, R.; Huber, G. W. Renewable Chemical Commodity Feedstocks from Integrated Catalytic Processing of Pyrolysis Oils. *Science* **2010**, *330*, 1222–1227.

7. He, J.; Huang, K.; Barnett, K. J.; Krishna, S.; Martin Alonso, D.; Brentzel, Z.; Burt, S. P.; Walker, T. W.; Banholzer, W.; Maravelias, C. T.; Hermans, I.; Dumesic, J. A.; Huber, G. W. New Catalytic Strategies for Alpha-Omega Diol Production from Lignocellulosic Biomass. *Faraday Discuss.* **2017**, *202*, 247-267.

8. 2016 Billion-Ton Report. United States Department of Energy: Washington, DC, 2016.

9. Werle, P.; Moraweitz, M.; Lundmark, S.; Sorenson, K.; Karvinen, E.; Lehtonen, J. Alcohols, Polyhydric. *Ulmann's Encyclopedia of Industrial Chemistry*; Wiley-VCH Verlag GmbH & Co. KGaA: Weinheim, Germany, 2008.

10. Xing, R.; Qi, W.; Huber, G. W. Production of Furfural and Carboxylic Acids from Waste Aqueous Hemicellulose Solutions from the Pulp and Paper and Cellulosic Ethanol Industries. *Energy Environ. Sci.* **2011**, *4* (6), 2193-2205.

11. Alonso, D. M.; Hakim, S. H.; Zhou, S.; Won, W.; Hosseinaei, O.; Tao, J.; Garcia-Negron, V.; Motagamwala, A. H.; Mellmer, M. A.; Huang, K.; Houtman, C. J.; Labbé, N.; Harper, D. P.; Maravelias, C.; Runge, T.; Dumesic, J. A. Increasing the Revenue from Lignocellulosic Biomass : Maximizing Feedstock Utilization. *Sci. Adv.* **2017**, *3* (5), 1-7.

12. Brentzel, Z. J.; Barnett, K. J.; Huang, K.; Maravelias, C. T.; Dumesic, J. A.; Huber, G. W. Chemicals from Biomass: Combining Ring-Opening Tautomerization and Hydrogenation Reactions to Produce 1,5-Pentanediol from Furfural. *ChemSusChem* **2017**, *10* (7), 1351–1355.

13. Huang, K.; Brentzel, Z. J.; Barnett, K. J.; Dumesic, J. A.; Huber, G. W.; Maravelias, C. T. Conversion of Furfural to 1,5-Pentanediol: Process Synthesis and Analysis. *ACS Sustain. Chem. Eng.* **2017**, *5* (6), 4699–4706.

14. Schneipp, L. E.; Geller, H. H. Preparation of Dihydropyran, δ-Hydroxyvaleraldehyde and 1,5-Pentanediol from Tetrahydrofurfuryl Alcohol. *J. Am. Chem. Soc.* **1946**, *68* (6), 1646–1648.

15. Sato, S.; Igarashi, J.; Yamada, Y. Stable Vapor-Phase Conversion of Tetrahydrofurfuryl Alcohol into 3,4-2H-Dihydropyran. *Appl. Catal. A Gen.* **2013**, *453*, 213–218.

16. De, B. K.; Battacharyya, K.; Bandyopadhyay, K. Bio- and Auto-Catalytic Esterification of High Acid Mowrah Fat and Palm Kernel Oil. *Eur. J. Lipid Sci. Technol.* **2002**, *104*, 167–173.

17. Schmitt, M.; Hasse, H. Chemical Equilibrium and Reaction Kinetics of Heterogeneously Catalyzed N-Hexyl Acetate Esterification. *Ind. Eng. Chem. Res.* **2006**, *45* (12), 4123–4132.

18. He, B.; Deng, T.; Li, J.; Yan, F.; Wang, H.; Huang, Y.; Peng, C. An Innovative Auto-Catalytic Esterification for the Production of Phytosterol Esters: Experiment and Kinetics. *RSC Adv.* **2014**, *4* (109), 64319–64327.

19. Schwach-Abdellaoui, K.; Monti, A.; Barr, J.; Heller, J.; Gurny, R. Optimization of a Novel Bioerodible Device Based on Auto-Catalyzed Poly(ortho Esters) for Controlled Delivery of Tetracycline to Periodontal Pocket. *Biomaterials* **2001**, *22* (12), 1659–1666.

20. Mohd-Adnan, A. F.; Nishida, H.; Shirai, Y. Evaluation of Kinetics Parameters for Poly(l-Lactic Acid) Hydrolysis under High-Pressure Steam. *Polym. Degrad. Stab.* **2008**, *93* (6), 1053–1058.

21. Fujishige, S.; Morita, R.; Brewer, J. R. Auto-Catalytic Cleavage of Poly (β-L-Malic Acid) in Aqueous Solution. *Makromol. Chem., Rapid Commun.* **1993**, *14*, 163–166.

22. Goje, A. S. Auto-Catalyzed Hydrolytic Depolymerization of Poly(Butylene Terephthalate) Waste at High Temperature. *Polym. Plast. Technol. Eng.* **2006**, *45* (2), 171–181.

23. Faris, A. H.; Rahim, A. A.; Mohamad Ibrahim, M. N.; Hussin, M. H.; Alkurdi, A. M.; Salehabadi, A. Investigation of Oil Palm Based Kraft and Auto-Catalyzed Organosolv Lignin Susceptibility as a Green Wood Adhesives. *Int. J. Adhes. Adhes.* **2017**, *74* (December 2016), 115–122.

24. Wei, W.; Wu, S.; Xu, S. Enhancement of Enzymatic Saccharification of Bagasse by Ethanol-Based Organosolv Auto-Catalyzed Pretreatment. *J. Chem. Technol. Biotechnol.* **2016**, *92*, 580–587.

25. Guo, Y.; Zhou, J.; Wen, J.; Sun, G.; Sun, Y. Structural Transformations of Triploid of Populus Tomentosa Carr. Lignin during Auto-Catalyzed Ethanol Organosolv Pretreatment. *Ind. Crops Prod.* **2015**, *76*, 522–529.

26. Wen, J. L.; Xue, B. L.; Sun, S. L.; Sun, R. C. Quantitative Structural Characterization and Thermal Properties of Birch Lignins after Auto-Catalyzed Organosolv Pretreatment and Enzymatic Hydrolysis. *J. Chem. Technol. Biotechnol.* **2013**, *88* (9), 1663–1671.

27. Chen, H.; Zhao, J.; Hu, T.; Zhao, X.; Liu, D. A Comparison of Several Organosolv Pretreatments for Improving the Enzymatic Hydrolysis of Wheat Straw: Substrate Digestibility, Fermentability and Structural Features. *Appl. Energy* **2015**, *150*, 224–232.

28. Yáñez-S, M.; Matsuhiro, B.; Nuñez, C.; Pan, S.; Hubbell, C. A.; Sannigrahi, P.; Ragauskas, A. J. Physicochemical Characterization of Ethanol Organosolv Lignin (EOL) from Eucalyptus Globulus: Effect of Extraction Conditions on the Molecular Structure. *Polym. Degrad. Stab.* **2014**, *110*, 184–194.

29. Rypkema, H. A.; Sinha, A.; Francisco, J. S. Carboxylic Acid Catalyzed Hydration of Acetaldehyde. *J. Phys. Chem. A* **2015**, *119* (19), 4581–4588.

30. Copelin, H. B. E. I. Du Pont de Nemours and Company, US Pat. 2,497,812, 1950.

31. Smith, C. W. E. I. Du Pont de Nemours and Company, US Pat. 2,546,019, 1951.

32. Heer, P. K. K. S.; Gaikar, V. G. Simulation of a Palm Fatty Acid Distillate-Based Biodiesel Plant Using Homogeneous and Heterogeneous Catalysts. *Chem. Eng. Technol.* **2016**, *39* (12), 2416–2426.

33. Su, F.; Guo, Y. Advancements in Solid Acid Catalysts for Biodiesel Production. *Green Chem.* **2014**, *16* (6), 2934-2957.

34. Sittiwong, W.; Richardson, M. W.; Schiaffo, C. E.; Fisher, T. J.; Dussault, P. H. Re2O7-Catalyzed Reaction of Hemiacetals and Aldehydes with O-, S-, and C-Nucleophiles. *Beilstein J. Org. Chem.* **2013**, *9*, 1526–1532.

35. Kavala, V.; Samal, A.; Patel, B. Water as Catalyst and Solvent: Tetrahydropyranylation of Alcohols in an Aqueous Medium. *Arkivoc* **2005**, (i), 20–29.

36. Casale, M. T.; Richman, A. R.; Elrod, M. J.; Garland, R. M.; Beaver, M. R.; Tolbert, M. A. Kinetics of Acid-Catalyzed Aldol Condensation Reactions of Aliphatic Aldehydes. *Atmos. Environ.* **2007**, *41* (29), 6212–6224.

37. Soghrati, E.; Choong, C.; Poh, C. K.; Kawi, S.; Borgna, A. Single-Pot Conversion of Tetrahydrofurfuryl Alcohol into Tetrahydropyran over a Ni/HZSM-5 Catalyst under Aqueous-Phase Conditions. *ChemCatChem* **2017**, *9* (8), 1402–1408.

38. Fogler, H. S. *Elements of Chemical Reaction Engineering*; Pearson Education Inc.: Upper Saddle River, New Jersey U.S.A., 2006.

Chapter 5. Hydration of Highly Reactive Vinyl Cyclic Ethers over Solid-acid Catalysts for the Production of C4-C6 α,ω-Diols

5.1 Introduction

Lignocellulosic biomass ia a low-cost and highly abundant resource for the production of renewable alternatives to oil-derived fuels and chemicals.[1–3] Much progress has been made in recent years in developing new catalytic routes to chemicals from biomass,[4,5] which increases the value of biomass conversion technologies and can potentially lower the cost of biofuels (Kefeng co-production).[6] One such class of chemicals are α,ω-diols, which are comprised of linear, aliphatic carbon chains with terminal hydroxyl groups.[7] The dual-functionality of α,ω-diols make them ideal molecules in the synthesis of several classes of polymers, including polyester polyols, polyurethanes, and polycarbonate diols.[8] Four to six carbon (C4-C6) α,ω-diols – including 1,4-butanediol (1,4-BD), 1,5-pentanediol (1,5-PD), and 1,6-hexanediol (1,6-HD) – together represent a $7 billion annual market that is growing at 7% per year.[9]

Recent work in our group has shown that 1,5-PD and 1,6-HD can be produced in a 3-step pathway from C5 and C6 biomass-derived molecules, tetrahydrofurfuryl alcohol (THFA) and tetehydropyran-2-methanol (THP2M), respectively (see Figure 5.1).[10,11] Both the C5 (Chapter 2) and C6 (Chapter 3) pathways undergo analogous chemistry, in which THFA or THP2M is subjected to gas phase dehydration, aqueous phase hydration, and aqueous phase hydrogenation, in that order. This Dehydration-Hydration-Hydrogenation route will be referred to as the "DHH" pathway from here forward. The DHH pathway for the C5 route was shown to greatly decrease

The content of this chapter is largely adapted from the following reference:

Kevin J. Barnett, Zachary J. Brentzel, James A. Dumesic, George W. Huber. Hydration of highly reactive vinyl cyclic ethers over solid-acid catalysts for the production of C4-C6 α,ω-diols. *In Preparation.*

* KJB performed experiments. ZJB performed thermochemistry calculations. *

1,5-PD production costs (including a 50x lower catalyst cost) versus the bimetallic, noble metal-catalyzed direct hydrogenolysis approach previously studied in the literature.[12–16]

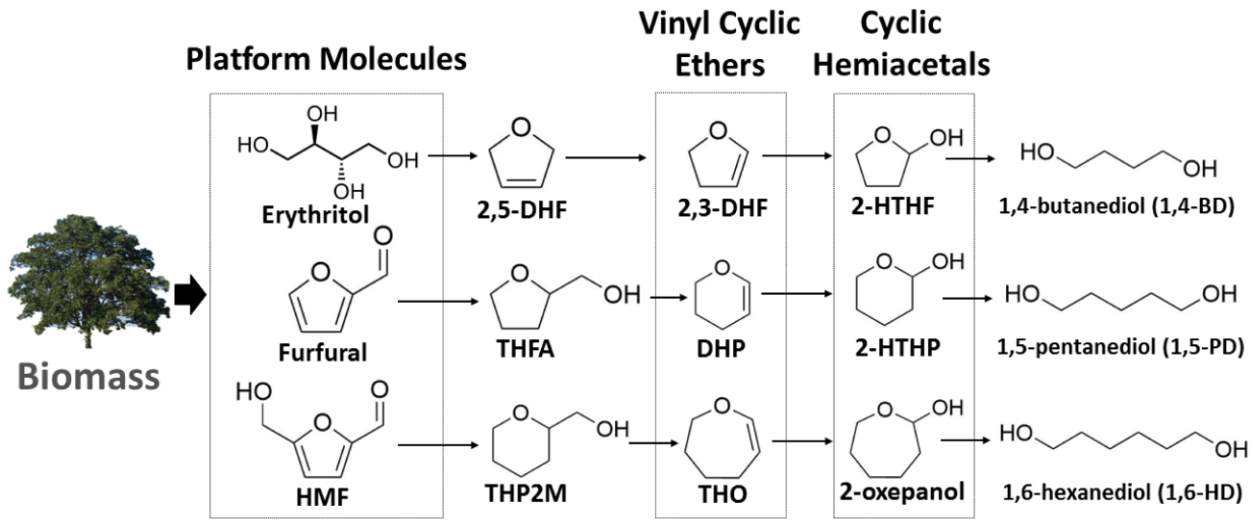

Figure 5.1 Roadmap for producing C4-C6 α,ω-diols from biomass-derived vinyl cyclic ethers.

The chemistry of the final hydrogenation step involves tautomerization of the cyclic hemiacetal to its ring-opened aldehyde form.[10] Hydration occurs prior to hydrogenation and this step has not been studied in detail. In both the C5 and C6 pathways, an α,β-unsaturated (or "vinyl") cyclic ether – 3,4-dihydropyran (3,4-DHP) and 2,3,4,5-tetrahydrooxepine (THO) in the C5 and C6 routes, respectively - is spontaneously hydrated in water without the addition of a catalyst, yielding near quantitative yields to the hydrated product.[11,17] Previous works have performed 3,4-DHP hydration in the presence of homogeneous acids.[18–20] The use of no catalyst or solid acid catalysts avoid the further downstream separation required with homogeneous acid catalyst.[21,22] In the present work, we investigate the relationship between the structures of vinyl cyclic ethers and their reactivity for hydration.

While the C5 and C6 vinyl cyclic ethers can be produced via high-temperature dehydration

of biomass-derived cyclic ethers THFA and THP2M, respectively, it is difficult to produce the C4 vinyl cyclic ether, 2,3-DHF, using dehydration chemistry (see Figure 5.1).[23] However, if 2,3-DHF could be synthesized from biomass, it could be subjected to similar hydration and hydrogenation reactions to produce 1,4-BD. In fact, this has been attempted once before in a patent by BASF, in which 2,3-DHF (50wt% in H_2O) was converted to 1,4-BD in 97% yields over an activated carbon-supported Cu catalyst at 170˚C and 50 bar H_2. (cite BASF).[24]

In the present work, we propose a pathway to produce 2,3-DHF from biomass-derived erythritol is proposed (Figure 5.1). Erythritol is a C4 polyol that is currently made industrially via microbial conversion of biomass-derived glucose.[25] Others have previously demonstrated the conversion of erythritol to 2,5-dihydrofuran (2,5-DHF) in yields up to 77% via the 2-step cyclodehydration of erythritol and dihydroxylation of the cyclic product.[26] Another study attempted the single-step conversion of erythritol to 2,5-DHF over homogeneous MO-based catalysts, but achieved lower overall yields of 39%.[27] While 2,5-DHF is an unsaturated cyclic ether (as described above), the location of the double bond at the β,γ position makes hydration of this molecule very slow. Unlike 2,5-DHF, as an vinyl cyclic ether 2,3-dihydrofuran (2,3-DHF) is able to rapidly hydrate to its cyclic hemiacetal 2-hydroxytetrahydrofuran (2-HTHF). In the present work, we demonstrate the isomerization the 2,5-DHF to 2,3-DHF in hydrogen atmosphere, hydration of 2,3-DHF to 2-HTHF, and hydrogenation of 2-HTHF to 1,4-BD over heterogeneous base-metal catalysts. Furthermore, we demonstrate all three reaction steps can occur in a single reactor with 82% overall 1,4-BD yields from 2,5-DHF.

The reaction rates for hydration of vinyl cyclic ethers with solid acid catalysts was also explored. In Chapter 4, the autocatalytic nature of the DHP hydration reaction was outlined,[17] in which we showed that the formation of liquid-phase acids in batch reactors and solid-phase acids

in continuous flow reactors improved DHP hydration rates by up to 28 times. Solid acid catalysts have been employed previously for DHP hydration,[28] but no systemic study of the solid acids and their kinetics has been attempted. In this chapter, we study the hydration kinetics of several solid acid catalysts and show improved reaction rates versus the autocatalytic hydration of DHP. We then utilize the higher reactivity of the solid acid catalysts in an attempt to improve the selectivity to α,ω-diols for the combined hydration-hydrogenation of vinyl cyclic ethers in a single reactor.

5.2 Experimental Methods

5.2.1 Materials

Chemicals used as feeds for hydration reactions include 3,4-dihydropyran (AK Scientific, 95%), 3,6-dihydropyran (Combi-Blocks, 96%), 2,3-dihydrofuran (Sigma Aldrich, 99%), 2,5-dihydrofuran (Combi-Blocks, 98%), furan (Sigma Aldrich, >99%), cyclohexene (Alfa Aesar, 99%), cyclopentene (Sigma Aldrich, 96%), 3-methyl-2-pentene (TCI, >99%), 2-methyl-1-pentene (Sigma Aldrich, >99%), 3-methyl-1-pentene (Alfa Aesar, 98%), and 1-penten-3-ol (Sigma Aldrich, 99%). Chemicals used for calibration standards for hydration products were 2-hydroxytetrahydropyran (Acros Organics, 90%), 2-hydroxytetrahydrofuran (Accela ChemBio, 95%), and cyclohexanol (Sigma Aldrich, 99%). 2-hexanol (Sigma Aldrich, 99%) was used as a calibration standard for the hydration products of 3-methyl-2-pentene (3M2P), 2-methyl-1-pentene (2M1P), and 3-methyl-1-pentene (3M1P) due to the lack of available standards and the similarity in chemical structure of 2-hexanol. Isopropyl amine (IPA) for temperature-programed desorption (TPD) studies was supplied by Sigma Aldrich (>99.5%).

5.2.2 Catalyst Synthesis

Solid Acid Catalysts. The zirconium phosphate (ZrP) catalyst was prepared by precipitation of $ZrCl_2O$-$8H_2O$ (Sigma Aldrich, 1 M, 70 mL) and $NH_4H_2PO_4$ (Sigma Aldrich, 1 M, 140 mL) at a molar ratio of P/Zr = 2. The solution was stirred and then filtered, washed with deionized (DI) water and dried overnight at 100˚C. The catalyst was calcined at 450˚C for 4 h (5˚C/min ramp) in static air prior to reaction.

Cesium phosphotungstic acid (CsPTA) was synthesized via dropwise addition of Cs_2CO_3 (0.1 M) to $H_3PW_{12}O_{40}$ (0.1 M) while stirring vigorously at room temperature. The Cs_2CO_3-PTA mixture was then pretreated in a muffle furnace at 450 C for 2h to remove water. The yellow precipitate was aged for 20 h at room temperature, filtered, and calcined in air at 300 C for 2h.

HZSM5 (SiO_2:Al_2O_3=30) and H-Beta (SiO_2:Al_2O_3=25) zeolites were provided in the by Zeolyst International. HZSM5 was provided in the ammonium form and H-β in the hydrogen form. Both zeolites were calcined in static air at 550˚C (1˚C/min ramp, 3h hold) to their final hydrogen form state. Amorphous SiO_2:Al_2O_3 (Grade 135, Sigma Aldrich) and γ- Al_2O_3 (Alfa Aesar) were calcined at 450˚C for 4h (5˚C/min ramp).

Nafion SAC-13 (Sigma Aldrich), Amberlyst 15 (Dry-hydrogen form, Sigma Aldrich), and Amberlyst 70 (Rohm and Haas) were crush to a powder and dried overnight in an oven at 110˚C prior to use.

Supported Metal Catalysts. Commercial 5wt% Ru/C (Sigma Aldrich) was reduced at 300˚C (2˚C/min ramp, 2h hold). Commercial 5wt% Pt/Al_2O_3 (Acros) was reduced at 300˚C (2˚C/min ramp, 2h hold).

All Cu- and Co-based catalysts were prepared by incipient wetness impregnation onto their respective supports. Supports used were Vulcan XC 72 carbon (Cabot), Grade 646 SiO_2 (150Å

pore size, Sigma Aldrich), Grade 9385 SiO_2 (60Å pore size, Sigma Aldrich), and Degussa P25 TiO_2 (Sigma Aldrich). The TiO_2 support was calcined in static air at 750˚C (4˚C/min ramp, 4h hold) to fully convert it to the rutile phase prior to impregnation. $Co(NO_3)_2 \cdot 6H_2O$ and $Cu(NO_3)_2 \cdot 3H_2O$ (Aldrich, ≥98%) were mixed with deionized (DI) water to the amount required to reach the incipient wetness point of the support. The nitrate solution was added dropwise to the incipient point and dried at 85˚C at vacuum (15in. Hg) for at least 4h. In some cases, multiple impregnation steps were required, in which the catalyst was dried similarly between each step. After drying, all catalysts were treated in N2 flow (100mL/min) at 350˚C (2˚C/min, 2h hold) to remove all nitrate precursors. Cu catalysts were then reduced at 350˚C (1˚C/min, 2h hold) and Co catalysts were reduced at 450˚C (1˚C/min, 2h hold) without removing the sample from the pretreatment setup. Strong metal-support interaction (SMSI) Co/TiO_2 was prepared similarly to non-SMSI Co/TiO_2 above, but with a 600˚C calcination in flowing air (100mL/min, 2˚C/min ramp, 2h hold) and a 600˚C reduction (1˚C/min ramp, 2h hold) following the same nitrate decomposition step at 350˚C.[29] All reduced catalysts were then transferred to a glovebox filled with inert UHP Ar (Airgas, 99.999%) without exposure to air.

5.2.3 Catalyst Characterization

IPA-TPD experiments were carried out using a Micromeritics Autochem II 2920 unit. Prior to IPA-TPD analysis, samples were pretreated in flowing Helium (Airgas UHP 99.999%) at 50mL/min at elevated temperature to remove water and any other adsorbates. SiO_2:Al_2O_3 , γ-Al_2O_3, ZrP, HZSM5, and H-β were treated at 500˚C (10˚C/min ramp, 1h hold) and CsPTA was treated at 200˚C (1˚C/min ramp, 1h hold) due to its lower thermal stability. The samples were then cooled to 50°C where 100μL IPA was dosed seven times to saturate the Brϕnsted acid sites on the catalyst surface. IPA adsorption was performed under 25mL/min Helium flow. IPA was

desorbed by increasing the sample temperature to 600˚C at 10˚C/min. The desorbed propene molecules formed during the temperature ramp were continuously monitored by a MKS Cirrus 2 quadrupole mass spectrometer (MS) recording the signals m/z = 41 (corresponding to propene). M/Z signals of 17, 18, and 58 were also recorded to analyze the emission of ammonia, water, and physisorbed IPA, respectively. Propene was quantified in the mass spectrometer by using a propene (Airgas, Polymer Grade) pulse calibration to obtain a MS to thermal conductivity detector (TCD) sensitivity ratio, in combination with a propene calibration curve generated in the TCD of the Autochem II 2920 unit by varying the propene concentration in helium.

5.2.4 Batch Reaction Studies

All reaction studies were performed in a 75mL Parr Hastelloy autoclave equipped with a magnetic stir bar and a stir rate of 750 rpm. For all reactions, the reactor was heated to the reaction temperature at ~4˚C/min, and zero time was defined as the point at which the reactor reached the final reaction temperature. All reactions were terminated by cooling in an ice water bath prior to product analysis. Reactor were purged twice with either Ar (Airgas, Industrial Grade) or hydrogen (Airgas, 99.999%) and the reaction pressures were set at 35.5 bar.

For the solid acid kinetic studies (See Table 5.3), 0.5wt% 3,4-DHP was added to DI water up to a total of 60g solution. This 3,4-DHP concentration was used due to the low solubility ~1wt% of 3,4-DHP in water. Hydrations occurred in Ar gas at a reaction temperature of 30˚C or 50˚C. At least four samples were taken through a dip-tube fitted with a 500 mesh steel filter during the course of each reaction in order to obtain reliable kinetic rate data.

For probe molecule hydrations (see Tables 5.1 and 5.2), 0.06M solution of the feed material in DI water was prepared with a total of 30g of solution. Hydrations occurred in Ar gas at a reaction temperature of 50˚C. For 3,4-DHP and 2,3-DHF, at least three samples were taken through a dip-

tube fitted with a 500 mesh steel filter during the course of each reaction in order to obtain reliable kinetic rate data. For the remaining probe molecules, multiple separate reactions were run for each data point (at least two reactions for each molecule) due to the more complex analysis of the two-phase systems (See Section 2.2.4).

For combined hydration-hydrogenation reactions (see Figures 5.5-5.8), stir bar and solid acid catalyst (if used) were first loaded outside of the glovebox. The reactor entered into the glovebox where the reduced metal catalysts were stored (see Section 5.2.2). The desired amount of metal catalyst was loaded into the reactor, all reactor valves shut, and the reactor was removed from the glovebox. 30mL of feed solution - 0.5wt% 3,4-DHP or 2,5-DHF in H_2O – was then pumped into the reactor after purging the lines of air. The reactions occurred in H_2 atmosphere at a reaction temperature of 100˚C for 2h reaction time. The aqueous liquid product was analyzed after quenching the reactor with an ice bath.

5.2.5 Product Analysis

Aqueous- and organic-phase products were filtered with 0.22μm polyethersulfone and polytetrafluoroethelyne filter membranes, respectively, prior to analysis. For reactions with cyclohexene, cyclopentene, 3M2P, 2M1P, 3M2P, and 1-penten-3-ol, 30mL cyclohexane or hexane was added to the product solution while stirring due to the insolubility of many of the probe molecules in water. Both the aqueous and organic phases were analyzed in the gas chromatograph (GC).

All liquid products were analyzed in a Shimadzu Gas Chromatograph equipped with a Flame Ionization Detector (FID). The FID and injection port temperatures were set to 240˚C. An injection volume of 1 μL and a split ratio of 100:1 were used. A Restek RTX-VMS capillary column (length: 30 m, ID: 0.25 mm, film thickness: 1.4 μm) was used as the GC column. The column

temperature program was as follows: hold at 40˚C for 1 min, ramp at 20˚C /min to 240˚C, and hold at 240˚C for 13 min.

5.3 Results and Discussion

The high reactivity of vinyl cyclic ethers was studied by comparing their hydration rates to those of other unsaturated species. First, cyclohexene and the vinyl cyclic ether, 3,4-DHP, were hydrated in a batch reactor over an HZSM5 solid acid catalyst. These molecules were chosen because cyclohexene and 3,4-DHP have identical chemical structures except for the presence of an ether oxygen atom in the 3,4-DHP (Figure 5.2). Therefore, any differences in reactivity would be solely due to this oxygen atom and its proximity to the double bond. Hydration of 0.5wt% 3,4-DHP and cyclohexene in water at 50˚C resulted in reaction rates of 2097 and 0.017 μmol/gcat-min, respectively - a difference of greater than 6 orders of magnitude. The cyclohexene hydration rate we obtained are similar to the results of Okuhara et. al, who achieved a rate of 31 μmol/gcat-min at higher temperature (100˚C) and higher cyclohexene concentration (12.8 wt%).[30]

We hypothesize the difference in reactivity of the 3,4-DHP and the cyclohexene is due to differences in the cationic intermediates formed during hydration (Figure 5.2). The abstraction of an acidic proton is widely accepted to be the initial step in most hydration reactions;[31] however, the resulting cationic intermediates of cyclohexene and 3,4-DHP are likely very different. Cyclohexene likely forms a secondary carbocation intermediate upon hydrogen abstraction, as shown in Figure 5.2A. 3,4-DHP forms a oxocarbenium carbocation at the 2-position of the 6-membered ring, which is resonance stabilized with the cyclic ether oxygen atom, as shown in Figure 5.2B. These oxocarbenium resonance-stabilized intermediates have been shown in past literature to be very stable and to exhibit much higher reaction rates compared to secondary carbocation intermediates in the hydrogenolysis of alcohols and cyclic ethers.[12]

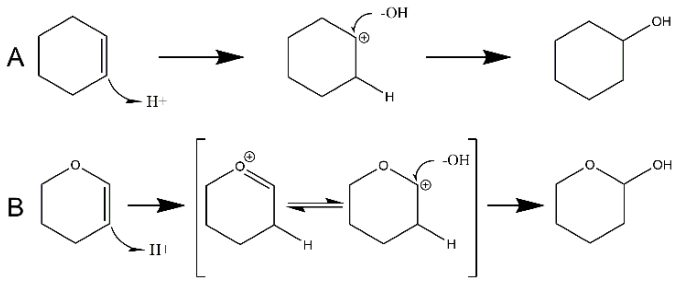

Figure 5.2 Proposed hydration mechanism of A) cyclohexene to cyclohexanol via a 2˚ carbocation intermediate and B) 3,4-DHP to 2-HTHP via an oxocarbenium intermediate.

Thermochemistry calculations on the intermediate species formed were performed using Gaussian 09 software (with hf/3-21g Hartree Fock functional set) and compared to the hydration rates of a variety of unsaturated species over an HZSM5 solid acid catalyst in an attempt to probe our hypothesis of increased reactivity with intermediate state stability. The probe molecules (Shown in Table 5.1 and Table 5.2) were chosen to span a large range of predicted intermediate structures with varying stabilities (i.e. 2˚ carbocation, 3˚ carbocation, and oxocarbenium).

Table 5.1 shows the calculated energies of all possible intermediates for the unsaturated probe molecules. Table 5.2 shows the alcohol production rates for HZSM5-catalyzed hydration at 50˚C. The hydration product formed from the more stable cationic intermediate (or more negative ΔG_{form}) from the thermochemistry calculations in Table 5.1 was the only observed product in all experiments performed. This is to be predicted by Markovnikov's Rule, particularly for species such as 3-methyl-2-pentene, for which the product that forms from the 3˚ carbocation (3-methyl-3-pentanol) being observed while the product forming from the 2˚ carbocation (3-methyl-2-pentanol) was not. What is striking, however, is the very large difference in stabilities for the vinyl cyclic ether oxocarbenium intermediates versus the 2˚ carbocation made from the same molecule (e.g. -863.2 kJ/mol vs. -703 kJ/mol for 3,4-DHP). This difference in stability explains why no

hydration was observe at the 3-position of 3,4-DHP and no hydration at all was observed for 3,6-DHP (Table 5.2).

Table 5.1 Gas-phase thermochemistry of carbocation and oxocarbenium ions formed in the hydration of vinyl cyclic ethers and various unsaturated species

Feed	Intermediate	Intermediate ΔG_{form} (kJ/mol)
3,4-DHP	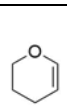	-863.2
		-703.7
2,3-DHF		-857.4
		-692.5
3-methyl-2-pentene	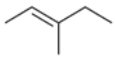	-824.0
	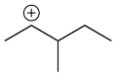	-769.2
2-methyl-1-pentene	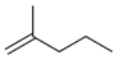	-822.3
	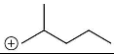	-688.5
Cyclohexene		-764.6
		
Cyclopentene		-757.9
		
3-methyl-1-pentene	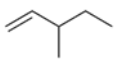	-778.8
	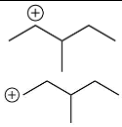	-721.7

* Gas phase thermochemistry values were calculated with Gaussian 09 software.
*Geometry optimizations and subsequent frequency calculations were performed using hf/3-21g at a temperature of 25˚C.

The results of the probe hydration study followed the hypothesized reactivity trends based on the gas-phase thermochemistry calculations, with hydration rates for various predicted cationic intermediate types increasing in the order: 2˚ carbocation < 3˚ carbocation < oxocarbenium (Table 5.2 and Figure 5.3). In fact, the vinyl cyclic ethers (3,4-DHP and 2,3-DHF) were by far the most reactive molecules, with rates of hydration 5 orders of magnitude greater than the next most

reactive molecule (2M1P). When plotting the log of the experimental hydration rates over HZSM5 (Table 5.1) against the calculated thermochemistry energies of the cationic intermediates (Table 5.2), a fairly linear trend over 9 orders of magnitude is observed. This indicates that the calculated energetics are in fact a good predictor for the hydration rates, although it should be noted that the energetics are predictions from gas-phase thermochemistry, while the hydration is taking part in the aqueous-phase on a solid surface.

Table 5.2 Batch reaction data for the hydration of unsaturated compounds in DI water over A-70 at 50˚C

Feed	Predicted Intermediate	Product	Production rate (μmol/gcat-min)
3,4-DHP 		 2-HTHP	2,097
2,3-DHF 		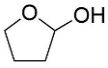 2-HTHF	1,147
3-methyl-2-pentene 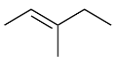	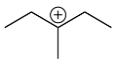	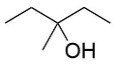 3-methyl-3-pentanol	0.064
2-methyl-1-pentene 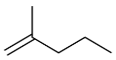	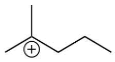	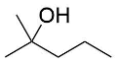 2-methyl-2-pentanol	0.025
Cyclohexene 		 Cyclohexanol	0.017
Cyclopentene 		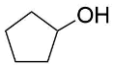 Cyclopentanol	0.0020
3-methyl-1-pentene 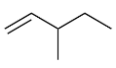	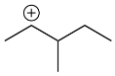	 3-methyl-2-pentanol	0.0018
1-penten-3-ol 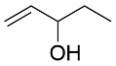	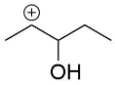	 2,3-pentanediol	-
3,6-DHP 		 4-HTHP	-
2,5-DHF 		 3-HTHF	-

* Feed Reactant Concentration: 0.06M

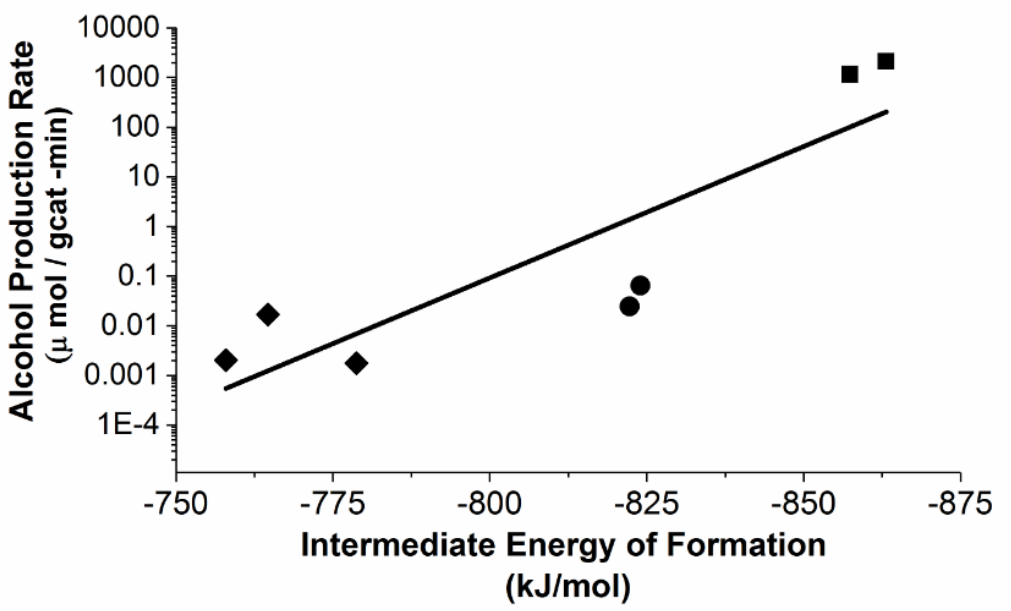

Figure 5.3 Alcohol product formation (on log scale) versus gas-phase cationic intermediate energy of formation during hydration of various unsaturated species.

Interestingly, the molecules that had double bonds at the β,γ (or "allyl") position relative to the oxygen atom (1-penten-3-ol, 3,6-DHP, and 2,5-DHF) exhibited no reactivity for hydration. This is further evidence that the location of the double bond in proximity to the oxygen is critical to high reactivity of the vinyl cyclic ethers, due to the oxocarbenium stabilized intermediate. This also shows that there is no double bond isomerization occurring at our reaction conditions – otherwise the allyl cyclic ethers would show considerable conversion.

A kinetic study of solid acid catalysts was then performed to learn more about the effect that certain acid site types and catalyst structures have on hydration rates. Conditions where the contribution from autocatalytic hydration was minimized - low temperature (30˚C) and 3,4-DHP concentrations (0.5wt%) – were used to extract only the solid acid contribution to the hydration rate. At these conditions, only 3.3% of the 3,4-DHP was converted in one hour of reaction time in the absence of a catalyst, which was accounted for in the solid acid kinetics calculations. Table 5.3 shows the multi-point rate data obtained for various solid acid catalysts, in addition to the

Brϕnsted site density and Brϕnsted site turnover frequency (TOF). Regarded as a predominantly Lewis acid catalyst, γ-Al_2O_3 gave very low rates of 3,4-DHP hydration, with no observed products above the baseline at 30˚C and a rate of only 4 μmol/gcat-min at 50˚C. Catalysts known for their high Brϕnsted site density, such as CsPTA, ZrP, Nafion SAC-13, HZSM5, H-Beta, Amberlyst-15 (A-15) , and A-70 gave hydration rates to 2-HTHP ranging from 206 μmol/gcat-min for CsPTA to 7289 μmol/gcat-min for A-70 at 30˚C. While this appears to be a large range of reactivity, when normalizing the rates to the density of Brϕnsted acid sites – as measured by IPA-TPD – the reactivity of these catalysts are much narrower; the most reactive catalyst on a TOF basis (CsPTA) is only 5x more reactive than the least active (HZSM5). These results combined suggest that 3,4-DHP hydration is largely a Brϕnsted acid catalyzed reaction with only slight differences in reactivity between the different Brϕnsted sites. This data also shows that solid acid catalysts have higher 3,4-DHP hydration rates than autocatalytic hydration.

Table 5.3 Comparison of 2-HTHP production rate and Brϕnsted acid site TOF for the hydration of 0.5wt% DHP in DI water over various solid acid catalysts in a batch reactor

Catalyst	**2-HTHP Production Rate (μmol/gcat-min)**	**Brϕnsted Site Fraction**	**Brϕnsted Site Density (mmol/g)**	**TOF (s^{-1})**	**Normalized TOF (s^{-1}) [HZSM5]**
γ-Al_2O_3	n.r. ; 4[a]	0.40[32]	0.04	n.r.; 0.0015[a]	n/a ; 0.020[a]
SiO_2-Al_2O_3	n.r. ; 13[a]	0.79[32]	0.28	n.r. ; 0.0008[a]	n/a ; 0.010[a]
CsPTA	206	-	0.05	0.064	4.9
ZrP	329	0.38[33]	0.31	0.018	1.4
Nafion SAC-13	449	∞[32]	0.14[32]	0.053	4.1
HZSM5	477	0.51[34]	0.61	0.013	1.0
H-Beta	1950	-	0.83	0.039	3.0
Amberlyst-70	5436	∞[32]	2.86[32]	0.026	2.0
Amberlyst-15	7289	∞[32]	4.70	0.032	2.4

Feed=0.5wt%DHP/H_2O, T=30˚C, P=500 psi Ar, Stir rate=750 rpm (T=50˚C[a] ; n.r. = no reaction)

A few interesting trends do appear in the TOF data, including the higher activity of H-Beta than HZSM5 and the very low activity of SiO_2-Al_2O_3. H-Beta exhibited 3x higher hydration rates than HZSM5 despite being similar silioca-aluminate zeolites with nearly identical SiO_2:Al_2O_3 ratios of 25 and 30, respectively. We hypothesize that this is due to the larger pore size of H-Beta, which enables the 3,4-DHP to access a higher number of the Brϕnsted acid sites that were measured by isopropyl amine during the IPA-TPD characterization. Another interesting result was the very low reactivity of amorphous SiO_2-Al_2O_3 as compared to the zeolite structured silico-aluminates (H-Beta and HZSM5). In fact, SiO_2-Al_2O_3 showed almost no reactivity towards hydration despite having a higher Brϕnsted-to-Lewis site ratio than the zeolites.

The increased activity of the solid acids versus the autocatalytic hydration can be used the increase α,ω-diol selectivity when combining the hydration and hydrogenation steps in one batch reactor. These two reaction steps can be combined by adding a metal hydrogenation catalyst to the reactor, which converts the cyclic hemiacetal hydration products (their ring-opened aldehydes) to α,ω-diols. As shown in Figure 5.4, when attempting to combine these two reaction steps, the saturated cyclic ether, THP, forms as a side product due hydrogenation of the unsaturated cyclic ether, 3,4-DHP.

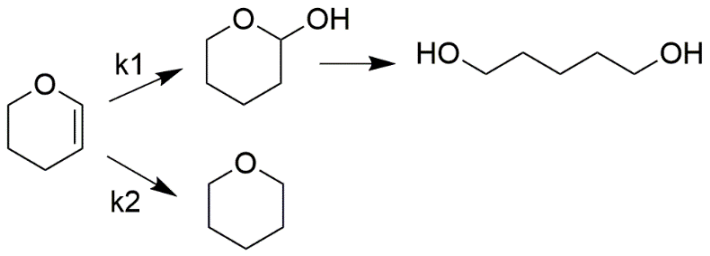

Figure 5.4 Reaction pathway for combined hydration-hydrogenation of 3,4-DHP.

The combined hydration-hydrogenation of 3,4-DHP was performed at 100˚C in hydrogen atmosphere with a Ru/C metal catalyst (Figure 5.5). Ru/C was chosen as the hydrogenation

catalyst due to its high 2-HTHP/5HVal hydrogenation rates and improved stability over other Ru-based catalysts.[10] As seen in the first data point in Figure 5.5, with no A-70 solid acid added, the yield of THP (~75%) is much higher than that of 1,5-PD (~20%). This is because the hydrogenation of 3,4-DHP to THP occurs rapidly over Ru/C, and the rate of autocatalytic hydration is too slow to convert the 3,4-DHP to 2-HTHP before hydrogenation occurs. However, when the A-70 is added to the reactor at increasing loading, the reaction network shifts to 2-HTHP over THP (i.e. k1>k2 in Figure 5.4), leading to an 86% maximum 1,5-PD yield at a A-70:Ru/C mass ratio of 1.0. Thus, the much higher hydration rates over the A-70 solid acid increased the 1,5-PD yields from 20% to 86% from the purely autocatalytic hydration.

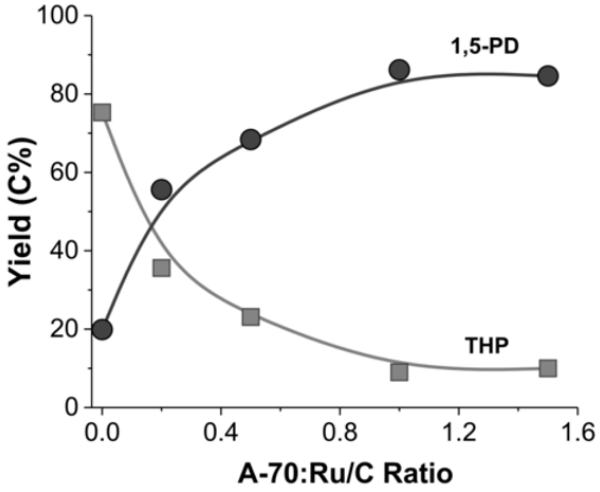

Figure 5.5 Effect of A-70 addition to Ru/C for the combined hydration-hydrogenation of 3,4-DHP in a batch reactor**.** Mass Ru/C: 25mg, Feed=0.5wt% in H_2O, Feed vol: 30mL, T=100˚C, P=500psi H_2, Reaction time=2h.

While Ru/C was chosen as the metal catalyst due to its high hydrogenation rates and improve stability, other metal catalysts – such as Co and Cu – are known to be much more selective for hydrogenation of C=O bonds over C=C bonds.[35] In Figure 5.6, we show the combined hydration-hydrogenation of 3,4-DHP over three different metal catalysts - Ru/C, Co/TiO_2, and

Cu/TiO_2 – with and without A-70 added to the reactor. The Ru/C data is the same as shown in Figure 5.5 (with 1,5-PD yields increasing from 20% to 86%); however, it can be seen that Co/TiO_2 and Cu/TiO_2 both exhibit much higher 1,5-PD yields, even with no A-70 added. Adding A-70 to the reactor increases the 1,5-PD yields from 72% to 88% for Co/TiO_2 and from 95% to 98% for Cu/TiO_2. Therefore, Co/TiO_2 does have some activity towards 3,4-DHP hydrogenation and adding the A-70 has a marked improvement on 1,5-PD yields, but Cu/TiO_2 has very little C=C hydrogenation capability to begin with. While these results suggest Co- and Cu-based catalysts should be used over Ru for combined hydration-hydrogenation, one should note that this study does not consider stability of the base metal catalysts in the aqueous phase.

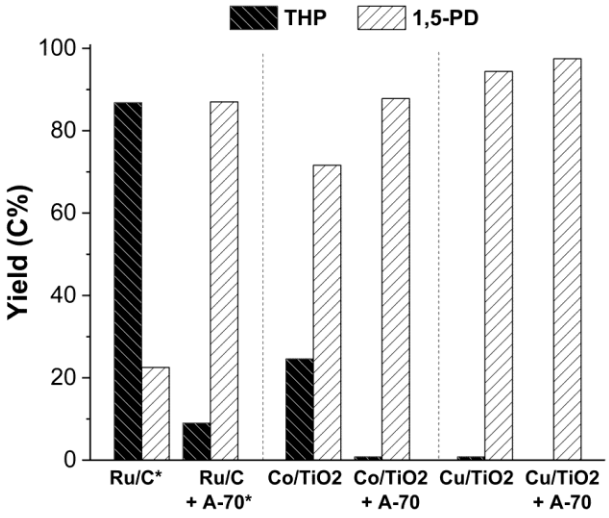

Figure 5.6 Combined hydration-hydrogenation of 3,4-DHP over various supported metal catalysts with and without A-70 solid acid catalyst**.** Feed=0.5wt% 3,4-DHP in H_2O, Feed vol: 30mL, T=100˚C, P=500psi H_2, Reaction time=2h. Mass Catalysts: Ru/C=25mg, Co/TiO_2=50mg, Cu/TiO_2=500mg, A-70=25mg. *Data also shown in Figure 5.5.

The hydration-hydrogenation chemistry shown for the C5 route above can be expanded to the C4 route from 2,3-DHF to 1,4-BD. However, 2,3-DHF is difficult to produce via high-temperature dehydration of biomass-derived cyclic ethers, such as THFA and THP2M in the C5

and C6 routes, respectively (see Figure 5.1). Therefore, we attempt the production of 1,4-BD from 2,5-DHF, which can be made from biomass-derived erythritol. 2,5-DHF must first be isomerized to 2,3-DHF prior to hydration-hydrogenation of 2,3-DHF to 1,4-BD (Figure 5.1).

In Figure 5.7, we show the results for the screening of metal catalysts with an HZSM5 solid acid catalyst for 2,5-DHF conversion in hydrogen atmosphere at 100˚C. We found that no conversion of 2,5-DHF occurred under inert atmosphere, indicating that both hydrogen and a metal catalyst are necessary for the initial isomerization step to proceed. All metal catalyst studied were able to fully convert the 2,5-DHF to one of two products: THF by hydrogenation of the C=C double bond or 1,4-BD by hydration of 2,3-DHF to 2-HTHF and hydrogenation of 2-HTHF to 1,4-BD. The catalyst screening results show that Co/TiO_2 gave the highest yield of 1,4-BD (~82%) over THF (~20%), much higher than those of Pt, Cu, or non-TiO_2 supported Co catalysts. Furthermore, we show that an SMSI-stabilized Co/TiO_2 catalyst (calcined and reduced at 600˚C) gave very similar results to Co/TiO_2 only reduced at 450˚C, which suggests stabilization techniques should not negatively affect 1,4-BD yields over Co/TiO_2 catalysts.

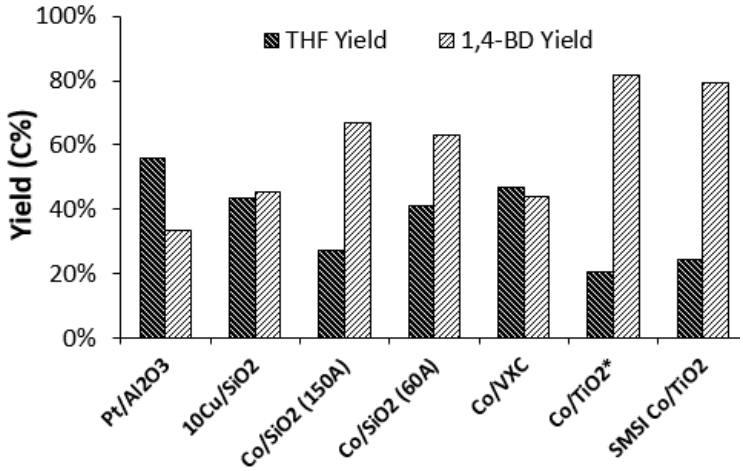

Figure 5.7 Combined isomerization-hydration-hydrogenation of 2,5-DHF over various supported metal catalysts with HZSM5 solid acid catalyst**.** Feed=0.5wt% 2,5-DHF in H_2O, Feed vol: 30mL, T=100˚C, P=500psi H_2, Reaction time=2h. Mass Catalysts: Pt/Al_2O_3=50mg, Cu/SiO_2=200mg, Co/SiO_2, Co/VXC, Co/TiO_2=100mg, HZSM5= 50mg in all reactions. *Data also shown in Figure 5.8.

Using the highly selective Co/TiO_2 as our metal catalyst, we then performed a study in which we varied the amount of HZSM5 solid acid catalyst used in order to observe the effect the hydration rate has on overall selectivity. Figure 5.8 shows that adding HZSM5 does in fact have a marked effect on 1,4-BD yields from 2,5-DHF, similar to the addition of A-70 in the hydration-hydrogenation of 3,4-DHP (Figure 5.5). Interestingly, when no HZSM5 catalyst is added to the reactor, there is no 1,4-BD formed, with product yields being split between THF (83%) and 1-butanol (19%). Thus, without HZSM5, none of the 2-HTHF hydration product and only hydrogenation products are able to be formed. However, upon addition of HZSM5 to the reactor, the 1,4-BD yields increase and THF/1-butanol side products decrease, with a maximum 1,4-BD yield of 82% being achieved at a HZSM5:Co/TiO_2 ratio of 0.5. Thus, for the single-step isomerization-hydration-hydrogenation of 2,5-DHF to 1,4-BD, addition of HZSM5 to Co/TiO_2 increases 1,4-BD yields from 0% to 82%, further evidence of the large impact solid acid catalysts have for improved α,ω-diol yields in combined hydration-hydrogenation reactions.

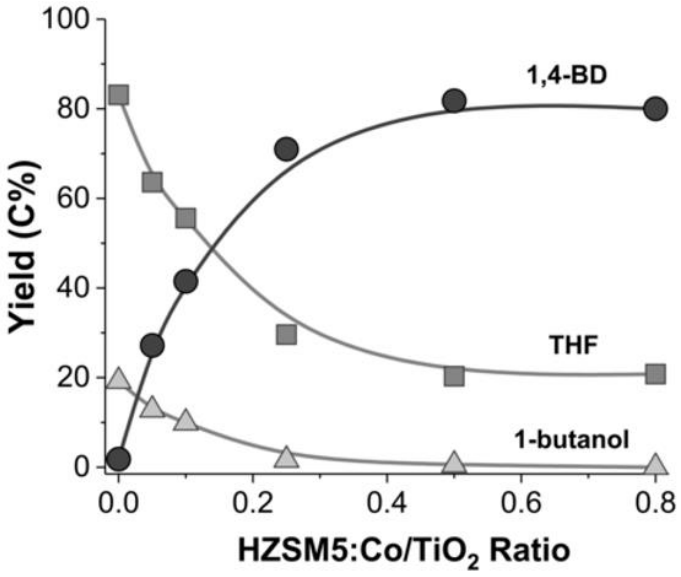

Figure 5.8 Effect of HZSM5 addition to Co/TiO_2 for the combined isomerization-hydration-hydrogenation of 2,5-DHF in a batch reactor**.** Mass Co/TiO_2: 100mg, Feed=0.5wt% in H_2O, Feed vol: 30mL, T=100˚C, P=500psi H_2, Reaction time=2h.

5.4 Conclusions

In this work, we were able to conclude that biomass-derived vinyl cyclic ethers exhibit extremely rapid hydration rates due to the formation of oxocarbenium-stabilized intermediate species upon hydration. These stable intermediates enabled hydration rates for vinyl cyclic ethers (3,4-dihydropyran) to exceed six orders of magnitude than those of compounds with the same chemical structure minus an ether oxygen atom (cyclohexene). This reactivity trend held true for several types of unsaturated species with a large range of different intermediate structures with varying stabilities (oxocarbenium, 3˚ carbocation, 2˚ carbocation). The addition of solid acid catalysts greatly improved the hydration rates of vinyl cyclic ethers as compared to the autocatalytic hydration. This was especially true of solid acids with high Brϕnsted acid content, for which the hydration rates largely normalized to Brϕnsted acid site density. These highly active Brϕnsted acid catalysts were utilized for the combined hydration-hydrogenation of 3,4-DHP to 1,5-PD, in which 1,5-PD yields increased from 20% to 86% when adding Amberlyst-70 to a Ru/C hydrogenation catalyst. Addition of HZSM5 to a Co/TiO_2 hydrogenation catalyst improved 1,4-BD yields from 0% to 82% in the combined isomerization-hydration-hydrogenation of 2,5-DHF. This result shows the large impact that solid acids have in increasing hydration rates and improving selectivities to desired α,ω-diol products and demonstrates the potential of a new route to the C4 α,ω-diol, 1,4-BD, from biomass in addition to the C5 and C6 routes discussed previously.

5.5 References

1. Huber, G. W.; Iborra, S.; Corma, A. Synthesis of Transportation Fuels from Biomass: Chemistry, Catalysts, and Engineering. *Chem. Rev.* **2006**, *106* (9), 4044–4098.
2. Chatterjee, C.; Pong, F.; Sen, A. Chemical Conversion Pathways for Carbohydrates. **2015**.
3. 2016 Billion-Ton Report. United States Department of Energy: Washington, DC, 2016.
4. Besson, M.; Gallezot, P.; Pinel, C. Conversion of Biomass into Chemicals over Metal Catalysts. *Chem. Rev.* **2014**, *114*, 1827–1870.

5. He, J.; Huang, K.; Barnett, K. J.; Krishna, S.; Martin Alonso, D.; Brentzal, Z.; Burt, S. P.; Walker, T. W.; Banholzer, W.; Maravelias, C. T.; et al. New Catalytic Strategies for Alpha-Omega Diol Production from Lignocellulosic Biomass. *Faraday Discuss.* **2017**, *202*, 247-267.

6. Huang, K.; Won, W.; Barnett, K. J.; Brentzel, Z. J.; Alonso, D. M.; Huber, G. W.; Dumesic, J. A.; Maravelias, C. T. Improving Economics of Lignocellulosic Biofuels: An Integrated Strategy for Coproducing 1,5-Pentanediol and Ethanol. *Appl. Energy* **2018**, *213* (July 2017), 585–594.

7. Sun, D.; Sato, S.; Ueda, W.; Primo, A. Production of C4 and C5 Alcohols from Biomass-Derived Materials. *Green Chem.* **2016**, *18*, 2579–2597.

8. Werle, P.; Moraweitz, M.; Lundmark, S.; Sorenson, K.; Karvinen, E.; Lehtonen, J. Alcohols, Polyhydric. *Ulmann's Encyclopedia of Industrial Chemistry*; Wiley-VCH Verlag GmbH & Co. KGaA: Weinheim, Germany, 2008.

9. MarketandMarkets. *1,6-Hexanediol Market by Application (Polyurethanes, Coatings, Acrylates, Adhesives, Polyester Resins, Plasticizers), and Region (Europe, North America, Asia-Pacific, South America, and Middle East & Africa) - Global Forecasts to 2021*; 2016.

10. Brentzel, Z. J.; Barnett, K. J.; Huang, K.; Maravelias, C. T.; Dumesic, J. A.; Huber, G. W. Chemicals from Biomass: Combining Ring-Opening Tautomerization and Hydrogenation Reactions to Produce 1,5-Pentanediol from Furfural. *ChemSusChem* **2017**, *10* (7), 1351–1355.

11. Burt, S. P.; Barnett, K. J.; McClelland, D. J.; Wolf, P.; Dumesic, J. A.; Huber, G. W.; Hermans, I. Production of 1,6-Hexanediol from Tetrahydropyran-2-Methanol by Dehydration–hydration and Hydrogenation. *Green Chem.* **2017**, *19* (5), 1390–1398.

12. Chia, M.; Pagán-Torres, Y. J.; Hibbitts, D.; Tan, Q.; Pham, H. N.; Datye, A. K.; Neurock, M.; Davis, R. J.; Dumesic, J. a. Selective Hydrogenolysis of Polyols and Cyclic Ethers over Bifunctional Surface Sites on Rhodium-Rhenium Catalysts. *J. Am. Chem. Soc.* **2011**, *133*, 12675–12689.

13. Chia, M.; O'Neill, B. J.; Alamillo, R.; Dietrich, P. J.; Ribeiro, F. H.; Miller, J. T.; Dumesic, J. a. Bimetallic RhRe/C Catalysts for the Production of Biomass-Derived Chemicals. *J. Catal.* **2013**, *308*, 226–236.

14. Karanjkar, P. U.; Burt, S. P.; Chen, X.; Barnett, K. J.; Ball, M. R.; Kumbhalkar, M. D.; Wang, X.; Miller, J. B.; Hermans, I.; Dumesic, J. A.; et al. Effect of Carbon Supports on RhRe Bifunctional Catalysts for Selective Hydrogenolysis of Tetrahydropyran-2-Methanol. *Catal. Sci. Technol.* **2016**, *6* (21), 7841–7851.

15. Koso, S.; Furikado, I.; Shimao, A.; Miyazawa, T.; Kunimori, K.; Tomishige, K. Chemoselective Hydrogenolysis of Tetrahydrofurfuryl Alcohol to 1,5-Pentanediol. *Chem. Commun.* **2009**, No. 15, 2035.

16. Tomishige, K.; Nakagawa, Y.; Tamura, M. Selective Hydrogenolysis and Hydrogenation Using Metal Catalysts Directly Modified with Metal Oxide Species. *Green Chem.* **2017**, *19*

(13), 2876–2924.

17. Barnett, K. J.; McClelland, D. J.; Huber, G. W. Autocatalytic Hydration of Dihydropyran to 1,5-Pentanediol Precursors via in Situ Formation of Liquid- and Solid-Phase Acids. *ACS Sustain. Chem. Eng.* **2017**, *5* (11), 10223–10230.

18. Schneipp, L. E.; Geller, H. H. Preparation of Dihydropyran, δ-Hydroxyvaleraldehyde and 1,5-Pentanediol from Tetrahydrofurfuryl Alcohol. *J. Am. Chem. Soc.* **1946**, *68* (6), 1646–1648.

19. Copelin, H. B. E. I. Du Pont de Nemours and Company, U.S. Patent 2,497,812, 1950.

20. Smith, C. W. E. I. Du Pont de Nemours and Company, U.S. Patent 2,546,019, 1951.

21. Heer, P. K. K. S.; Gaikar, V. G. Simulation of a Palm Fatty Acid Distillate-Based Biodiesel Plant Using Homogeneous and Heterogeneous Catalysts. *Chem. Eng. Technol.* **2016**, *39* (12), 2416–2426.

22. Guo, Y.; Zhou, J.; Wen, J.; Sun, G.; Sun, Y. Structural Transformations of Triploid of Populus Tomentosa Carr. Lignin during Auto-Catalyzed Ethanol Organosolv Pretreatment. *Ind. Crops Prod.* **2015**, *76*, 522–529.

23. Wilson, C. L. Reactions of Furan Compounds. VII. Thermal Interconversion of 2,3-Dihydrofuran and Cyclopropane Aldehyde. *J. Am. Chem. Soc.* **1947**, *69* (12), 3002–3004.

24. Pinkos, R.; Fischer, H.; Breitscheidel, F.; Palanek, P. BASF, U.S. Patent 5,945,571, 1996.

25. Moon, H. J.; Jeya, M.; Kim, I. W.; Lee, J. K. Biotechnological Production of Erythritol and Its Applications. *Appl. Microbiol. Biotechnol.* **2010**, *86* (4), 1017–1025.

26. Arceo, E.; Marsden, P.; Bergman, R. G.; Ellman, J. A. An Efficient Didehydroxylation Method for the Biomass-Derived Polyols Glycerol and Erythritol. Mechanistic Studies of a Formic Acid-Mediated Deoxygenation. *Chem. Commun.* **2009**, No. 23, 3357.

27. Dethlefsen, J. R.; Lupp, D.; Teshome, A.; Nielsen, L. B.; Fristrup, P. Molybdenum-Catalyzed Conversion of Diols and Biomass-Derived Polyols to Alkenes Using Isopropyl Alcohol as Reductant and Solvent. *ACS Catal.* **2015**, *5* (6), 3638–3647.

28. Dickey, J. B.; Joyner, F. B. Eastman Kodak Company, U.S. Patent 2,808,440, 1957.

29. Lee, J.; Burt, S. P.; Carrero, C. A.; Alba-Rubio, A. C.; Ro, I.; O'Neill, B. J.; Kim, H. J.; Jackson, D. H. K.; Kuech, T. F.; Hermans, I.; et al. Stabilizing Cobalt Catalysts for Aqueous-Phase Reactions by Strong Metal-Support Interaction. *J. Catal.* **2015**, *330*, 19–27.

30. Nakato, T.; Toyoshi, Y.; Kimura, M.; Okuhara, T. Unique Catalysis of an Acidic Salt of Heteropoly Acid ,. **1999**, *52*, 23–28.

31. Rekasheva, A. F. The Dependence of the Mechanism of the Hydrolysis, Trans-Esterification, and Trans-Etherification of α,β-Alkenyl Ethers and Esters on Their Structure. *Russ. Chem. Rev.* **1968**, *37* (12), 1009–1022.

32. Weingarten, R.; Tompsett, G. a.; Conner, W. C.; Huber, G. W. Design of Solid Acid

Catalysts for Aqueous-Phase Dehydration of Carbohydrates: The Role of Lewis and Brønsted Acid Sites. *J. Catal.* **2011**, *279* (1), 174–182.

33. Weingarten, R.; Kim, Y. T.; Tompsett, G. a.; Fernández, A.; Han, K. S.; Hagaman, E. W.; Conner, W. C.; Dumesic, J. a.; Huber, G. W. Conversion of Glucose into Levulinic Acid with Solid Metal(IV) Phosphate Catalysts. *J. Catal.* **2013**, *304*, 123–134.

34. Cheng, Y. T.; Jae, J.; Shi, J.; Fan, W.; Huber, G. W. Production of Renewable Aromatic Compounds by Catalytic Fast Pyrolysis of Lignocellulosic Biomass with Bifunctional Ga/ZSM-5 Catalysts. *Angew. Chemie - Int. Ed.* **2012**, *51* (6), 1387–1390.

35. Gallezot, P.; Richard, D. Selective Hydrogenation of α,β-Unsaturated Aldehydes. *Catal. Rev.* **1998**, *40* (1&2), 81–126.

Chapter 6. Hydrogenation of γ-Butyrolactone to 1,4-Butanediol over Bimetallic CuCo/TiO_2 Catalysts

6.1 Introduction

1,4-Butanediol (1,4-BD) is an industrially important chemical that can be used to produce many basic chemicals such as tetrahydrofuran (THF), polybutylene terephthalate (PBT), polybutylene succinate (PBS), polyurethane, and polyester polyols.[1,2] The global 1,4-BD market was valued at 6.19 billion USD in 2015 and is expected to grow at a Compound Annual Growth Rate of 7.7% in the next 8 years.[1] 1,4-BD is commercially produced by three major routes: 1) hydrogenation of butynediol produced via carbonylation of acetylene with formaldehyde (Reppe process), 2) hydrogenation of maleic anhydride (MA), and 3) acetoxylation of butadiene.[3,4] Hydrogenation of MA (made via oxidation of n-butane) is attracting growing interest due to its safe operational advantages and the low cost of n-butane feedstock.[3,5,6] The hydrogenation of MA or MA-derived dialkyl esters to produce 1,4-BD has been reported to proceed via the reaction intermediate γ-butyrolactone (GBL) over various noble metal and copper catalysts at temperatures and pressures between 170-260˚C and 3-7 MPa, respectively.[5-10] Combined 1,4-BD and GBL selectivities above 94% are obtained from MA-derived dialkyl esters with Cu-based catalysts.[5, 9,10]

1,4-BD can also be produced from renewable platform molecules including succinic acid (SA) and furfural, as shown in Figure 6.1.[2,4,11-16] The annual market volume for 1,4-BD (2000 kton/yr), while the current volumes for SA and furfural are 60 and 604 kton/yr, respectively. The

The content of this chapter is largely adapted from the following reference, Copyright (2017), reproduced by permission of the American Chemical Society:

Zhiwei Huang[#], Kevin J. Barnett[#], Joseph P. Chada, Zachary J. Brentzel, Zhuoran Xu, James A. Dumesic, George W. Huber. Hydrogenation of gamma-Butyrolactone to 1,4-Butanediol over CuCo/TiO2 Bimetallic Catalysts. ACS Catalysis. **2017**. *7* (12), 8429-8440. #Authors contributed equally to this work.

* KJB designed research and experiments. ZH performed experiments. * JPC performed STEM. ZJB performed NMR.

hydrogenation of SA and the oxidation-hydrogenation of furfural to 1,4-BD proceed via the same GBL intermediate (Figure 6.1).[2,4,11-17] Many noble metals, including Rh, Pt, Pd and Ru, have been studied for the direct SA hydrogenation into 1,4-BD.[12,13,15,16] Rh/C, Pt/C, and Pd/C gave high selectivities to 1,4-BD (70-90%) at above 60% conversions, while Ru produced large amounts of THF.[15] Re has been used as an additive for Ru and Pd catalysts in SA hydrogenation to promote the conversion of the GBL intermediate to 1,4-BD, increasing the rate of 1,4-BD production by 29 times.[12,17,18] Furfural can be oxidized to form SA,[19] MA[20,21] and 2(5H)-furanone,[4,19] all of which can be hydrogenated to GBL[19] and further converted to 1,4-BD.[4,14] For example, Yuan et al.[4] achieved a 85% 1,4-BD yield from furfural over a Pt/TiO_2-ZrO_2 catalyst via the 2-step oxidation-hydrogenation of furfural.

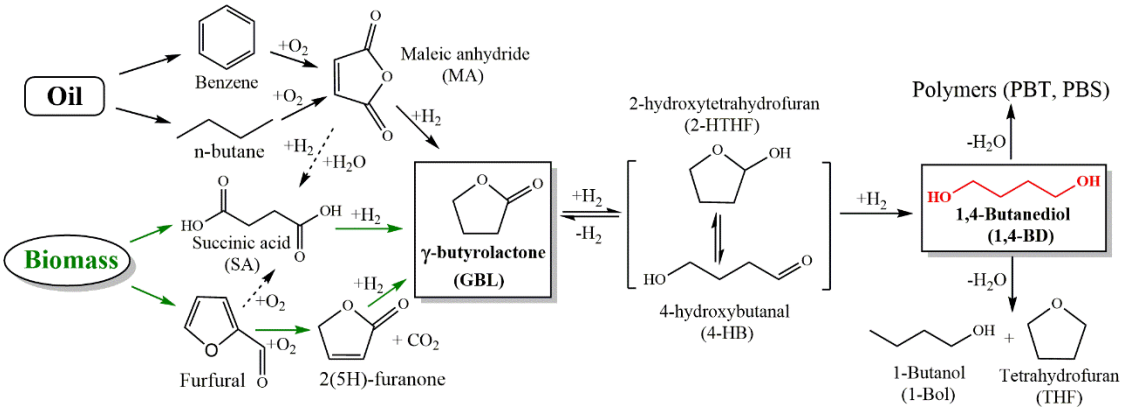

Figure 6.1 Reaction route for the production of 1,4-BD from petroleum- and biomass- derived GBL.

Cu- and Pd-based heterogeneous catalysts have been studied for GBL hydrogenation due to their high C=O hydrogenation activity.[2] Hydrogenation of GBL under batch conditions over a heterogeneous Pd/C catalyst using ethanol as solvent at 180˚C and 10 MPa H_2 pressure resulted in 88.6% 1,4-BD selectivity at 98% conversion[22], and reaction over a FeO_x modified Pd/C catalyst using water as solvent at 200 °C and 5 MPa H_2 gave a 70.8% 1,4-BD selectivity at 76.4% conversion.[13] Over a $MgSiO_3$ supported multicomponent Cu-Pd-KOH catalyst, GBL was

hydrogenated to 1,4-BD in the liquid-phase with 99.0% selectivity at 96.5% conversion under 160˚C and 6.2 MPa H_2.[23] In the liquid-phase hydrogenation of a 70:30 GBL-dimethyl succinate (DMS) mixture over Cu/ZnO at 180-220 ºC and 8 MPa H_2, 90.5% 1,4-BD and 9.0% THF selectivities were obtained at 90% GBL conversion (98% DMS conversion).[24] Vapor-phase GBL hydrogenation over $CuCrO_x$ at 210°C produced 1,4-BD selectively (87-97%) at 60-70% conversions, with 1-butanol (1-Bol) and THF selectivities up to 1.1% and 5.5%, respectively.[25] In addition, homogeneous Ru catalysts have been studied for GBL hydrogenation, achieving a 99% 1,4-BD yield over a Ru complex of tetradentate bipyridine ligand at 25°C.[26]

Clearly, it is highly desirable to develop efficient earth-abundant heterogeneous catalysts to catalyze the hydrogenation of GBL at lower temperature and pressure to produce 1,4-BD. In the present work, up to 95% 1,4-BD yield was achieved over a bimetallic $Cu_{0.1}Co_{0.9}/TiO_2$ catalyst at relatively mild conditions of 140 ºC and 3.4 MPa H_2. This Cr-free non-noble $CuCo/TiO_2$ bimetallic catalyst had over a two times higher 1,4-BD selectivity than Pt/C, Pd/C, and Ru/C catalysts. However, the reaction rate on a total mole of metal basis for GBL hydrogenation on Ru/C was 2.5 times greater than on the $Cu_{0.1}Co_{0.9}/TiO_2$ catalyst. The $CuCo/TiO_2$ bimetallic catalyst had an activity up to 11 times higher than that of a commercial copper chromite catalyst. The correlations between the catalyst structural and catalytic performance of the $Cu\text{-}Co/TiO_2$ catalysts with different Co contents are discussed to gain insights into the probable active sites and reaction mechanism.

Despite previous research on GBL hydrogenation, the mechanism of GBL ring-opening/hydrogenation to 1,4-BD remains unclear. Recent research on the production of C_5 and C_6 diols from biomass-derived hemiacetals provides insight into the mechanism of GBL hydrogenation to 1,4-BD. Brentzel et. al.[27,28] reported a 3-step dehydration-hydration-

hydrogenation (DHH) pathway for the production of 1,5-pentanediol (1,5-PD) from furfural. The final step in this process involves hydrogenation of the hemiacetal 2-hydroxytetrahydropyran (2-HTHP) to 1,5-PD, which occurs by tautomerization of the 2-HTHP to the ring-opened aldehyde, 5-hydroxyvaleraldehyde.[27] The same chemistry was shown to proceed in the analogous C_6 route from tetrahydropyran-2-methanol to 1,6-hexanediol.[29] It will be shown in this paper that the C_4 hemiacetal analog of 2-HTHP, 2-hydroxytetrahydrofuran (2-HTHF), is likely formed by hydrogenation of GBL (Figure 6.1). Accordingly, 2-HTHF can similarly undergo a ring-opening tautomerization to form 4-hydroxybutanal (4-HB)[30], the latter of which has been reported to be a reaction intermediate in the production of GBL by 1,4-BD dehydrogenation.[31,32] Hamminga et al.[33] used *in situ* ATR-FTIR spectroscopy to study the mechanism of liquid-phase hydrogenation of GBL over Cu-ZnO. Neither 2-HTHF nor 4-HB was observed in their study. Thus, another key objective of this work is to elucidate the reaction pathways for GBL hydrogenation over Cu-Co/TiO_2 bimetallic catalyst based on the effect of reaction parameters, catalytic performance of different model compounds and ^{13}C variable temperature NMR.

6.2 Experimental Methods

6.2.1 Catalyst Synthesis

Cu-Co/TiO_2 catalysts with various Co molar percentages (0, 25%, 50%, 75%, 90%, 95%, 100%) were prepared by incipient wetness (co)impregnation. A commercial P25 TiO_2 (Aldrich) was used as the support. We chose TiO_2 as support because it is a stable support that we have used for other aqueous phase reactions and it has low Brønsted surface acidity.[34] The support was calcined at 750 ^oC (4 ^oC/min) for 4 h before (co)impregnating with an aqueous solution containing the calculated amounts of $Co(NO_3)_2 \cdot 6H_2O$ and $Cu(NO_3)_2 \cdot 3H_2O$ (Aldrich, ≥98%). The total metal loading was set at 1.8 mmol/g. After impregnation, the materials were kept at room temperature

for 2 h, dried at 110 ^{o}C overnight, and then calcined at 450 ^{o}C for 3 h in a muffle furnace with a ramp rate of 3 ^{o}C/min. The Cu-rich (Cu mol% ≥75%) Cu-Co/TiO_2 catalysts were reduced under H_2 flow (80 ml/min, >99.99%, Airgas) at 300 ^{o}C (ramping rate: 1 ^{o}C /min) for 2 h. Co-rich (Co mol% ≥50%) catalysts were reduced at 450^{o}C (ramping rate: 2^{o}C /min) for 2 h. The calcined and reduced catalysts are denoted as $Cu_{1-x}Co_x/TiO_2$-C and $Cu_{1-x}Co_x/TiO_2$-R, respectively, where x refers to the molar fraction of Co in decimal form. The Cu and Co content of the catalysts measured from the ICP results were similar to the amount expected from impregnation (Table 6.1).

Copper chromite ($CuCrO_x$) and 5%Ru/C were purchased from Aldrich. 5%Pd/C and 5%Pt/C were supplied by Strem Chemicals Inc. The copper chromite was reduced at the same conditions as monometallic Cu/TiO_2. The Pd, Pt and Ru catalysts were reduced under H_2 flow (80 ml/min, >99.99%, Airgas) at 300 ^{o}C (ramping rate: 4 ^{o}C /min) for 2 h. All the above reduced catalysts were stored in a glove box in Ar (>99.99%, Airgas) to avoid oxidation.

6.2.2 Catalyst Characterization

The elemental compositions of the synthesized samples were analyzed by ICP-OES (Varian Vista-MPX CCD Simultaneous ICP-OES) after the samples (50 mg) were digested with a mixture of 2 mL nitric acid (Fisher, 69.2 wt%), 6 mL hydrochloric acid (Fisher, 37.4 wt%), and 10 mL hydrofluoric acid (Acros Organics, 48–51%) in a Teflon beaker at 100 ^{o}C for 24 h. Cobalt and copper standards for the ICP analysis were prepared from copper (Fluka, 1000 ± 2 mg/L) and cobalt (Fluka, 1000 ± 2 mg/L) ICP standards.

X-ray powder diffraction (XRD) patterns of the samples were obtained in the scanning angle (2θ) range of 20-80° on a Bruker D8 Discover diffractometer using Cu Kα1 radiation (λ = 1.5406 Å) operated at 50 kV and 1000 mA. The crystallite sizes (*d*) of CuO and Cu in the samples

were calculated by the Scherrer equation: $d = k\lambda/\beta_L \cos\theta$, where k is the Debye-Scherrer constant (0.90), θ is the diffraction angle and β_L is the full width at half maximum.

Thermogravimetric analysis (TGA) of the spent catalyst was performed with a TA Instruments Q500 system. Approximately 12 mg of the sample was loaded onto a Pt pan in 100 mL/min N_2 flow, ramped at 10 °C/min from room temperature to 100 °C, held for 20 min, and then ramped at 10 °C/min to 800 °C.

The Brunauer–Emmett–Teller (BET) surface area was calculated from nitrogen adsorption data at liquid nitrogen temperature obtained on a Micromeritics ASAP 2020 system. Prior to the BET measurements, samples were degassed under vacuum at 250 °C for 4 h. The BET surface areas of the calcined samples were in the range of 12.8 to 15.6 m^2/g (Table 6.1).

Scanning transmission electron microscopy (STEM) was performed using a Cs-corrected FEI Titan microscope operated at 200 kV. Prior to STEM analysis, the samples were passivated in 1% oxygen after reduction. Catalyst powders were dispersed in ethanol and ultrasonicated for 30 min and deposited on either carbon-coated Cu or Au grids and plasma cleaned prior to insertion into the microscope. Images were collected with high-angle annular dark-field (HAADF) STEM, with collection angles of 54-270 mrad, probe convergence angle of 24.5 mrad, and probe current of 25 pA. Energy-dispersive x-ray spectra (EDS) and electron energy loss spectra (EELS) were collected on the same microscope with a EDAX SiLi and Gatan GIF 865 detector, respectively. Spectral images (SI) were collected in EFSTEM with an energy resolution of 0.8 eV. The SIs were de-noised by a weighted principal component analysis (PCA) using temDM software, a plugin for DigitalMicrograph.[35,36] 12 principle components were retained. Relative composition maps were generated from the SI by standard background extrapolation and subtraction techniques for the

core-loss Ti, Co, and Cu L-edges. Approximately 100-200 particles were analyzed for each particle size distribution. In the case of the bimetallic samples, bimodal distribution of particle sizes was observed. Since it was very difficult for us to quantify the exact ratio of small (<4 nm) to large (>4 nm) nanoparticles, an equally number of both sizes were counted.

Temperature-programmed reduction (TPR) was carried out on a Micromeritics AutoChem II 2920 unit. Before TPR, the as-prepared calcined samples (100 mg) were pretreated in helium at 150 ^{o}C for 30 min. A TPR run was carried out with a 10% H_2/Ar mixture gas at a flow rate of 50 mL/min and the temperature was increased to 800 ^{o}C at a temperature ramp rate of 10 ^{o}C/min. A dry ice/acetone cooling bath was used to remove moisture from the TPR effluent stream. The H_2 consumption was monitored by a thermal conductivity detector (TCD) and quantified based on H_2 consumption of a TPR standard (Ag_2O).

NH_3-TPD measurements were carried out using a Micromeritics Autochem II 2920 unit. Prior to NH_3-TPD analysis, samples were reduced at 300 °C for Cu_1/TiO_2 and $CuCrO_x$ and 450 °C for $CuCo/TiO_2$ bimetallic catalysts for two hours (2 °C/min) under a flow of 10% H_2 in Ar. Then samples were cooled to 100 °C for NH_3 adsorption. Adsorption was performed under a flow of 15%NH_3–He (Airgas, 50 mL/min) for 30 min. NH_3 was desorbed under a He flow of 50 mL/min with 10° C/min ramp rate to 700 °C. The desorbed NH_3 molecules were continuously monitored by a MKS Cirrus 2 quadrupole mass spectrometer recording the signals m/z = 17 and 16 (corresponding to NH_3). The density of acid sites was quantified by calibrating the MS signals with NH_3/He gas flows at several different concentrations.

A 10 wt% 2-hydroxytetrahydrofuran (2-HTHF) (Accela ChemBio, 95%) in 1,4-dioxane-d8 (Aldrich, ≥ 99 atom% deuterium) sample was prepared for nuclear magnetic resonance (NMR) spectroscopy. Variable temperature NMR experiments were performed on a Bruker Avance-III

500 MHz spectrometer with a broadband fluorine observe probe. The ^{2}H signal from 1,4-dioxane-d8 was used as the field-frequency lock. The magnetic field shimming was performed on the ^{2}H solvent signals. ^{1}H and ^{13}C chemical shifts were referenced against solvent. Spectra were collected from 24 to 82 °C. The sample was equilibrated at each temperature for 15 minutes before collecting the spectrum. ^{1}H experiments were performed with a Bruker standard 1D pulse sequence, 'zg30'. The inter-scan relaxation delay, sweep width, acquisition time, and number of scans were 2 s, 20 ppm centered at 10 ppm, 3.3 s, and 8 scans, respectively. ^{13}C spectra were collected with a quantitative ^{1}H decoupled pulse sequence, 'zgig30'. The inter-scan relaxation delay, sweep width, acquisition time, and number of scans were 2 s, 284 ppm centered at 110 ppm, 2 s, and 32 scans, respectively.

6.2.3 Reaction Kinetics Measurements

GBL hydrogenation batch reactions were carried out in a hastelloy autoclave (50 ml) at a stirring speed of 750 rpm. The reduced active catalysts were loaded into the reactor in the glove box. In a typical run, 20 g of 10 wt% GBL (Aldrich, 99%) in 1,4-dioxane (Acros, >99%, stabilized with BHT) solution and 0.4 g of reduced catalyst were introduced into the autoclave. The reactor was then purged with H_2 three times, pressurized with H_2 to 3.4 MPa, and heated to the desired reaction temperature, which was held constant for the duration of the reaction. The reactor was quenched in an ice bath to terminate the reaction. THF (Acros, 99.9%, stabilized with BHT), ethanol (Decon Labs Inc., 100%), and deionized water were used to study the effect of solvents.

Continuous reaction studies with the $Cu_{0.1}Co_{0.9}/TiO_2$ catalyst were carried out with the $Cu_{0.1}Co_{0.9}/TiO_2$ catalyst in an up-flow configuration at 140 ^{o}C and 3.4 MPa. The calcined catalyst sample (0.6 g) was loaded into a ¼" OD (0.18" ID) 316 stainless steel tube and secured in place by alternating layers of quartz wool (Grace) and granular silicon dioxide (Sigma, 99.9%, 4-20

mesh). The reactor tube was contained inside a tube furnace equipped with aluminum filler rods for uniform heat distribution. Both ends of the furnace were sealed with quartz wool. The reactor was pressurized with H_2 gas to 3.4 MPa. The reactor furnace controller was set to the desired reaction temperature. The catalyst was reduced at the same conditions as for batch reactor. After the temperature of the catalyst bed was decreased to the reaction temperature, a solution of 10 wt% GBL in 1,4-dioxane was pumped into the reactor with an HPLC pump (Lab Alliance Series I) at a speed of 1.2 mL/h. The H_2 to GBL mole ratio was 50. Liquid products accumulated in a stainless-steel gas–liquid separator (300 mL) above the reactor outlet. Liquid samples were analyzed by gas chromatography (Shimadzu GC2010) equipped with a flame ionization detector (FID) and a ZB-5MS capillary column (30 m × 0.25 mm × 0.5 μm). The products were also confirmed by GC-MS (Shimadzu GCMS-QP2010S) equipped a Restek RTX-VMS capillary column (30 m × 0.25 mm × 1.4 μm). The gaseous products from batch reactions were collected using a gas-bag and analyzed using a gas chromatograph (Shimadzu GC-2014) with both TCD (fitted with a GS-CarbonPLOT column) and FID (fitted with a Rt-Q-Bond capillary column). Only negligible amounts of CH_4, CO and CO_2 (in total <0.1%) were detected in gas products. GBL conversion, product selectivities and product production rates were calculated on carbon basis and are defined as follows：

$$\text{Conversion (\%)} = \frac{\text{mol of GBL charged - mol of GBL left}}{\text{mol of GBL charged}} \times 100$$

$$\text{Selectivity (\%)} = \frac{\text{mol of product x C atoms in product}}{\text{(mol of GBL charged - mol of GBL left) x C atoms in GBL}} \text{x}\,100$$

$$\text{Reaction rate } (\text{mol}_{\text{prod}}/\text{mol}_{\text{metal}}\ \text{h}^{-1}) = \frac{\text{mol of GBL converted} \times \text{Product selectivity}}{\text{mol of active metal} \times \text{reaction time}}$$

In the hydrogenation of 10 wt% GBL in 1,4-dioxane, 4-hydroxybutyl,4-hydroxybutanoate (4-HHB) was formed by the esterification of GBL with the 1,4-BD product. The formation of 4-HHB was also confirmed by separate reaction studies using equal amounts (5 wt%) of GBL and 1,4-BD in 1,4-dioxane catalyzed by either acid (eg. HY zeolite) or base (eg. CaO) in an oil bath at 60 °C. Due to the unavailability of the standard for 4-HHB, its GC response factor was assumed to be the sum of that for GBL and 1,4-BD. In most cases, the carbon balances were 100 ± 4%. Because small concentrations of products were detected when ethanol and water were separately used as solvent, the selectivity (%) for ethyl 4-hydroxybutanoate and 4-hydroxybutanoic acid was estimated by subtracting the sum of the known products from 100%.

6.3 Results and discussion

The XRD patterns of calcined and reduced monometallic and bimetallic Cu/Co catalysts are shown in Figure 6.2. The monometallic Co_1/TiO_2-C displayed the characteristic peaks of Co_3O_4 (PDF # 43-1003) and rutile TiO_2, while the pattern of the monometallic Cu_1/TiO_2-C showed the characteristic peaks of CuO (PDF # 05-0661) and rutile TiO_2 (Figure 6.2A). The crystallite sizes of Co_3O_4 and CuO were estimated to be 18.0 and 21.7 nm, respectively, from the Scherrer equation (Table 6.1). The intensity of the Co_3O_4 diffractions decreased for the $Cu_{0.1}Co_{0.9}/TiO_2$-C sample with the (311) peak at 36.8° possibly decomposing into two peaks centered at 36.7 and 36.8° (Figure 6.2B). The shift of the Co_3O_4 (311) peak to lower 2θ reflects the possible expansion of Co_3O_4 lattice by addition of Cuinto the lattice[37], with the lattice parameter increased from 2.437 to 2.444 Å. Only a broad shoulder at around $2\theta = 36.7°$ was seen for $Cu_{0.5}Co_{0.5}/TiO_2$-C (Figure 6.2B). Note that due to the overlapping of the diffraction peaks for Co_3O_4 and $CuCo_2O_4$, it is difficult to distinguish the two components by XRD patterns.[37,38] No diffraction peaks corresponding to CuO

could be seen in bimetallic $Cu_{0.5}Co_{0.5}/TiO_2$-C and $Cu_{0.1}Co_{0.9}/TiO_2$-C samples (Figure 6.2B). This result indicates that large CuO crystallites only existed in the monometallic Cu_1/TiO_2-C sample, and Cu species were highly dispersed in the bimetallic samples. This behavior is in agreement with the work of Wang et al.[38]

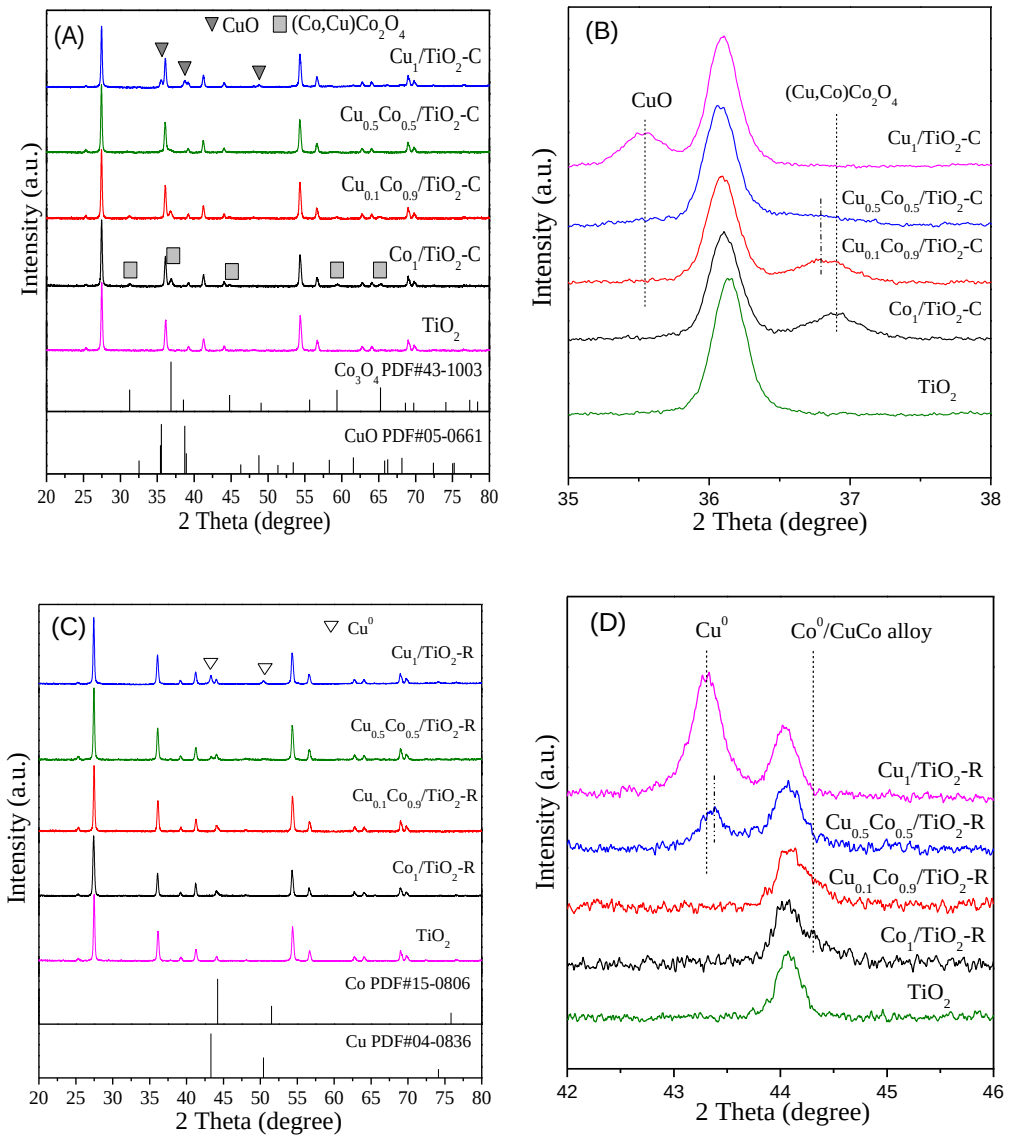

Figure 6.2 (A,B) XRD patterns of calcined catalyst samples with (B) magnified (2θ = 35–38°); (C, D) XRD of reduced catalysts with (D) magnified (2θ = 42–46°).

After reduction at 450 °C, the diffractions of Co_3O_4 for both monometallic Co_1/TiO_2-R and bimetallic $CuCo/TiO_2$-R samples disappeared and no other peaks related to CoO could be observed (Figure 6.2C). Only a shoulder peak at $2\theta = 44.3°$, assigned to Co^0, could be observed in Co_1/TiO_2-R (Figure 6.2D) because of the overlapping of the intense diffraction peaks of the TiO_2 support. The broad shoulder peak at $2\theta = 44.3°$ in $Cu_{0.1}Co_{0.9}/TiO_2$-R is either metallic Co or a Co phase that has small amounts of Cu in the lattice. Diffraction peaks assigned to Cu^0 were clearly observed in monometallic Cu_1/TiO_2-R. The intensity of these peaks decreased with increasing Co content, and almost disappeared in $Cu_{0.1}Co_{0.9}/TiO_2$-R. The slight shift of 2θ value for Cu (111) from 43.3° for Cu_1/TiO_2-R to 43.4° in $Cu_{0.5}Co_{0.5}/TiO_2$-R, probably corresponded to a Cu phase that has some Co in the lattice.[37, 39,40]

Table 6.1 Metal loadings, textural properties and reduction degrees of $CuCo/TiO_2$ catalyst samples with different Co contents

Sample	Composition (wt%) [a]		S_{BET} (m^2/g)	CuO/Co_3O_4 crystallite size (nm) [b]	Particle size (nm) [c]	Extent of reduction (%)[e]
	Cu	Co				
Cu_1/TiO_2-C	11.93	-	12.8	21.7/-	2.6, >20 [d]	62.7
$Cu_{0.5}Co_{0.5}/TiO_2$-C	5.78	5.19	15.6	N.D/N.D	2.3, 16.5[d]	50.2
$Cu_{0.1}Co_{0.9}/TiO_2$-C	1.20	9.36	14.6	N.D/16.3	1.6, 21.3 [d]	48.1
Co_1/TiO_2-C	-	10.53	13.3	-/18.0	19.8	34.6

[a] Obtained from ICP analysis.
[b] The crystallite sizes calculated by the Scherrer equation. N.D: Not detected.
[c] Particle size measured by STEM
[d] Bimodal size distribution of particles measured by STEM
[e] From H_2-TPR.

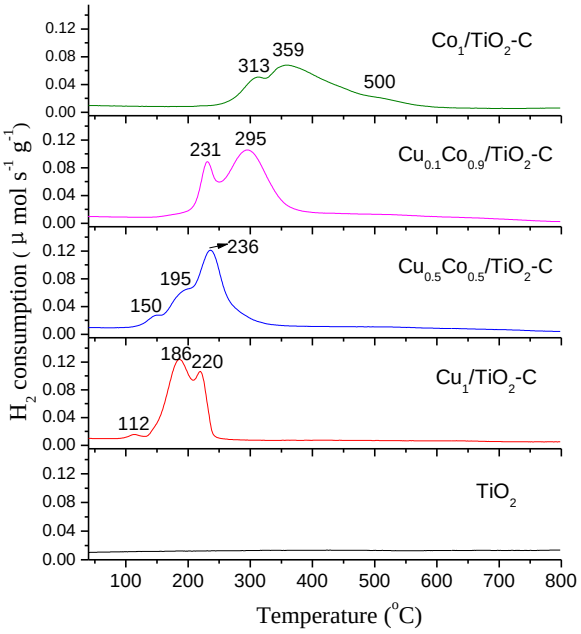

Figure 6.3 Temperature-programmed reduction profiles of calcined catalyst samples and TiO_2 support.

Figure 6.3 shows the H_2-TPR profiles of the calcined catalyst precursors. No H_2 consumption was seen for the TiO_2 support demonstrating that a metal is needed to reduce the TiO_2 consistent with previous studies.[41,42] The TPR profile of monometallic Co_1/TiO_2 gave an initial reduction peak at 313 °C followed by a broad peak at 359 °C. This TPR behavior has been described previously for the two-step reduction of Co_3O_4 to Co^0.[38, 41, 43,44] The shoulder peak at ~500 °C is likely associated with reduction of TiO_x overcoated CoO_x particles.[34] The monometallic Cu_1/TiO_2-C showed three peaks at 112, 186 and 220°C. The reduction of CuO occurs at lower temperature than the reduction of CoO_x, which is consistent with the works of Ávila-Neto et al.[4] and Wang et al.[38] The addition of a small amount of Cu (10 mol%) to the Co led to a large decrease in the reduction temperature for the $Cu_{0.1}Co_{0.9}/TiO_2$-C sample (down to 231 and 295 °C). The TPR of the $Cu_{0.5}Co_{0.5}/TiO_2$-C sample had three peaks at even lower temperatures (150, 195 and 236 °C) than the $Cu_{0.1}Co_{0.9}/TiO_2$-C sample. It is likely that Cu^0 species initiates the reduction process by

activation of H_2 and the adsorbed hydrogen is transferred to cobalt oxides by a spillover mechanism.[34,45]

The extent of reduction of the catalysts is shown in Table 6.1. Only 34.6% of the cobalt was reduced in the Co_1/TiO_2-R catalyst sample while 62.7 % of the copper was reduced in the Cu_1/TiO_2-R. The low reduction degree of Co_1/TiO_2-R is in agreement with our previous studies.[44] The extent of reduction of $Cu_{0.1}Co_{0.9}/TiO_2$-R and $Cu_{0.5}Co_{0.5}/TiO_2$-R was 48.1% and 50.2%, respectively. If we assume that 62.7% of the Cu is reduced in the bimetallic catalysts, then the extent of reduction of Co in $Cu_{0.1}Co_{0.9}/TiO_2$-R and $Cu_{0.5}Co_{0.5}/TiO_2$-R is 45.0 and 30.8%, respectively. It is likely that the extent of reduction under reaction conditions is different than the extent of reduction reported in Table 6.1 because of differences in the hydrogen partial pressure.

Figure 6.4 shows the STEM micrographs of $CuCo/TiO_2$-R catalysts with different Co contents. The majority of the Cu particles in the monometallic Cu_1/TiO_2-R catalyst were quasi-circular with an average diameter of 2.6 nm (Figure 6.4a). Small amounts of large Cu aggregates (> 20 nm) were observed in this catalyst (Figure 6.4a). The presence of some large Cu particles in Cu_1/TiO_2-R catalyst explains the much larger crystallite size (25.4 nm) determined by XRD (Figure 6.2c). A bimodal distribution of dispersed small particles (average particle sizes ~ 2.3 nm) and large particles (average particle sizes ~16.5 nm) was observed for $Cu_{0.5}Co_{0.5}/TiO_2$-R. Larger particles were observed in both $Cu_{0.1}Co_{0.9}/TiO_2$-R (21.3nm) and Co_1/TiO_2-R (19.8nm) catalysts compared to the catalysts which had more Cu. A few small particles (< 3 nm) were also observed in $Cu_{0.1}Co_{0.9}/TiO_2$-R; however, this catalyst had fewer of these smaller particles than the $Cu_{0.5}Co_{0.5}/TiO_2$-R catalyst. Accordingly, $Cu_{0.1}Co_{0.9}/TiO_2$-R has less of a bimodal character than $Cu_{0.5}Co_{0.5}/TiO_2$-R. The Co_1/TiO_2 sample consisted exclusively of larger (19.8 nm average size) particles.

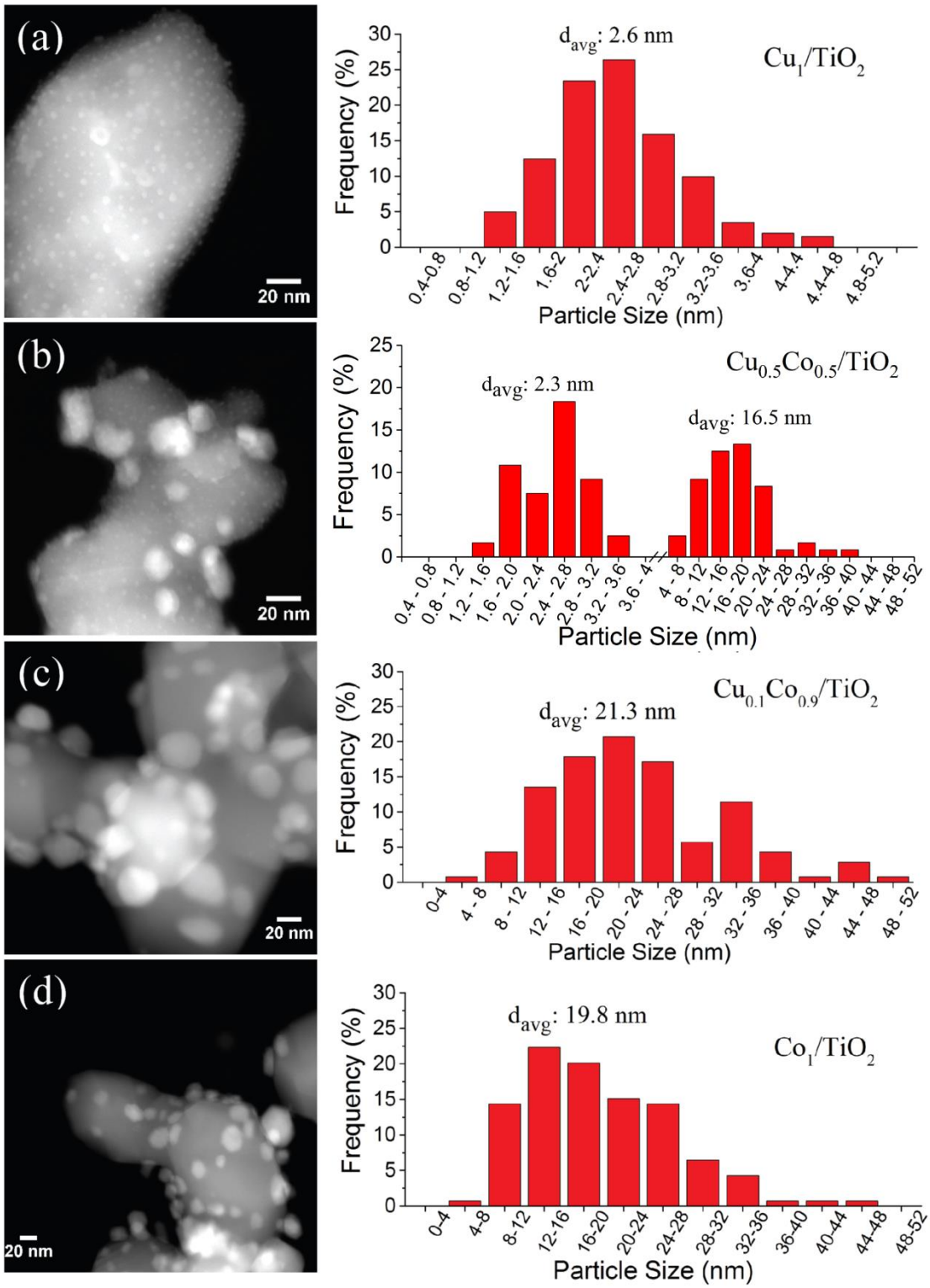

Figure 6.4 STEM micrographs of $CuCo/TiO_2$ catalysts with different Co contents: (a) Cu_1/TiO_2-R; (b) $Cu_{0.5}Co_{0.5}/TiO_2$-R; (c) $Cu_{0.1}Co_{0.9}/TiO_2$-R and (d) Co_1/TiO_2-R.

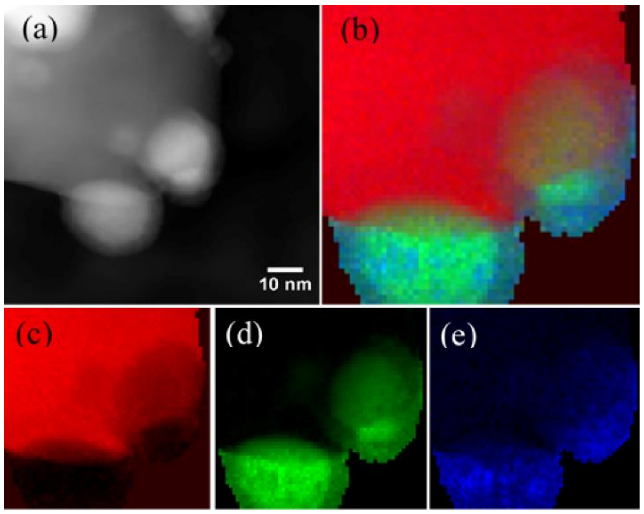

Figure 6.5 Spectral image analysis of $Cu_{0.1}Co_{0.9}/TiO_2$-R bimetallic nanoparticles: (a) STEM-HAADF image; (b) RGB composite map of two-dimensional EELS (red: Ti L map, green: Co L map, and blue: Cu L map); (c) elemental projection of Ti; (d) elemental projection of Co and (e) elemental projection of Cu.

EELS and EDS studies were conducted on several nanoparticles to investigate the elemental composition and distribution of elements in the $Cu_{0.1}Co_{0.9}/TiO_2$-R catalyst. Accurate elemental mapping of the small nanoparticles (<3 nm) was not possible due to damage by the electron beam before a sufficient signal-to-noise could be obtained, although Cu and Co both appear to exist to some extent in these particles. EELS of the large (~20 nm) nanoparticles revealed that Co and Cu formed bimetallic nanoparticles and were in close contact (Figure 6.5b). The composition maps showed highly concentrated Co signals in the core and more concentrated Cu signals on the outer surfaces of the nanoparticles (Figure 6.5b, d), suggesting that Cu prefers to deposit on the outer surface of the Co nanoparticles. EDS spot scans of several large nanoparticles were in agreement with the observation from EELS. The co-existence of Cu and Co, especially at the outer surface of the bimetallic nanoparticles (Figure 6.5b, d, e), suggests the formation of a CuCo alloy shell structure. Note that similar core-shell CuCo bimetallic nanoparticles with a Co-rich core and Cu-rich shell were also determined in $Cu_{0.5}C_{0.5}/TiO_2$ by EELS and EDS spot scans. The formation of such Co-

rich core and CuCo alloy near-surface shell particles is driven by the lower surface energy of Cu compared with Co (1.93 J/m^2 vs. 2.71 J/m^2).[38, 46-48]. The positive segregation energy (+0.73 eV) for Co-core and Cu-shell alloy nanoparticles calculated by DFT-PW91 also indicates the preferable formation of such core-shell configuration.[49] A similar Co-rich core and a Cu-dominated outer shell catalyst has also been recently prepared by Xiang et al. using a co-precipitation method.[50]

Table 6.2 Effect of different catalysts and solvents on GBL hydrogenation at 100°C

Catalyst	Solvent	Conversion (%)	Reaction rate ($mmol_{BDO}$/ $mol_{metal}\cdot h^{-1}$)	Carbon Selectivity (%)	
				1,4-BD	Byproducts
Blank	1,4-Dioxane	0	0	0	0
5%Pd/C	1,4-Dioxane	0	0	0	0
5%Pt/C	1,4-Dioxane	2.2	22.4	56.9	1-Bol (3.6)
5%Ru/C	1,4-Dioxane	23.1	75.2	34.5	1-Prol (7.5)
$CuCrO_x$	1,4-Dioxane	8.8	5.7	100	0
$Cu_{0.1}Co_{0.9}/TiO_2$-R	1,4-Dioxane	11.5	30.1	100	0
$Cu_{0.1}Co_{0.9}/TiO_2$-R	THF	0.9	1.2	100	0
$Cu_{0.1}Co_{0.9}/TiO_2$-R	Ethanol	9.3	5.9	23.7	EHB (76.3)
$Cu_{0.1}Co_{0.9}/TiO_2$-R	H_2O	16.8	0	0	4-HBA (100)

Reaction conditions: 20 g 1 wt% GBL in different solvents, 0.20 g catalyst, 100 °C, 3.4 MPa H_2, 24 h. The reaction rate is defined as mmol of 1,4-BD generated per mol of active metal per h. 1,4-BD: 1,4-butanediol; 1-Bol: 1-butanol; 1-Prol: 1-propanol; EHB: ethyl 4-hydroxybutanoate; 4-HBA: 4-hydroxybutanoic acid.

Table 6.2 shows the catalytic performance of different catalysts for hydrogenation of 1 wt% GBL at 100 °C in a batch reactor. Carbon-supported noble metal catalysts either presented low activity (rates <30 $mmol_{1,4\text{-}BD}/mol_{metal}\cdot h^{-1}$ for Pd/C and Pt/C) or low 1,4-BD selectivity (<57% for Ru/C, Pd/C, and Pt/C). Conversion to undetected humins or GBL adsorption onto Pt/C and Ru/C (similar as with GBL analog γ-valerolactone on Ru/C[51]) may have caused the low observed 1,4-BD selectivities over these catalysts. A commercial copper-chromite catalyst showed moderate

GBL hydrogenation activity (5.7 $mmol_{1,4\text{-}BD}/mol_{metal}\cdot h^{-1}$) and up to 100% 1,4-BD selectivity; however, the use of Cr-containing catalysts are undesirable because of the high toxicity of Cr(VI).[52,53] The $Cu_{0.1}Co_{0.9}/TiO_2$-R bimetallic catalyst exhibited high 1,4-BD production rate (30.1 $mmol_{1,4\text{-}BD}/mol_{metal}\cdot h^{-1}$) while maintaining 100% 1,4-BD selectivity.

A range of commonly used solvents was studied for GBL hydrogenation with the $Cu_{0.1}Co_{0.9}/TiO_2$-R catalyst, as shown in Table 6.2. Almost no reaction took place (GBL conversion <1%) when the reaction was carried out in THF. In ethanol and water, low selectivities to 1,4-BD (<24%) were obtained due to the formation of ester (ethyl 4-hydroxybutanoate, EHB) or acid (4-hydroxybutanoic acid, 4-HBA) byproducts, respectively. The highest activity and selectivity to 1,4-BD (100%) was attained when 1,4-dioxane was used as solvent. Previous studies also found 1,4-dioxane as a suitable solvent for 1,4-diols production from GBL,[33] SA[17] and levulinate esters[54].

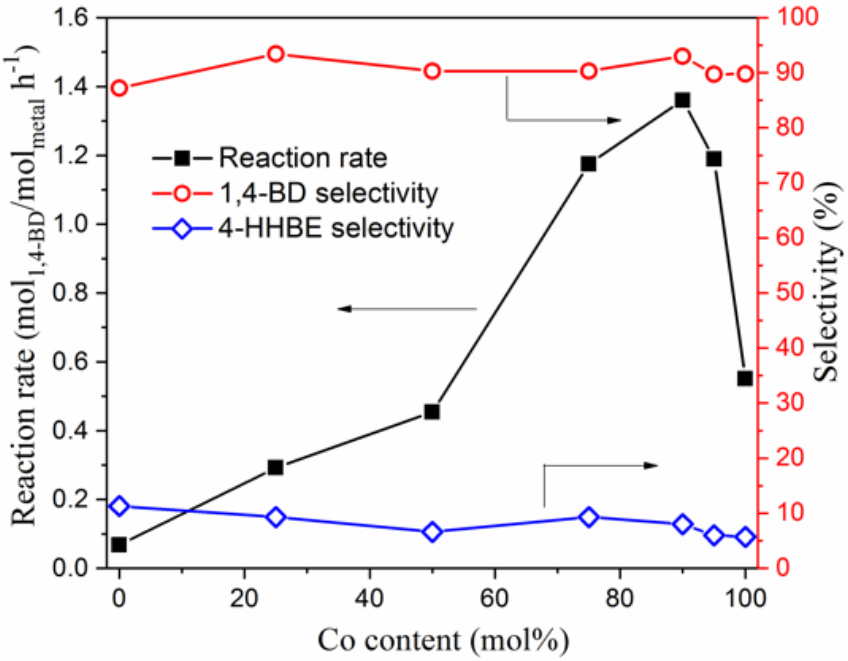

Figure 6.6 Effect of cobalt content on the catalytic activity and selectivity of $CuCo/TiO_2$-R catalysts at fixed Cu + Co molar amount (1.8 mmol/g) for GBL hydrogenation. The Co content is the amount of Co in the Cu+Co bimetallic catalyst. (Reaction conditions: 20 g 10 wt% GBL in 1,4-dioxane, 0.40 g catalyst (0.80 g for Cu_1/TiO_2-R), 140°C, 3.4 MPa H_2, 5-24 h, ~20% conversion).

Figure 6.6 shows the reaction rate and selectivity to major products for hydrogenation of 10 wt% GBL in 1,4-dioxane over $CuCo/TiO_2$-R catalysts as a function of Co content. The 1,4-BD production rate increased from 0.068 $mol_{1,4\text{-}BD}/mol_{metal}\cdot h^{-1}$ for monometallic Cu_1/TiO_2 to a maximum of 1.36 $mol_{1,4\text{-}BD}/mol_{metal}\cdot h^{-1}$ at 90 mole% Co content for $Cu_{0.1}Co_{0.9}/TiO_2$-R and then decreased to 0.55 $mol_{1,4\text{-}BD}/mol_{metal}\cdot h^{-1}$ for monometallic Co_1/TiO_2-R. The 1,4-BD selectivity did not vary significantly (maintained in the range of 87.2-93.4%) with the change in Co content, with the $CuCo/TiO_2$ bimetallic catalysts having a slightly higher selectivity than their Cu and Co monometallic counterparts. In contrast to experiments performed at low GBL concentrations (1 wt%; Table 6.2), the higher GBL concentrations (10 wt%) used in this experiment resulted in formation of 4-hydroxybutyl,4-hydroxybutanoate (4-HHB) with selectivities up to 12.5%. Other byproducts detected were small amounts of THF (≤0.3%) and 1-Bol (≤0.2%) (not shown).

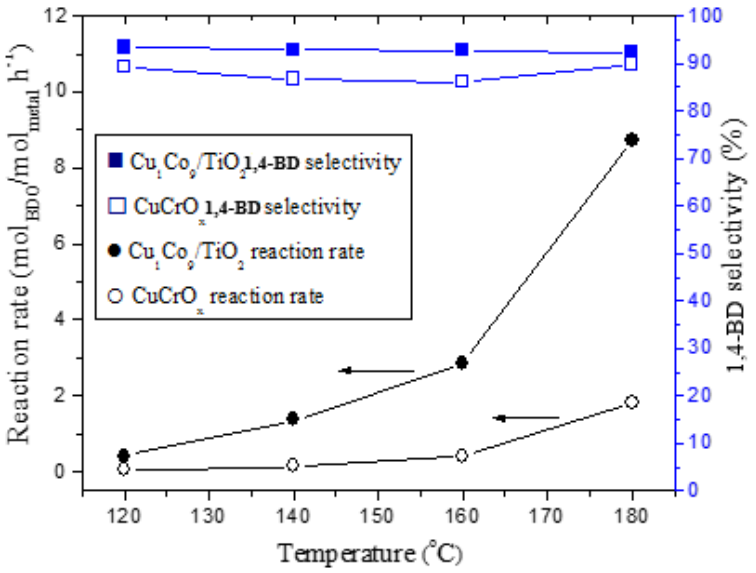

Figure 6.7 Effect of reaction temperature for hydrogenation of GBL on $Cu_{0.1}Co_{0.9}/TiO_2$-R and commercial $CuCrO_x$ catalysts. (Reaction conditions: 20 g 10 wt% GBL in 1,4-dioxane, 0.40 g catalyst, 3.4 MPa H_2, ~20% conversion, 0.6-28 h reaction).

Figure 6.7 shows the reaction rate and 1,4-BD product selectivity of GBL hydrogenation over $Cu_{0.1}Co_{0.9}/TiO_2$-R and a commercial $CuCrO_x$ catalyst as a function of reaction temperature

from 120 to 180 °C. At a temperature of 120 °C, the rate of 1,4-BD production over $Cu_{0.1}Co_{0.9}/TiO_2$-R (0.412 $mol_{1,4\text{-}BD}/mol_{metal}\cdot h^{-1}$) is 11.4 times higher than over $CuCrO_x$ (0.036 $mol_{1,4\text{-}BD}/mol_{metal}\cdot h^{-1}$) on a mol active metal basis (for $CuCrO_x$ is based on mol of Cu). At 180 °C the rate of 1,4-BD production for $Cu_{0.1}Co_{0.9}/TiO_2$-R (8.711 $mol_{1,4\text{-}BD}/mol_{metal}\cdot h^{-1}$) is 4.8 times higher than over $CuCrO_x$ (1.803 $mol_{1,4\text{-}BD}/mol_{metal}\cdot h^{-1}$). The apparent activation energy (Ea) for $Cu_{0.1}Co_{0.9}/TiO_2$-R is 75 kJ/mol, versus 93 kJ/mol for $CuCrO_x$. The 1,4-BD selectivity for $Cu_{0.1}Co_{0.9}/TiO_2$-R slightly declined from 93.4 to 92.3% with increasing temperature from 120 to 180 °C. The 1,4-BD selectivity for $Cu_{0.1}Co_{0.9}/TiO_2$-R was higher than the 1,4-BD selectivity for $CuCrO_x$ (86-89.9%) over the entire temperature range studied. The rather low surface acidity of the $Cu_{0.1}Co_{0.9}/TiO_2$ bimetallic catalyst (~1/9 of $CuCrO_x$ catalyst, Figure 6.8) explains its higher 1,4-BD selectivity for GBL hydrogenation, as acid sites catalyzed the dehydration of 1,4-BD to form THF and 1-Bol byproducts.[13,31,55,56]

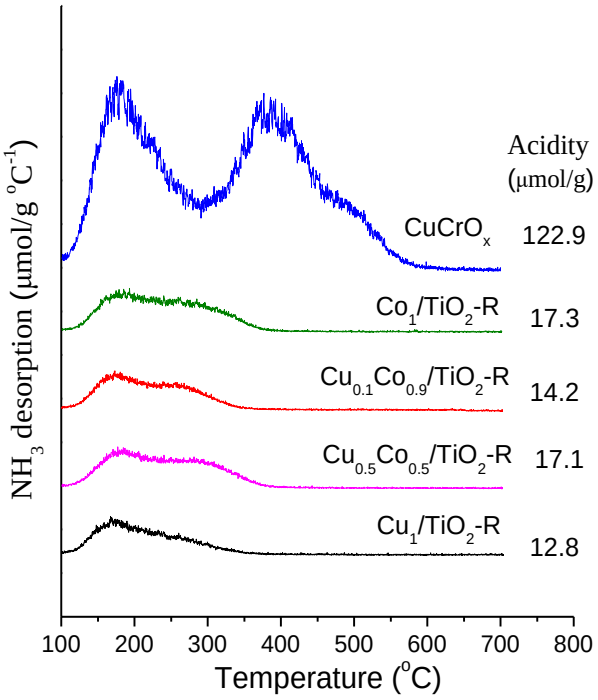

Figure 6.8 NH_3-TPD of a commercial $CuCrO_x$ catalyst and $CuCo/TiO_2$-R catalysts with different Co contents.

Figure 6.9 shows the time course of GBL hydrogenation over $Cu_{0.1}Co_{0.9}/TiO_2$-R catalyst at 140 °C and 3.4 MPa H_2. The concentration of GBL decreased significantly in the first 24 h - with a corresponding increase in the concentration of 1,4-BD - before stabilizing at 0.06 mol/L C after 36 h. The concentration of 4-HHB went through a maximum at 8 h, after which it was likely converted to 1,4-BD. A maximum in 1,4-BD yield (95.2%) was achieved at 36 h, followed by a decrease in1,4-BD concentration from 4.60 at 36 h to 4.38 mol/L C at 48 h due to over-conversion of 1,4-BD to THF, 1-Bol, and 1-Prol through a series of secondary reactions. THF, 1-Bol, and 1-Prol concentrations were minimal even after 48 h: 0.22, 0.05 and 0.08 mol/L C, respectively. No 2-HTHF or 4-HB was observed in this reaction even though they are likely reaction intermediates.

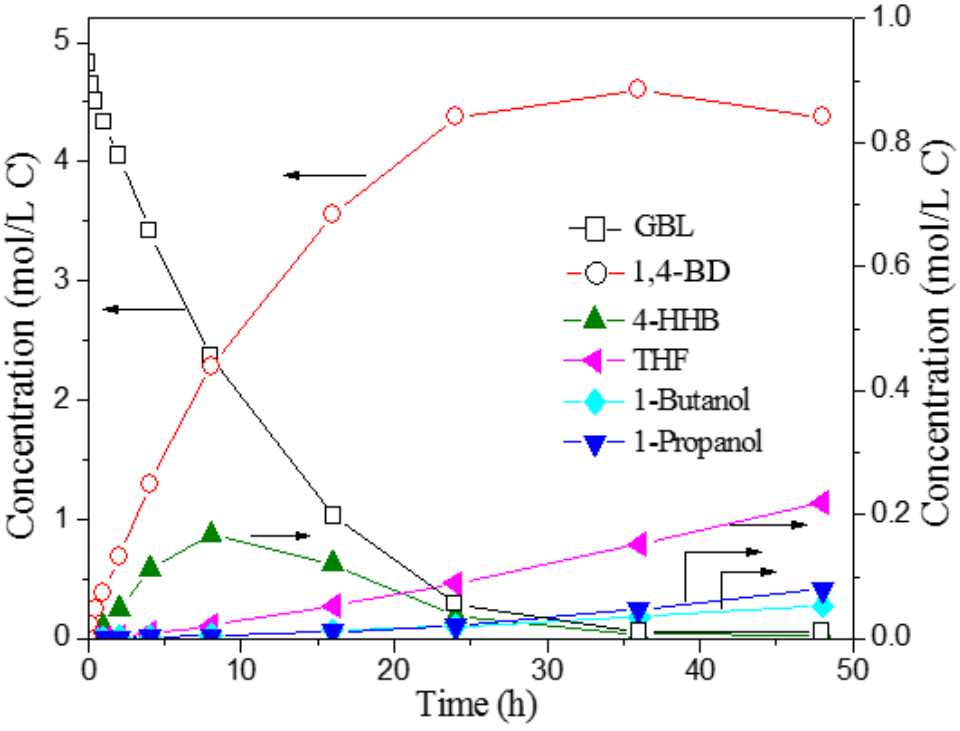

Figure 6.9 GBL hydrogenation over $Cu_{0.1}Co_{0.9}/TiO_2$-R as a function of reaction time (Reaction conditions: 30 g 10 wt% GBL in 1,4-dioxane, 1.2 g catalyst, 140 °C and 3.4 MPa H_2).

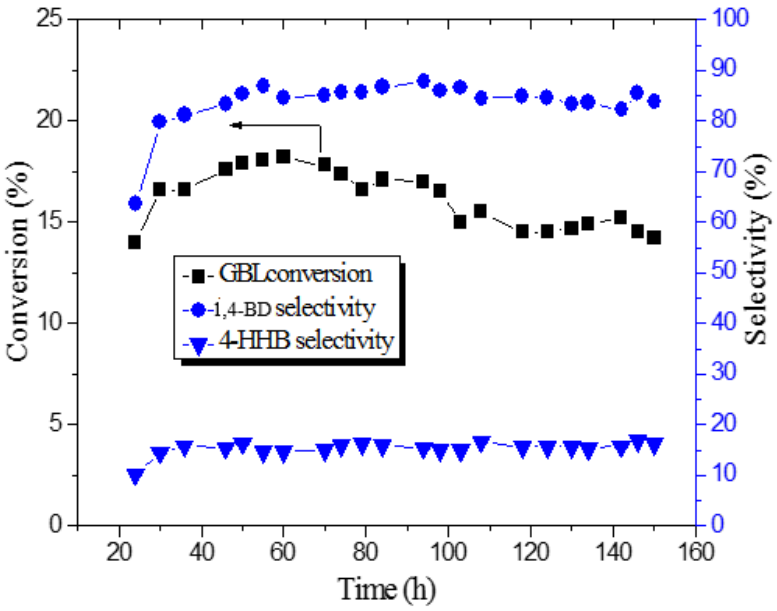

Figure 6.10 GBL hydrogenation with $Cu_{0.1}Co_{0.9}/TiO_2$-R in a continuous flow reactor. (Reaction conditions: 10 wt% GBL in 1,4-dioxane, 0.60 g catalyst, 140°C , 3.4 MPa H_2, WHSV of GBL = 0.2 h^{-1}, and H_2/GBL mole ratio = 50.

The long-term stability of the $Cu_{0.1}Co_{0.9}/TiO_2$-R bimetallic catalyst for GBL hydrogenation was carried out using a fixed-bed flow reactor as shown in Figure 6.10. The GBL conversion remained constant between 16.5-18.2% for 98 h before slowly declining to 14.2% after 150 h time-on-stream. The 1,4-BD (81.2-87.8%) and 4-HHB intermediate (11.7-17.2%) selectivities were stable from 30-150 h time-on-stream. The total selectivity to the THF, 1-Bol, and 1-Prol byproducts remained below 0.6% during the entire reaction.

The spent catalyst after the 150 h reaction was characterized by XRD, TGA, ICP, BET, and STEM. No perceptible structure changes were observed by XRD as compared with the reduced fresh catalyst (Figure 6.11). The BET surface area of the spent catalyst (12.0 m^2/g) was nearly unchanged from the fresh catalyst (11.6 m^2/g). ICP analysis showed no leaching of Cu or Co during the reaction. In addition, no detectable weight loss due to the desorption/decomposition of coke

can be seen from the TG profile. While it is possible that a small amount of sintering occurred, there were no large particle size changes observed by the STEM between fresh and spent $Cu_{0.1}Co_{0.9}/TiO_2$-R (Figure 6.12). It is possible that slight restructuring of the surface morphology of Cu and Co occurred and caused deactivation.

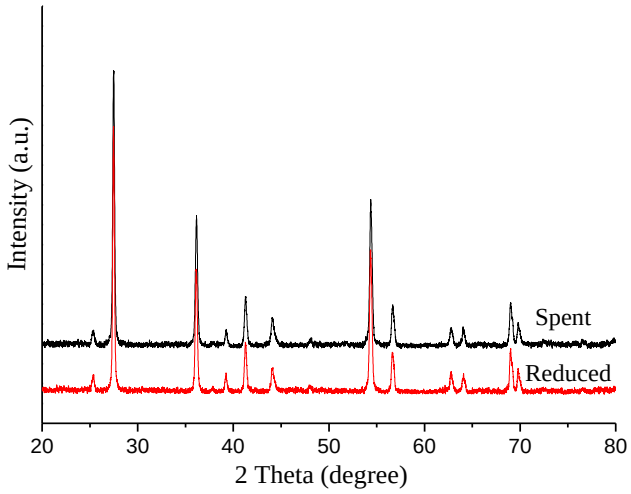

Figure 6.11 XRD spectrum of the $Cu_{0.1}Co_{0.9}/TiO_2$-R catalyst before and after the 150 h time-on stream GBL hydrogenation reaction.

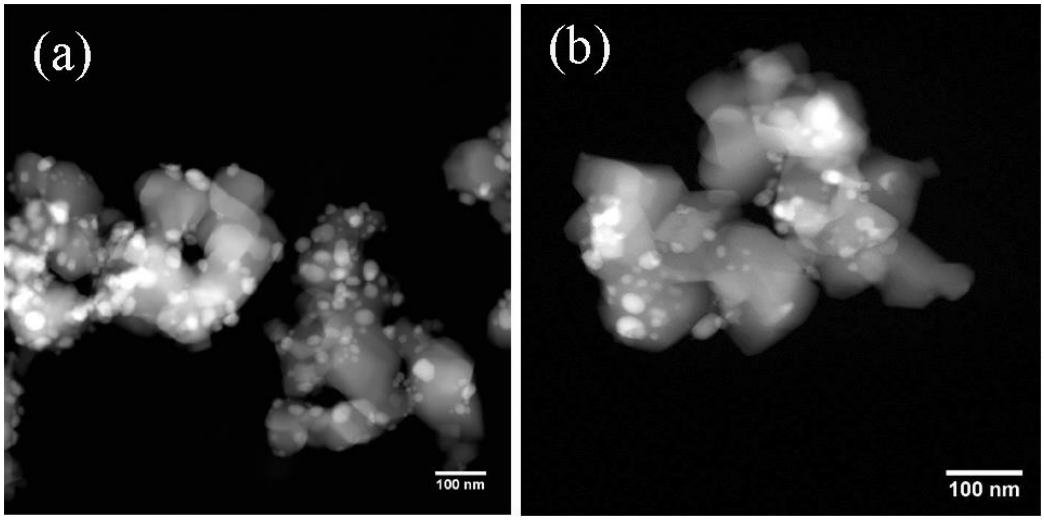

Figure 6.12 STEM image of fresh (a) and spent $Cu_{0.1}Co_{0.9}/TiO_2$ after 150 h time-on steam (b). No appreciable sintering of active particles was observed.

Table 6.3 shows the reaction rate for hydrogenation of different model compounds over the $Cu_{0.1}Co_{0.9}/TiO_2$-R catalyst at 100 ^oC. Butyraldehyde, ethyl butyrate, and butyric acid were used as the corresponding model compounds for 4-HB, 4-HHB, and 4-HBA due to the unavailability of the latter compounds. The reaction rate for hydrogenation of 2-HTHF and butyraldehyde is ~700 and ~400 times higher than the reaction rate for hydrogenation of GBL, explaining why these intermediates were not detected by GC. The similar conversion rates of 2-HTHF and butyraldehyde are further evidence that conversion of 2-HTHF to 1,4-BD proceeds via hydrogenation of the aldehyde group of 4-HB. Note that a small amount (4.5%) of GBL was detected at the beginning (conversion < 20%) of 2-HTHF hydrogenation, which further confirms that 2-HTHF is a reaction intermediate for GBL hydrogenation. The reaction rate of the other molecules was much lower than 2-HTHF and butyraldehyde and decreased in the order GBL > ethyl butyrate > butyric acid.

Table 6.3 Reaction results of various substrates hydrogenation over $Cu_{0.1}Co_{0.9}/TiO_2$-R catalyst at 100 ^oC

Substrates	Time (h)	Catalyst amount (g)	Conversion (%)	Rate (mol_{prod} /mol_{metal}·h^{-1})	Carbon Selectivity (%)		
					1,4-BD	GBL	1-Butanol
GBL	24	0.2	11.5	0.03	100	-	0
2-HTHF	0.5	0.02	18.2	21.1	95.5	4.5	0
Butyraldehyde	1	0.02	15.4	11.7	0	0	100
Ethyl butyrate	24	0.2	1.4	0.004	0	0	100
Butyric acid	24	0.2	0	0	0	0	0

* Reaction conditions: 20 g 1 wt% substrate in 1,4-dioxane, 100 °C, 3.4 MPa H_2

In situ NMR spectroscopy measurements were collected to determine the equilibrium of 2-HTHF and its ring-opened tautomer, 4-HB, in 1,4-dioxane at varying temperature (24 to 82 °C), as shown in Figure 6.13. At 24 °C 5.8% of the cyclic hemiacetal, 2-HTHF, exists in its ring-open

form (4-HB). The equilibrium shifts towards the ring-opened product at elevated temperatures as a result of endothermic tautomerization, with up to 20% of 2-HTHF transformed to 4-HB at 82 °C. Extrapolation of the NMR ring-opening equilibrium data suggests that the equilibrium is 28.4% and 65% ring-opened to 4-HB at a reaction temperature of 100 and 140 °C, respectively.

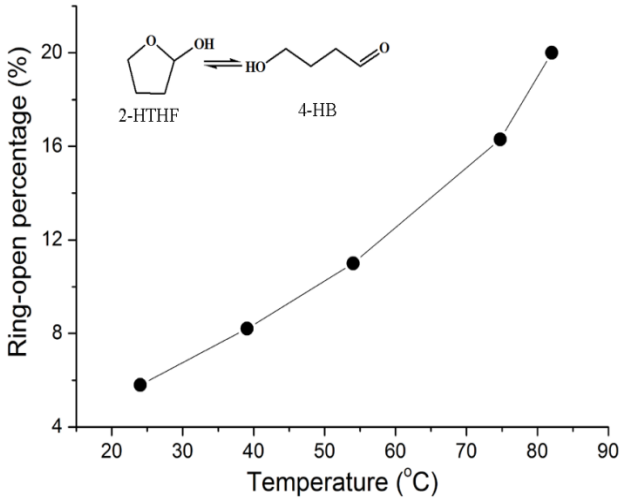

Figure 6.13 Variable temperature NMR of 2-HTHF in 1,4-Dioxane.

Based on the time-course reaction studies, variable temperature NMR measurements, and probe reaction studies, we propose the reaction pathway for the production of 1,4-BD and byproducts shown in Figure 6.14. GBL is initially hydrogenated to 2-HTHF, which then equilibrates with its ring-opened tautomer, 4-HB. This equilibration to the ring-opened form is followed by the rapid hydrogenation to 1,4-BD over metallic active sites. This reaction pathway is similar to the hydrogenation of other hemiacetals including the hydrogenation of the hemiacetal 2-hydroxytetrahydropyran (2-HTHP) to 1,5 pentanediol[27] and an analogous C_6 route from tetrahydropyran-2-methanol to 1,6-hexanediol.[29] Higher feedstock concentrations lead to the formation of the ester 4-HHB from the GBL reactant and the 1,4-BD product. The ester can be further hydrogenated to 1,4-BD. The dehydration and hydrogenolysis of 1,4-BD generates the

byproducts THF and 1-Bol, respectively.[13,31,55,56] The 1-propanol (1-Prol) byproduct is likely formed via the decarbonylation of 4-HB. 4-HBA is formed when water is a solvent but not in 1,4-dioxane.

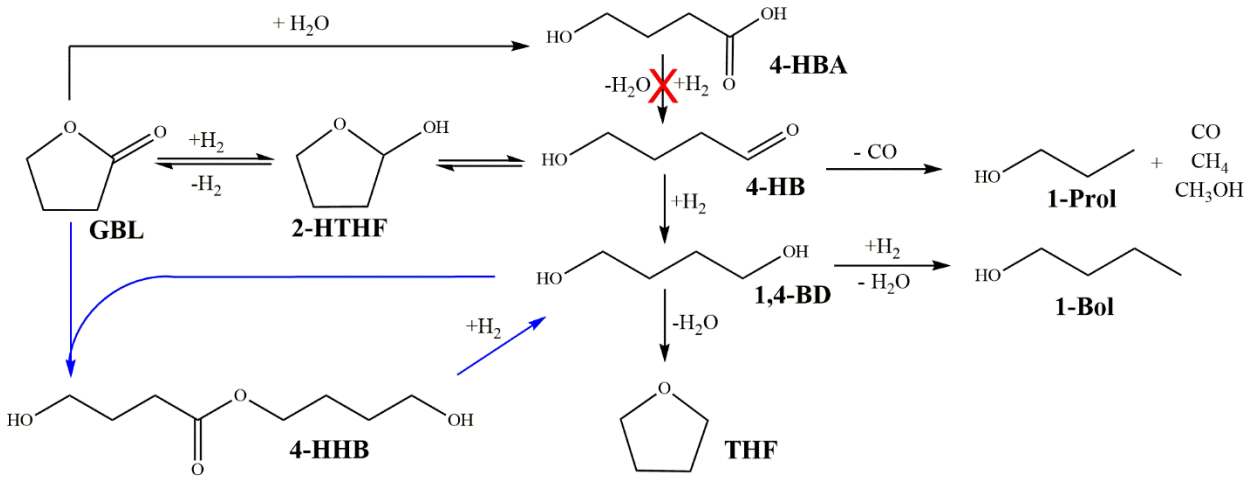

Figure 6.14 Proposed reaction pathway for the production of 1,4-BD and byproducts (The blue arrows show that 4-HHB is a reaction intermediate that can be further converted to 1,4-BD).

Although Cu-based catalysts have been widely used for the production of 1,4-diols by the hydrogenation of GBL, γ-valerolactone, ester derivatives of SA and MA,[2,5,6,8,10,33,57] our findings show that Co_1/TiO_2-R is more than 8 times active than Cu_1/TiO_2-R for GBL hydrogenation. The reaction rate is further enhanced by 2.1-2.5 times by the addition of small amount of Cu (5~25 mol%) into the Co catalyst (Figure 6.6). Cu has a low solubility in Co with a maximum of 9 at% Cu that can be dissolved in Co at 1050 °C, according to the binary Cu-Co phase diagram.[58] The amount of Cu that can form a Cu-Co solution decreases with decreasing temperature. However, recent studies indicate that CuCo alloy particles can be formed in nanoparticles below 100 nm.[46,47,50,59-61] A variety of experimental techniques, including STEM-EDS(EDX) chemical analysis,[46,59-61,63,64] high-resolution TEM,[46,63] Atom probe tomography (APT)[50], and X-ray photoelectron spectroscopy (XPS) with Ar^+ ions etching[47,62] have been applied to confirm the

formation of CuCo nanoalloy particles. In the present work, STEM-EELS (Figure 6.5) and STEM-EDS showed the formation of Co-rich core and CuCo alloy near-surface shell nanoparticles in the $Cu_{0.1}Co_{0.9}/TiO_2$-R bimetallic catalyst. XRD results (Figure 6.2) also provided evidence for the formation of CuCo bimetallic phase in the $CuCo/TiO_2$ bimetallic catalysts. CuCo bimetallic nanoparticles have been reported to have higher activity than their monometallic counterparts in many catalytic reactions.[50, 60-63,65] Prieto et al.[60] ascribed the high activity of a $CuCo/MoO_x$ catalyst in synthesis gas hydrogenation to the formation of a nanosized CuCo alloy phase at a Co/(Cu + Co) ratio of 0.65. Therefore, the higher reaction rate and 1,4-BD selectivity obtained with the Co-rich $CuCo/TiO_2$ bimetallic catalysts is likely due to the formation of CuCo alloy shell nanoparticles.

6.4 Conclusions

It was demonstrated that GBL can be selectively hydrogenated into 1,4-BD in a 1,4-dioxane solvent with Cu-Co/TiO_2 catalysts. The rate of GBL hydrogenation increases with increasing Co content with a maximum at around 90 mol% Co-10 mol% Cu. The $Cu_{0.1}Co_{0.9}/TiO_2$ bimetallic catalyst had ~11, 2.5 and 20 times higher activity than a commercial copper chromite, monometallic Co and monometallic Cu catalysts, respectively. A small amount of Cu (~10 mol%) in the bimetallic catalyst increased the reducibility of the Co and resulted in the formation of Co-rich core and CuCo alloy near-surface shell nanoparticles, leading to higher activity and selectivity of the catalyst. GBL hydrogenation in ethanol and water produced EHB and 4-HBA, respectively, as the major products. GBL hydrogenation in 1,4-dioxane produced up to 95% yield of 1,4-BD with $Cu_{0.1}Co_{0.9}/TiO_2$ in a batch reactor under relatively mild conditions of 140˚C and 3.4 MPa H_2. The $Cu_{0.1}Co_{0.9}/TiO_2$ also exhibited good stability for GBL hydrogenation in a continuous flow reactor, maintaining about 80% of its activity after 150 h time-on stream. The rate of hydrogenation

of 2-HTHF and butyraldehyde (a model of 4-HB) in 1,4-dioxane is ~700 and ~400 times greater than the rate of hydrogenation of GBL, respectively, indicating GBL hydrogenation likely goes through 2-HTHF and 4-HB intermediates. In 1,4-dioxane, 2-HTHF undergoes facile ring opening tautomerization to 4-HB, with approximately 65% of 2-HTHF converting to 4-HB at 140˚C.

6.5 References

1. Grand View Research. *1,4 Butanediol (1,4-BD) Market Analysis by Application (Tetrahydrofuran (THF), Polybutylene Terephthalate (PBT), Gamma-Butyrolactone (GBL), Polyurethane (PU)), By Region (North America, Europe, Asia Pacific, CSA, MEA), And Segment Forecasts, 2014-2025*; 2017.
2. Sun, D.; Sato, S.; Ueda, W.; Primo, A.; Garcia, H.; Corma, A. Production of C4 and C5 alcohols from biomass-derived materials. *Green Chem.* **2016,** *18*, 2579-2597.
3. Haas, T.; Jaeger, B.; Weber, R.; Mitchell, S. F.; King, C. F. New Diol Processes: 1,3-Propanediol and 1,4-Butanediol. *Appl. Catal. A Gen.* **2005**, *280* (1), 83–88.
4. Li, F.; Lu, T.; Chen, B.; Huang, Z.; Yuan, G. Pt Nanoparticles over TiO2-ZrO2mixed Oxide as Multifunctional Catalysts for an Integrated Conversion of Furfural to 1,4-Butanediol. *Appl. Catal. A Gen.* **2014**, *478*, 252–258.
5. Chen, L. F.; Guo, P. J.; Zhu, L. J.; Qiao, M. H.; Shen, W.; Xu, H. L.; Fan, K. N. Preparation of Cu/ SBA-15 catalysts by different methods for the hydrogenolysis of dimethyl maleate to 1,4-butanediol. *Appl. Catal. A* **2009,** *356*, 129-136.
6. Ohlinger, C.; Kraushaar-Czarnetzki, B. Improved processing stability in the hydrogenation of dimethyl maleate to γ-butyrolactone, 1,4-butanediol and tetrahydrofuran*Chem. Eng. Sci.* **2003,** *58*, 1453-1461.
7. Meyer, C. I.; Regenhardt, S. A.; Marchi, A. J.; Garetto, T. F. Gas phase hydrogenation of maleic anhydride at low pressure over silica-supported cobalt and nickel catalysts.*Appl. Catal. A* **2012,** *417*, 59-65.
8. Schlander, J. H.; Turek, T. Gas-Phase Hydrogenolysis of Dimethyl Maleate to 1,4-Butanediol and γ-Butyrolactone over Copper/Zinc Oxide Catalysts. *Ind. Eng. Chem. Res*. **1999**, *38*, 1264-1270.
9. Pillai, U. R.; Sahle-Demessie, E.; Young, D. Maleic anhydride hydrogenation over Pd/Al2O3 catalyst under supercritical CO2 medium. *Appl. Catal. B.* **2003**, *43*, 131-138.
10. Ding, G.; Zhu, Y.; Zheng, H.; Zhang, W.; Li, Y. Study on the reaction pathway in the vapor-phase hydrogenation of biomass-derived diethyl succinate over CuO/ZnO catalyst. *Catal. Commun.* **2010**, *11*, 1120-1124.

11. Besson, M.; Gallezot, P.; Pinel, C. Conversion of Biomass into Chemicals over Metal Catalysts. *Chem. Rev.* **2014**, *114*, 1827–1870.

12. Kang, K. H.; Han, S. J.; Lee, J. W.; Kim, T. H.; Song, I. K. Effect of Boron. Content on 1,4-Butanediol Production by Hydrogenation of Succinic Acid over. Re-Ru/BMC (Boron-modified Mesoporous Carbon) Catalysts. *Appl. Catal. A.* **2016**, *524*, 206-213.

13. Liu, X.; Wang, X.; Xu, G.; Liu, Q.; Mu, X.; Liu, H. Tuning the catalytic selectivity in biomass-derived succinic acid hydrogenation on FeOx-modified Pd catalysts. *J. Mater. Chem. A.* **2015**, *3*, 23560-23569.

14. Li, X.; Jia, P.; Wang, T. Furfural: A Promising Platform Compound for Sustainable Production of C4 and C5 Chemicals. *ACS Catal.* **2016**, *6*, 7621-7640.

15. Luque, R.; Clark, J. H.; Yoshida, K.; Gai, P. L. Efficient aqueous hydrogenation of biomassplatform molecules using supported metal nanoparticles on Starbons®. *Chem. Commun*. **2009**, 5305-5307.

16. Corbel-Demailly, L.; Ly, B. K.; Minh, D. P.; Tapin, B.; Especel, C.; Epron, F.; Cabiac, A.; Guillon, E.; Besson, M.; Pinel, C. Heterogeneous catalytic hydrogenation of biobased levulinic and succinic acids in aqueous solutions. *ChemSusChem* **2013**, *6*, 2388-2395.

17. Kang, K. H.; Hong, U. G.; Bang, Y.; Choi, J. H.; Kim, J. K.; Lee, J. K.; Han, S. J.; Song, I. K. Hydrogenation of Succinic Acid to 1,4-Butanediol over Re-Ru. Bimetallic Catalysts Supported on Mesoporous Carbon. *Appl. Catal. A* **2015**, *490*, 153-162.

18. Minh, D. P.; Besson, M.; Pinel, C.; Fuertes, P.; Petitjean, C. Aqueous-phase hydrogenation of biomass-based succinic acid to 1, 4-butanediol over supported bimetallic catalysts. *Top. Catal.* **2010**, *53*, 1270-1273.

19. Li, X.; Lan, X.; Wang, T. Highly selective catalytic conversion of furfural to γ-butyrolactone. Green Chem. **2016**, *18*, 638-642.

20. Alonso-Fagúndez, N.; Ojeda, M.; Mariscal, R.; Fierro, J. L. G.; López Granados, M. Gas phase oxidation of furfural to maleic anhydride on V2O5/c-Al2O3 catalysts: Reaction conditions to slow down the deactivation. *J. Catal*. **2017**, *348*, 265-275.

21. Li, X.; Hoa, B.; Zhang, Y. Selective aerobic oxidation of furfural to maleic anhydride with heterogeneous Mo–V–O catalysts. *Green Chem.* **2016**, *18*, 2976-2980

22. Fuchigami, T.; Wakasa, N.; Iwai, N. J.P. Patent 7082189A, 1995.

23. Thomas, D.; Taylor, P. D. U.S. Patent 4797382, 1989.

24. Bertola, A. U.S. Patent 6191322, 2001.

25. Cawse, J. N.; Johnson, N. E.; Whitaker, M. T. U.S. Patent 4652685, 1987.

26. Li, W.; Xie, J. H.; Yuan, M. L.; Zhou, Q. L. Ruthenium complexes of tetradentate bipyridine ligands: highly efficient catalysts for the hydrogenation of carboxylic esters and lactones. *Green Chem*. **2014**, *16*, 4081-4085.

27. Brentzel, Z. J.; Barnett, K. J.; Huang, K.; Maravelias, C. T.; Dumesic, J. A.; Huber, G. W. Chemicals from Biomass: Combining Ring-Opening Tautomerization and Hydrogenation Reactions to Produce 1,5-Pentanediol from Furfural. *ChemSusChem* **2017**, *10* (7), 1351–1355.

28. Huang, K.; Brentzel, Z. J.; Barnett, K. J.; Dumesic, J. A.; Huber, G. W.; Maravelias, C. T. Conversion of Furfural to 1,5-Pentanediol: Process Synthesis and Analysis. *ACS Sustain. Chem. Eng.* **2017**, *5* (6), 4699–4706.

29. Burt, S. P.; Barnett, K. J.; McClelland, D. J.; Wolf, P.; Dumesic, J. A.; Huber, G. W.; Hermans, I. Production of 1,6-Hexanediol from Tetrahydropyran-2-Methanol by Dehydration–hydration and Hydrogenation. *Green Chem.* **2017**, *19* (5), 1390–1398.

30. Leite, L.; Lebedevs, A.; Stonkus, V.; Fleisher, M. Transformation of 4-hydroxybutanal over porcelain. *J. Mol. Catal. A* **1999**, *144*, 323-328.

31. Zhang, B.; Zhu, Y.; Ding, G.; Zheng, H.; Li, Y. Modification of the supported Cu/SiO2 catalyst by alkaline earth metals in the selective conversion of 1,4-butanediol to gamma-butyrolactone. *Appl. Catal. A* **2012**, *443*, 191-201.

32. Ichikawa, N.; Sato, S.; Takahashi, R.; Sodesawa, T.; Inui, K. Dehydrogenative cyclization of 1,4-butanediol over copper-based catalyst. *J. Mol. Catal. A* **2004**, *212*, 197-203.

33. Hamminga, G. M.; Mul, G.; Moulijn, J. A. Real-time in situ ATR-FTIR analysis of the liquid phase hydrogenation of γ-butyrolactone over Cu-ZnO catalysts: A mechanistic study by varying lactone ring size. *Chem. Eng. Sci.* **2004**, *59*, 5479-5485.

34. Lee, J.; Burt, S. P.; Carrero, C. A.; Alba-Rubio, A. C.; Ro, I.; O'Neill, B. J.; Kim, H. J.; Jackson, D. H. K.; Kuech, T. F.; Hermans, I.; et al. Stabilizing Cobalt Catalysts for Aqueous-Phase Reactions by Strong Metal-Support Interaction. *J. Catal.* **2015**, *330*, 19–27.

35. Bosman, M.; Watanabe, M.; Alexander, D. T. L.; Keast, V. J. Mapping chemical and bonding information using multivariate analysis of electron energy-loss spectrum images. *Ultramicroscopy* **2006**, *106*, 1024-1032.

36. Potapov, P.; Longo, P.; Okunishi, E. Enhancement of noisy EDX HRSTEM spectrum-images by combination of filtering and PCA. *Micron* **2017**, *96*, 29-37.

37. Su, J.; Mao, W.; Xu, X. C.; Yang, Z.; Li, H.; Xu, J.; Han, Y. F. Kinetic study of higher alcohol synthesis directly from syngas over CoCu/SiO2 catalysts. *AIChE J.* **2014**, *60*, 1797-1809.

38. Wang, J.; Chernavskii, P. A.; Khodakov, A. Y.; Wang, Y. Structure and catalytic performance of alumina-supported copper–cobalt catalysts for carbon monoxide hydrogenation. *J. Catal.* **2012**, *286*, 51-61.

39. Liu, G.; Pan, D.; Niu, T.; Cao, A.; Yue, Y.; Liu, Y. Nanoparticles of Cu–Co alloy supported on high surface area LaFeO3—preparation and catalytic performance for higher alcohol synthesis from syngas. *RSC Adv.* **2015**, *5*, 31637-31647.

40. Xiao, K.; Qi, X.; Bao, Z.; Wang, X.; Zhong, L.; Fang, K.; Lin, M.; Sun, Y. CuFe, CuCo and CuNi nanoparticles as catalysts for higher alcohol synthesis from syngas: a comparative study. *Catal. Sci. Technol.* **2013**, *3*, 1591-1602.

41. Bertella, F.; Concepción, P.; Martínez, A. TiO2 polymorph dependent SMSI effect in Co-Ru/TiO2catalysts and its relevance to Fischer-Tropsch synthesis. *Catal. Today* **2017**, *289*, 181-191.

42. Jongsomjit, B.; Wongsalee, T.; Praserthdam, P. Characteristics and catalytic properties of Co/TiO2 for various rutile:anatase ratios. *Catal. Commun.* **2005**, *6*, 705-710.

43. Srivastava, S.; Jadeja, G. C.; Parikh, J. A versatile bi-metallic copper–cobalt catalyst for liquid phase hydrogenation of furfural to 2-methylfuran. *RSC Adv.* **2016**, *6*, 1649-1658.

44. Ávila-Neto, C. N.; Zanchet, D.; Hori, C. E.; Ribeiro, R. U.; Bueno, J. M. C. Interplay between particle size, composition, and structure of MgAl2O4-supported Co–Cu catalysts and their influence on carbon accumulation during steam reforming of ethanol. *J. Catal.* **2013**, *307*, 222-237.

45. Anton, J.; Nebel, J.; Song, H.; Froese, C.; Weide, P.; Ruland, H.; Muhler, M.; Kaluza, S. Structure–activity relationships of Co-modified Cu/ZnO/Al2O3 catalysts applied in the synthesis of higher alcohols from synthesis gas. *Appl. Catal. A* **2015**, *505*, 326-333.

46. Gao, W.; Zhao, Y.; Chen, H.; Chen, H.; Li, Y.; He, S.; Zhang, Y.; Wei, M.; Evans, D. G.; Duan, X. Core–shell Cu@(CuCo-alloy)/Al2O3catalysts for the synthesis of higher alcohols from syngas. *Green Chem.* **2015**, *17*, 1525-1534.

47. Ahmed, J.; Ganguly, A.; Saha, S.; Gupta, G.; Trinh, P.; Mugweru, A. M.; Lofland, S. E.; Ramanujachary, K. V.; Ganguli, A. K. Enhanced Electrocatalytic Activity of Copper–Cobalt Nanostructures. *J. Phys. Chem. C* **2011**, *115*, 14526-14533.

48. Liu, G.; Niu, T.; Pan, D.; Liu, F.; Liu, Y. Preparation of bimetal Cu–Co nanoparticles supported on meso–macroporous SiO2 and their application to higher alcohols synthesis from syngas. *Appl. Catal. A* **2014**, *483*, 10-18.

49. Wang, L. L.; Johnson, D. D. Predicted Trends of Core−Shell Preferences for 132 Late Transition-Metal Binary-Alloy Nanoparticles. *J. Am. Chem. Soc.* **2009**, *131*, 14023-14029.

50. Xiang, Y.; Chitry, V.; Liddicoat, P.; Felfer, P.; Cairney, J.; Ringer, S.; Kruse, N. Long-Chain Terminal Alcohols through Catalytic CO Hydrogenation. *J. Am. Chem. Soc.* **2013**, *135*, 7114-7117.

51. Ding, D.; Wang, J.; Xi, J.; Liu, X.; Lu, G.; Wang, Y. High-yield production of levulinic acid from cellulose and its upgrading to γ-valerolactone. *Green Chem*. **2014**, *16*, 3846-3853.

52. Scancar, J.; Milacic, R. A critical overview of Cr speciation analysis based on high performance liquid chromatography and spectrometric techniques. *J. Anal. At. Spectrom.* **2014**, *29*, 427-443.

53. Ma, Y.; Hooda, P. S. Chromium, Nickel and Cobalt. In Trace Elements in Soils; Hooda, P. S., Ed.; Blackwell Publishing, Ltd: Hoboken, NJ, 2010; pp 470-472.

54. Ren, D.; Wan, X.; Jin, F.; Song, Z.; Liu, Y.; Huo, Z. Selective hydrogenation of levulinate esters to 1,4-pentanediol using a ternary skeletal CuAlZn catalyst. *Green Chem.* **2016**, *18*, 5999-6003.

55. Reddy, K. H. P.; Anand, N.; Prasad, P. S. S.; Rao, K. S. R.; Raju, B. D. Influence of method of preparation of Co-Cu/MgO catalyst on dehydrogenation/dehydration reaction pathway of 1, 4-butanediol. *Catal. Commun.* **2011**, *12*, 866-869.

56. Guo, P. J.; Chen, L. F.; Yan, S. R.; Dai, W. L.; Qiao, M. H.; Xu, H. L.; Fan, K. N. One-step hydrogenolysis of dimethyl maleate to tetrahydrofuran over chromium-modified Cu–B/γ-Al2O3 catalysts. *J. Mol. Catal. A* **2006**, *256*, 164-170.

57. Christian, R. V.; Brown, H. D.; Hixon, R. M. Derivatives of γ-Valerolactone, 1,4-Pentanediol and 1,4-Di-(β-cyanoethoxy)-pentane. *J. Am. Chem. Soc.* **1947**, *69*, 1961-1963.

58. Rocha, A. L.; Solórzano, I. G.; Vander Sande, J. B. Heterogeneous and homogeneous nanoscale precipitation in dilute Cu–Co alloys. *Mater. Sci. Eng. C* **2007**, *27*, 1215-1221.

59. Carenco, S.; Tuxen, A.; Chintapalli, M.; Pach, E.; Escudero, C.; Ewers, T. D.; Jiang, P.; Borondics, F.; Thornton, G.; Alivisatos, A. P.; Bluhm, H.; Guo, J.; Salmeron, M. Dealloying of Cobalt from CuCo Nanoparticles under Syngas Exposure. *J. Phys. Chem. C* **2013**, *117*, 6259-6266.

60. Prieto, G.; Beijer, S.; Smith, M. L.; He, M.; Au, Y.; Wang, Z.; Bruce, D. A.; de Jong, K. P.; Spivey, J. J.; de Jongh, P. E. Design and Synthesis of Copper–Cobalt Catalysts for the Selective Conversion of Synthesis Gas to Ethanol and Higher Alcohols. *Angew. Chem. Int. Ed.* **2014**, *53*, 6397-6401.

61. Bulut, A.; Yurderi, M.; Ertas, İ. E.; Celebi, M.; Kaya, M.; Zahmakiran, M., Carbon dispersed copper-cobalt alloy nanoparticles: A cost-effective heterogeneous catalyst with exceptional performance in the hydrolytic dehydrogenation of ammonia-borane. *Appl. Catal. B* **2016**, *180*, 121-129.

62. Li, J.; Zhu, Q. L.; Xu, Q. Non-noble bimetallic CuCo nanoparticles encapsulated in the pores of metal–organic frameworks: synergetic catalysis in the hydrolysis of ammonia borane for hydrogen generation. *Catal. Sci. Technol.* **2015**, *5*, 525-530.

63. Wen, C.; Cui, Y.; Yin, A.; Fan, K.; Dai, W. L. Remarkable Improvement of Catalytic Performance for a New Cobalt-Decorated Cu/HMS Catalyst in the Hydrogenation of Dimethyloxalate. *ChemCatChem* **2013**, *5*, 138-141.

64. Cao, A.; Liu, G.; Yue, Y.; Zhang, L.; Liu, Y. Nanoparticles of Cu–Co alloy derived from layered double hydroxides and their catalytic performance for higher alcohol synthesis from syngas. *RSC Adv.* **2015**, *5*, 58804-58812.

65. Chen, B.; Li, F.; Huang, Z.; Yuan, G. Carbon-coated Cu-Co bimetallic nanoparticles as selective and recyclable catalysts for production of biofuel 2,5-dimethylfuran. *Appl. Catal. B* **2017**, *200*, 192-199.

Chapter 7. Conclusions and Future Directions

7.1 Conclusions

Four to six carbon (C4-C6) α,ω-diols were synthesized from biomass-derived oxygenates. The C5 platform molecule, furfural, was hydrogenated to tetrahydrofurfuryl alcohol (THFA) prior to further upgrading to 1,5-pentanediol (1,5-PD). The Dehydration-Hydration-Hydrogenation (DHH) pathway to produce α,ω-diols was studied as an alternative to the more costly direct hydrogenolysis over oxophilically-promoted noble metal catalysts (e.g. RhRe). 1,5-PD was produced in 87% overall yields from THFA utilizing the DHH chemistry. The use of low-cost catalysts (γ-Al_2O_3, Ru/C) combined with much higher reaction rates led to a >50x decrease in catalyst cost and a 6.6x decrease in the non-feedstock production costs versus the direct hydrogenolysis of THFA over a RhRe catalyst.

The reaction mechanism and kinetics for each of the three reaction steps in the DHH pathway were studied to uncover the underlying cause for the high reactivities and product selectivities obtained in the DHH pathway. Nuclear magnetic resonance (NMR) spectroscopy of the reaction products of carbon-13 labelled THFA definitely showed the reaction mechanism proceeds through γ-Al_2O_3-catalyzed ring-opening followed by a Wagner-Meerwien rearrangement to the dihydropyran (DHP) product. Gas-phase thermodynamic calculations showed the DHP product was highly favorable when compared to various ring-rearrangement side products. As such, overall DHP yields of 90% were obtained in the THFA dehydration reaction step over a γ-Al_2O_3 catalyst.

The DHP was then hydrated to the 2-hydroxytetrahydropyran (2-HTHP) product in near quantitative yields without the use of any externally added catalyst. It was shown that the *in situ* formation of liquid acidic species during hydration in water further increased the hydration rate,

autocatalyzing the reaction. Solid acid coke species formed at higher temperatures (>130˚C) in continuous flow reactors were shown to increase hydration rates by at least 28x will still maintaining near quantitative yields to the desired hydration products. The addition of pre-synthesized solid acid catalysts resulted in much improved rates over the autocatalytic hydration and improved product selectivities to in the combined hydration-hydrogenation of vinyl cyclic ethers to α,ω-diols.

The underlying reason for the rapid hydration of DHP in water was studied by comparing DHP hydration rates to those of similar molecules with no cyclic ether oxygen atom present (e.g. cyclohexene). Vinyl cyclic ethers such as DHP were shown to hydrate over 5 orders of magnitude faster than any other type of compound studied and over 7 orders of magnitude faster than cyclohexene. Gas-phase thermochemistry calculations of the intermediates formed upon hydration showed that the increased rates of vinyl cyclic ether hydration was due to the formation of very stable oxocarbenium intermediates.

The last step of the DHH pathway - conversion of the cyclic hemiacetal 2-hydroxytetrahydropyran (2-HTHP) to 1,5-PD - was shown to proceed through the hydrogenation of the ring-opened tautomer of 2-HTHP, 5-hydroxyvaleraldehye (5HVal). Variable temperature NMR revealed ring-opening of 2-HTHP occurred spontaneously in solution, forming a ~50:50 mixture of 2-HTHP:5HVal at our hydrogenation temperature of 120˚C. The ability to simply hydrogenate the aldehyde group of 5HVal to the 1,5-PD product allowed for the use of monometallic catalysts such as Ru/C, which gave much higher reaction rates than the RhRe-catalyzed direct hydrogenolysis of THFA.

The DHH chemistry was studied for the analogous C6 route for THP2M conversion to 1,6-hexanediol (1,6-HD). Lower overall yields to the α,ω-diol product (34%) were achieved than for the C5 route due to the increased thermodynamic favorability of over-conversion of the dehydration product 2,3,4,5-tetrahydrooxepine (THO). A detailed reaction pathway for the THP2M dehydration step was proposed based on the change in observed product selectivities with catalyst contact time in a continuous flow reactor. The hydration-hydrogenation chemistry was shown to proceed through a similar cyclic hemiacetal intermediate as the C5 route and gave an 86% overall 1,6-HD yield from THO.

New conversion routes from biomass to the C4 α,ω-diol, 1,4-butanediol (1,4-BD), were studied based on the chemistries outlined above for the C5 and C6 routes. A new pathway from biomass-derived erythritol to 1,4-BD was proposed. Erythritol can be converted to 2,5-DHF in two-reaction steps. Our work demonstrated the combined isomerization-hydration-hydrogenation of 2,5-DHF to 1,4-BD in up to 82% yields in a single batch reactor over a solid acid hydration catalyst and a metal hydrogenation catalyst. Another route to 1,4-BD was demonstrated via the hydrogenation of furfural-derived γ-butryolactone (GBL) to 1,4-BD. 1,4-BD yields above 95% were obtained from GBL over bimetallic $CuCo/TiO_2$ catalysts. Moreover, GBL hydrogenation rates were improved by 2.5x over monometallic Co and 20x over monometallic Cu catalysts, respectively, when employing a bimetallic $CoCu/TiO_2$ catalyst with a 90:10 Co:Cu ratio.

7.2. Future Directions

7.2.1 Improved Stability of Solid Acid Catalysts

Multiple reaction steps in the DHH pathway can be improved by increasing the stability of the heterogeneous catalysts employed. In the DHP hydration step, it was shown in Chapter 5 that the addition of solid acid catalysts can greatly improve the hydration rate as compared to the

homogeneous, autocatalytic hydration. These solid acid catalysts showed no signs of leaching of acid sites during the low temperature (30˚C), low concentration (0.5wt% DHP/H_2O) batch kinetic experiments. However, upon increasing the temperature and DHP concentration in water, both Amberlyst-70 (A-70) and HZSM5 catalysts exhibited significant deactivation in flow reactors. In fact, x-ray diffraction (XRD) of fresh and spent HZSM5 showed a 29% loss in crystallinity of the zeolite structure in the hydration of 20wt% DHP/H_2O in a flow reactor. While the flow reactor temperature (50-70˚C) was higher than for the batch kinetic studies, A-70[1,2] and HZSM5[3–5] have previously been shown to be hydrothermally stable at much higher temperatures (>160˚C), indicating that the presence of high concentration of organics may have an effect on the catalyst stability. Increased coking is also a likely primary deactivation mechanism at these higher concentrations of DHP, as observed by the formation of solid humins and lower carbon balances at increased temperatures. It is thus our suggestion that more work be done in i) studying the effect various organic species have on the structural stability of different zeolite structures and ii) investigating the factors that limit coking reactions at high concentrations of organics in water (i.e. effect of SiO_2:Al_2O_3 ratio or zeolite cage structure). The knowledge gained from these studies could then be used to implement improved solid acid catalysts for hydration of highly concentrated organic species in aqueous systems.

7.2.2 Improved Stability of Base-metal Catalysts

The stability of base-metal catalysts (e.g. Co and Ni) should be further studied for aqueous-phase upgrading of biomass-derived oxygenates. It was shown in prior work that base-metal catalysts could be stabilized in aqueous-phase reactions by atomic-layer-deposition (ALD)[6] and strong metal-support interactions (SMSI).[7] However, both of these studies were performed with dilute feed concentrations (2wt%) in a water solvent.[6,7] When attempting to employ ALD and

SMSI-stabilized Ni and Co catalysts for higher concentrations (20wt%) of 2-HTHP in water (for 1,5-PD production), significant deactivation in the form of leaching and sintering was observed. This indicates that the organic species (2-HTHP) has a large effect on the base metal stability, likely in the form of chelation.[8,9] Most prior work in the deactivation of base metals in aqueous systems has focused on the leaching of cationic metal atoms (e.g. Ni^{2+} and Co^{2+}) through their interactions with water molecules,[10,11] but not much research has focused on the effect the organic species concentration and functionality has on the leaching of the base metals. Recent work in a related thesis has shown that different functionalities (aldehydes, ketones, carboxylic acids) as well as the number (i.e. mono-functional vs. bi-functional) and proximity of functionalities in a molecule indeed has a large effect on the stability of supported Ni catalysts in solution.[12] While this work is important in that it introduces these chelation effects on stability, more work needs to be done in identifying the mechanism of chelation and what effect chelation has on different supported base-metal systems at varying reaction conditions (temperature, pressure, atmosphere, concentration, etc.). This knowledge can then be used for the design of base-metal systems with improved stability in highly concentrated organic systems.

7.2.3 Outlook

The C5 route from furfural to 1,5-pentanediol (1,5-PD) is currently being commercialized in the form of a start-up company called Pyran. The success of this project can be partly attributed our dedication to fundamental chemistry and catalysis research with a focus on potential applicability, in combination with macro-scale technoeconomic simulations (see Chapter 2). Our focus on the fundamentals led to the discovery of the tetrahydrofurfuryl alcohol dehydration mechanism (Chapter 2), autocatalytic hydration of dihydropyran (Chapter 4), enhanced hydration rates of vinyl cyclic ethers (Chapter 5), and spontaneous ring-opening of cyclic hemiacetals

(Chapter 2). These basic discoveries of the dehydration-hydration-hydrogenation (DHH) chemistries explained how high yields in the DHH pathway were achieved, and the resulting knowledge gained can be applied to similar chemistries to improve or discover new biomass-upgrading reactions.

Catalysts displaying a balance of high activity, high stability, and *low costs* then had to be developed. All of these factors are related, but the fact that all were considered in our research led to the optimal results. Catalytic testing was scaled from batch reactors and low feed concentrations to continuous flow reactors at high feed concentrations, with *catalyst stability* being a primary goal in addition to high activity. The results of these experiments were simultaneously inputted into a technoeconomic model, which allowed for real-time feedback on the effect certain reaction conditions had on the minimum selling price of 1,5-PD. This allowed for an iterative research approach that led to an enhanced focus on the important parameters related to the industrial applicability of the 1,5-PD process. It is my suggestion that other research groups take this iterative approach between experiment and simulation whenever possible.

The commercialization of bio-derived 1,5-PD through Pyran brings up the question of whether it is preferred to produced new chemicals from biomass or to make drop-in replacements for petroleum-derived chemicals. 1,5-PD is currently only produced in very small quantities from oil, so it will largely replace 1,4-butanediol (1,4-BD) and 1,6-hexanediol (1,6-HD) in industry. The fact that 1,5-PD is not a pure drop-in does create a risk for companies looking to replace oil-derived diols with 1,5-PD, but not as much a risk as if 1,5-PD was very chemically different from 1,4-BD or 1,6-HD. This is the issue with many biomass-derived chemicals: the inherent functionality of biomass allows for the development of many new types of molecules that cannot be made from petroleum, but there is thus little current market for these new chemicals. A great

example of this is the C6 chemistry from cellulose to 1,6-HD, where several new types of molecules have been discovered by our research group, including levoglucosenone, cyrene, levoglucosanol, 1,2,5,6-tetrol, 1,2,6-hexanetriol, and tetrahydrofuran di-methanol. Each of these molecules have unique functionalities that would likely enable commercial applications, but little effort has been done previously to test the properties or uses of these molecules in end-products. It is thus my suggestion that more coordination occur between researchers who develop new bio-chemicals and researchers who can test for potential applications in the form of specialty chemicals, solvents, or polymeric materials.

7.3 References

1. Weingarten, R.; Conner, W. C.; Huber, G. W. Production of Levulinic Acid from Cellulose by Hydrothermal Decomposition Combined with Aqueous Phase Dehydration with a Solid Acid Catalyst. *Energy Environ. Sci.* **2012**, *5* (6), 7559.
2. Guilera, J.; Ramírez, E.; Fité, C.; Iborra, M.; Tejero, J. Thermal Stability and Water Effect on Ion-Exchange Resins in Ethyl Octyl Ether Production at High Temperature. *Appl. Catal. A Gen.* **2013**, *467*, 301–309.
3. Ravenelle, R. M.; Schübler, F.; Damico, A.; Danilina, N.; Van Bokhoven, J. A.; Lercher, J. A.; Jones, C. W.; Sievers, C. Stability of Zeolites in Hot Liquid Water. *J. Phys. Chem. C* **2010**, *114* (46), 19582–19595.
4. Lutz, W.; Toufar, H.; Kurzhals, R.; Suckow, M. Investigation and Modeling of the Hydrothermal Stability of Technically Relevant Zeolites. *Adsorption* **2005**, *11* (3–4), 405–413.
5. Gardner, D. W.; Huo, J.; Hoff, T. C.; Johnson, R. L.; Shanks, B. H.; Tessonnier, J. P. Insights into the Hydrothermal Stability of ZSM-5 under Relevant Biomass Conversion Reaction Conditions. *ACS Catal.* **2015**, *5* (7), 4418–4422.
6. O'Neill, B. J.; Jackson, D. H. K.; Crisci, A. J.; Farberow, C. a.; Shi, F.; Alba-Rubio, A. C.; Lu, J.; Dietrich, P. J.; Gu, X.; Marshall, C. L.; et al. Stabilization of Copper Catalysts for Liquid-Phase Reactions by Atomic Layer Deposition. *Angew. Chemie - Int. Ed.* **2013**, *52*, 13808–13812.
7. Lee, J.; Burt, S. P.; Carrero, C. A.; Alba-Rubio, A. C.; Ro, I.; O'Neill, B. J.; Kim, H. J.; Jackson, D. H. K.; Kuech, T. F.; Hermans, I.; et al. Stabilizing Cobalt Catalysts for

Aqueous-Phase Reactions by Strong Metal-Support Interaction. *J. Catal.* **2015**, *330*, 19–27.

8. Egneus, B.; Uppstrom, L. Extraction of Boric Acid with Aliphatic 1,3-Diols and Other Chelating Agents. *Anal. Chim. Acta* **1973**, *66*, 211–229.

9. Martell, A. E.; Hancock, R. D.; Motekaitis, R. J. Factors Affecting Stabilities of Chelate, Macrocyclic and Macrobicyclic Complexes in Solution (Doctoral Dissertation). *Coord. Chem. Rev.* **1994**, *133*, 39–65.

10. Haasterecht, T. Van; Ludding, C. C. I.; Jong, K. P. De; Bitter, J. H. Toward Stable Nickel Catalysts for Aqueous Phase Reforming of Biomass-Derived Feedstock under Reducing and Alkaline Conditions. *J. Catal.* **2014**, *319*, 27–35.

11. Shabaker, J. W.; Simonetti, D. A.; Cortright, R. D.; Dumesic, J. A. Sn-Modified Ni Catalysts for Aqueous-Phase Reforming: Characterization and Deactivation Studies. *J. Catal.* **2005**, *231* (1), 67–76.

12. Brentzel, Z. J. Catalytic Upgrading of Biologically-Derived Chemicals via Ring-Opening Reactions (Doctoral Dissertation), University of Wisconsin-Madison, 2017.